CHEMICAL
RESEARCH,
DEVELOPMENT &
ENGINEERING
CENTER

CRDEC-CR-058

INTERIOR FLUID DYNAMICS OF LIQUID-FILLED PROJECTILES

Thorwald Herbert

OHIO STATE UNIVERSITY
Columbus, OH 43210

December 1989

U.S. ARMY
ARMAMENT
MUNITIONS
CHEMICAL COMMAND

Aberdeen Proving Ground, Maryland 21010-5423

Disclaimer

The findings in this report are not to be construed as an official Department of the Army position unless so designated by other authorizing documents.

Distribution Statement

Approved for public release; distribution is unlimited.

REPORT DOCUMENTATION PAGE

Form Approved
OMB No. 0704-0188

1a REPORT SECURITY CLASSIFICATION: UNCLASSIFIED	1b RESTRICTIVE MARKINGS
2a SECURITY CLASSIFICATION AUTHORITY	3 DISTRIBUTION/AVAILABILITY OF REPORT: Approved for public release; distribution is unlimited.
2b DECLASSIFICATION/DOWNGRADING SCHEDULE	
4 PERFORMING ORGANIZATION REPORT NUMBER(S): CRDEC-CR-058	5 MONITORING ORGANIZATION REPORT NUMBER(S)
6a NAME OF PERFORMING ORGANIZATION: Ohio State University; 6b OFFICE SYMBOL (If applicable)	7a NAME OF MONITORING ORGANIZATION
6c ADDRESS (City, State, and ZIP Code): Columbus, OH 43210	7b ADDRESS (City, State, and ZIP Code)
8a NAME OF FUNDING/SPONSORING ORGANIZATION: CRDEC; 8b OFFICE SYMBOL (If applicable): SMCCR-RSP-A	9 PROCUREMENT INSTRUMENT IDENTIFICATION NUMBER: DAAA15-85-K-0012
8c ADDRESS (City, State, and ZIP Code): Aberdeen Proving Ground, MD 21010-5423	10 SOURCE OF FUNDING NUMBERS: PROGRAM ELEMENT NO; PROJECT NO; TASK NO; WORK UNIT ACCESSION NO

11 TITLE (Include Security Classification)
Interior Fluid Dynamics of Liquid-Filled Projectiles

12 PERSONAL AUTHOR(S)
Herbert, Thorwald*

13a TYPE OF REPORT	13b TIME COVERED	14 DATE OF REPORT (Year, Month, Day)	15 PAGE COUNT
Contractor	FROM 85 Jul TO 88 Dec	1989 December	121

16 SUPPLEMENTARY NOTATION *At the time the work was started Mr. Herbert was employed by Virginia Polytechnic Institute and State University.
COR: Miles Miller, SMCCR-RSP-A, (301) 671-2186

17 COSATI CODES			18 SUBJECT TERMS (Continue on reverse if necessary and identify by block number)
FIELD	GROUP	SUB-GROUP	Projectile stability; Liquid payloads; Aeroballistics
01	01		
20	04		

19 ABSTRACT (Continue on reverse if necessary and identify by block number)

Theoretical and numerical studies were conducted to analyze the flow in spinning and coning liquid-filled payload cylinders and to provide efficient tools for estimating and calculating the liquid moments as input data for flight simulations. Earlier analytical studies for cylinders of large aspect ratio were extended to the nonlinear problem to provide estimates for all moments. This perturbation analysis is currently used to investigate the influence of partial liquid fills, central rods, and two-fluid fills on the moments. A new method was developed to obtain the moments from volume integrals rather than surface integrals and thus increase the accuracy of the results at fixed numerical approximation. An efficient spectral code has been developed for routine application to solve the three-dimensional Navier-Stokes equations. Utility of this code for efficient flight simulations has been demonstrated. The code has been
(continued on reverse)

20 DISTRIBUTION/AVAILABILITY OF ABSTRACT	21 ABSTRACT SECURITY CLASSIFICATION
☒ UNCLASSIFIED/UNLIMITED ☐ SAME AS RPT ☐ DTIC USERS	UNCLASSIFIED
22a NAME OF RESPONSIBLE INDIVIDUAL: SANDRA L. JOHNSON	22b TELEPHONE (Include Area Code): (301) 671-2914 / 22c OFFICE SYMBOL: SMCCR-SPS-T

DD Form 1473, JUN 86 — Previous editions are obsolete — SECURITY CLASSIFICATION OF THIS PAGE

19. Abstract (Continued)

applied to investigate liquid moments, velocity field, and pressure field in situations of pure forcing as well as resonance with inertial waves at Reynolds numbers up to 2000. For the linearized problem, a simplified set of equations has been developed that permits closed-form solutions for spatial eigenfunctions and highly efficient solution by spectral methods.

Summary

Theoretical and numerical studies were conducted to analyze the flow in spinning and coning liquid-filled payload cylinders and to provide efficient tools for estimating and calculating the liquid moments as input data for flight simulations. Earlier analytical studies for cylinders of large aspect ratio were extended to the nonlinear problem to provide estimates for all moments. This perturbation analysis is currently used to investigate the influence of partial liquid fills, central rods, and two-fluid fills on the moments. A new method was developed to obtain the moments from volume integrals rather than surface integrals and thus increase the accuracy of the results at fixed numerical approximation. An efficient spectral code has been developed for routine application to solve the three-dimensional Navier-Stokes equations. Utility of this code for efficient flight simulations has been demonstrated. The code has been applied to investigate liquid moments, velocity field, and pressure field in situations of pure forcing as well as resonance with inertial waves at Reynolds numbers up to 2000. For the linearized problem, a simplified set of equations has been developed that permits closed-form solutions for spatial eigenfunctions and highly efficient solution by spectral methods.

BLANK

PREFACE

The work described in this report was authorized under Contract No. DAAA15-85-K-0012. This work was started in July 1985 and completed in December 1988.

The use of trade names or manufacturers' names in this report does not constitute an official endorsement of any commercial products. This report may not be cited for purposes of advertisement.

BLANK

CONTENTS

BLANK

INTERIOR FLUID DYNAMICS
OF LIQUID-FILLED PROJECTILES

1. Research Objectives

The project "Interior Fluid Dynamics of Liquid-Filled Projectiles" under Contract DAAA15-85-K-0012 of the Department of the Army, AMCCOM, was originally planned as a three-year effort with the working period 07/01/85 - 06/30/88 and Thorwald Herbert as principal investigator. The working period was extended at no cost until 12/31/88.

A detailed description of the research objectives has been given in section 2.2 of the original proposal. In summary, the research aimed at understanding the origin of the flight instability of projectiles with liquid payloads and at estimating and accurately calculating the liquid-induced moments to obtain the data necessary for the design of future projectiles. This effort was directly related to the experimental studies conducted at CRDEC and to numerical studies performed at BRL. In detail, the work under this contract was planned to extend our earlier analysis in three directions:

(1) Fully exploit the potential of the linearized solution with regard to yaw moment, pitch moment, and temperature effects on the viscosity. Extend the solution to unsteady (e.g. spin-up) situations.

(2) Perform a perturbation analysis of the nonlinear effects that produce radial and azimuthal velocity components and modify the axial component. Study the effect of the cylinder end walls on the flow field and the pressure. Investigate the onset and nature of cellular motions at higher Reynolds numbers.

(3) Develop a highly efficient computer code for calculating the steady flow field and liquid moments on the basis of the Navier-Stokes equations. Implement spectral approximations in all space variables. Extend the analysis to unsteady problems (spin-up, spin-down, yaw-angle growth). Incorporate the flow computations into an existing six-degree-of-freedom code.

As will be discussed in the next section, most of these goals have been reached. Various other results have been achieved that were not anticipated at initiation of this contract. The work on unsteady aspects of the problem was initiated but not finished within the period of this contract.

Owing to Th. Herbert's accepting a new position at The Ohio State University (OSU) beginning with the academic year 1987/88 on October 1, 1987, only a part of the program was conducted at the Virginia Polytechnic Institute and State University (VPI). A part of the remaining funds was made available through a subcontract to The Ohio State University to continue the research. The research equipment acquired within this contract remained at VPI. The lack of this equipment required time-consuming modifications of our research codes and caused delays in the research program.

2. Research Achievements

After initiation of this contract, work was simultaneously conducted on all three topics. Rapid progress was made until summer 1987 in close cooperation of the principal investigator with Rihuá Li who worked as a postdoctoral associate. At this time, Dr. Li accepted a similar position at the University of Arizona since the funds available at OSU were insufficient for his remaining in the program. At OSU, M. Selmi continued Dr. Li's work after some training period.

Most of the results of our research have been reported in publications (see section 4) and more detailed papers are in preparation. Therefore, we can restrict this report to a brief overview of the achievements.

Our earlier analytical studies for cylinders of large aspect ratio (Herbert 1986) were extended to the nonlinear problem by use of a perturbation method. The small expansion parameter is $\varepsilon = \tau\sin\theta$, where $\tau = \Omega/\omega$, Ω the nutation rate, ω the spin rate, and θ the angle between the two axes of rotation. The solution up to second order is obtained in closed form, while the third-order contributions are determined numerically. Higher-order terms are small such that good estimates of all liquid moments can be obtained from the closed-form approximation. The effect of finite aspect ratios has been evaluated by comparison with results of the spectral code (see below). This evaluation and the comparison of flight simulations based on analytical and numerical results shows that the estimates are conservative and therefore useful for preliminary design studies. Recently, the analysis has been extended to obtain results for partially filled cylinders with an axisymmetric void, for cylinders with a central rod, and for the case of two immiscible fluids of different viscosities and densities separated by a cylindrical interface.

Various studies have been performed to evaluate existing Navier-Stokes solvers (Vaughn et al. 1985a, Strikwerda & Nagel 1985). These efforts were kindly supported by M. Nusca, BRL, who provided data for comparison and the latest version of the Sandia code. The previous codes are primarily based on finite-difference approximations with relatively coarse grid and were designed without insight into the nature of the fluid motion. As a result, these codes provide solutions only for relatively small Reynolds numbers and have to compromise between numerical approximation and computational expense. Guided by our analytical work, we have directed our efforts toward tailoring the Navier-Stokes code to the nature of the fluid motion and obtaining more accurate moments from a given numerical approximation for the flow fields.

Previous numerical work determined the moments from surface integrals over normal stresses and shear stresses which involve the pressure and velocity gradients at the boundary. However, boundary quantities are obtained with numerical errors typically much larger than the velocity in the interior. We have developed a method to determine the moments by integration over the volume of the cylinder. This integration requires only the knowledge of the fundamental Fourier component of the axial velocity and the mean (streaming) component of the azimuthal velocity. The pressure and velocity gradients are eliminated from this formulation. In comparison with the traditional surface approach, the smoothing by integration in three space directions and the use of well-approximated data provides moments of superior accuracy with the same original data, i.e. with the same amount of computer time. The method is generic in the sense that it is valid not only for cylinders but as well for arbitrary closed containers. Moreover, the method is not only useful for purely numerical work but especially for perturbation approaches that provide the fundamental Fourier component of the axial velocity at first order and the mean component of the azimuthal velocity at second order.

The design of the spectral code for solving the Navier-Stokes equations was guided by analytical studies, the anticipated use for flight simulations, and the desire to keep the code open for extension to unsteady problems. The latter demand prevented the use of artificial (non-physical) time dependence to obtain the steady solution. Since the structure of the equations clearly exhibits the dominance of the linear terms at the usually small values of ε, a good approximation for the solution can be obtained by solving the linear system. This solution is improved by iteration to account for nonlinearity. Besides the linearization in ε, a second type of linearization can be made in the velocity deviation from rigid-body motion. A third type of linearization is about a known solution at neighboring parameters. While the second type is used in absence of prior knowledge, the third type is especially suited for continuation of the solution and moment calculations in flight simulations which are characterized by a slow variation of the parameters along the trajectory.

The utility of the spectral code for fundamental studies of the fluid motion (Herbert & Li 1987) and its efficiency for flight simulations (Herbert 1988) has been verified. The flight simulations were based on a slightly modified version of the code developed by Vaughn et al. (1985b). More recent work was dedicated to the range of high Reynolds numbers and to the viscous effects on the resonance with inertial waves. For sufficiently small ε the spectral solutions of the nonlinear problem agree well with the results of Hall et al. (1987) obtained by spatial eigenfunction expansions of the linearized problem.

The eigenfunction expansions used by Hall, Sedney & Gerber (1987) require numerical determination of eigenvalues and eigenfunctions from an eigenvalue problem for a system of ordinary differential equations. We have developed an equivalent but much simpler set of equations that permits closed-form solutions for the spatial eigenfunctions (Li & Herbert 1988) and thus avoids the high computational expense for generating numerical solutions. The eigenvalues are obtained as solutions of a transcendental equation. Our formulation of the problem clearly reveals the structure of the eigenvalue spectrum and explains the empirical results of Hall et al. on the grouping of the eigenfunctions. The eigenvalues have been generated for Reynolds numbers as high as 10^6. The numerical problems of using modified Bessel functions of large complex arguments at these high Reynolds numbers are not yet fully overcome.

Besides solving the new formulation in terms of eigenfunction expansions, we apply spectral expansions in Chebyshev series. The otherwise two-step solution procedure (generation of functions, solving for the expansion coefficients) reduces in this case to a single step. Although this code has not yet matured for routine applications, experience in the range up to Reynolds numbers of the order of 10^3 is very encouraging.

Various studies have been performed to adapt the existing analytical and numerical methods to the unsteady problem. These studies concentrate on more efficient solution of linear and weakly nonlinear algebraic systems with iterative methods.

With the work under this contract, we have deepened the understanding of the fluid motion in liquid-filled cylinders. The analytical work provides estimates for the moments in various cylindrical configurations, guidance for the design of numerical methods, and an improved basis for calculation of the moments. Spectral codes for solving the linear and nonlinear problem have been developed and verified to efficiently calculate the liquid moments up to Reynolds numbers of the order of $2 \cdot 10^4$. The spectral code for the linear problem will be further developed to overlap with the boundary-layer methods in the range of high Reynolds numbers.

3. Personnel

During the working period, the following personnel were partly supported under Contract DAAA15-85-K-0012:

Thorwald Herbert, Professor, Principal Investigator
Rihua Li, Postdoctoral Associate
Relja Zivojnovic, Graduate Student (M.S. level)
Stephen D. Greco. Graduate Student (Ph.D. level)
Mohamed Selmi, Graduate Student (Ph.D. level)
Charlotte R. Hawley, Research Specialist
Vineet Mehta, Undergraduate Student
David Pierpont, Undergraduate Student

Rihua Li developed the volume approach for the calculation of the liquid moments and implemented this method into the numerical work. Li analyzed the problems associated with corners of the computational domain for spectral codes and contributed both to the analytical and numerical aspects of the research program. In 1987, Li developed the simplified formulation of the linear problem and the closed-form solution for the eigenfunctions. Dr. Li is presently Postdoctoral Associate in the Department of Aerospace and Mechanical Engineering at the University of Arizona.

R. Zivojnovic and S. Greco were involved in developing the perturbation approach and solving the perturbation equations numerically. Owing to the complexity of the problem, they cooperated only for a short time in the program.

Mohamed Selmi has continued the work of Dr. Li at OSU. He developed codes for determining the expansion coefficients of the linear solution in terms of eigenfunctions and for direct solution of the linear system by spectral methods.

Charlotte Hawley was responsible for computer operations and software, project administration, and technical manuscripts. Since December 1987, she is Research Assistant at OSU and continues her cooperation in the research program.

4. Publications (Note: See Appendices A-H)

The following publications, reports, and communications were prepared with support by contract DAAA15-85-K-0012:

(1) "Visualization of the Flow in a Spinning and Nutating Cylinder," by Th. Herbert and D. Pierpont, in: *Proc. 1985 Scientific Conf. on Chemical Defense Research, Aberdeen Proving Ground, Maryland, 1985.* (Ed.) M. Rausa, Report CRDC-SP-86007, pp. 989-994 (1986).

(2) "Analytical and Computational Studies of the Fluid Motion in Liquid-Filled Shells," by Th. Herbert, in: *Trans. Fourth Army Conf. on Applied Mathematics and Computing, Ithaca, New York, 1986.* ARO Report 87-1, pp. 627-636 (1987).

(3) "Numerical Study of the Flow in a Spinning and Nutating Cylinder," by Th. Herbert and R. Li, AIAA Paper No. 87-1445 (1987).

(4) "A Spectral Navier-Stokes Solver for the Flow in a Spinning and Nutating Cylinder," by Th. Herbert, in. *Proc. 1986 Scientific Conf. on Chemical Defense Research, Aberdeen Proving Ground, Maryland, 1986.* (Ed.) M. Rausa, Report CRDC-SP-87005, pp. 455-460

(1987).

(5) "Flight Simulation for Liquid-Filled Projectiles," by Th. Herbert, *Proc. 1987 U.S. Army CRDEC Scientific Conference on Chemical Defense Research, Aberdeen Proving Ground, Maryland (1987).* Report CRDC-SP-88013, pp. 377-385 (1988).

(6) "Computational Study of the Flow in a Spinning and Nutating Cylinder," by Th. Herbert and R. Li, *AIAA J.* (1988), under review.

(7) "Symbolic Computations with Spectral Methods," by Th. Herbert, ASME, AMD-Vol. 97, in *Symbolic Computation in Fluid Mechanics and Heat Transfer*, pp. 25-32 (1988).

(8) "High-Reynolds-Number Flows in a Spinning and Nutating Cylinder," by Rihua Li and Th. Herbert, in: *Proc. 1988 Scientific Conf. on Chemical Defense Research, Aberdeen Proving Ground, Maryland, 1988.* To appear.

The following papers reporting results obtained under the support by this contract are in preparation:

(9) "Perturbation Analysis of the Flow in a Spinning and Nutating Cylinder of Large Aspect Ratio," by Th. Herbert and R. Li, Physics of Fluids.

(10) "Calculation of the Liquid Moments in a Spinning and Nutating Cylinder," by R. Li and Th. Herbert, J. Guidance, Control, and Dynamics

(11) "Spatial Eigenfunction Expansion for the Flow in a Spinning and Nutating Cylinder," by R. Li and Th. Herbert, J. Fluid Mech.

5. Technical Presentations

The following papers were presented at meetings, conferences and seminars:

(1) "On the Domain of Stable Taylor-Vortex Flow," by Th. Herbert and R. Li, Proc. Conference on Mathematics Applied to Fluid Mechanics and Stability - Dedicated in Memory of Richard C. DiPrima, Troy, New York (Sept. 1985).

(2) "Zur Stabilität axialsymmetrischer Taylor Wirbel," Institut für Aerodynamik und Gasdynamik, Universität Stuttgart (Oct. 1985).

(3) "State Selection for Taylor-Vortex Flow," by R. Li and Th. Herbert, 22nd Annual Meeting of the Society of Engineering Science, University Park, Pennsylvania (Oct. 1985).

(4) "On the Fluid Motion in Liquid-Filled Shells," Scientific Conference on Chemical Defense Research, Aberdeen Proving Ground, Maryland (Nov. 1985).

(5) "State Selection in Taylor-Vortex Flow," Th. Herbert and R. H. Li, Meeting of the Division of Fluid Mechanics of the American Physical Society, Tucson, Arizona (Nov. 1985).

(6) "Fluid Motion in Liquid-Filled Shells," Fourth Army Conference on Applied Mathematics and Computing, Ithaca, New York (May 1986).

(7) "Anatomy of the Viscous Flow in a Spinning and Nutating Cylinder," Lockheed-Georgia, Marietta, Georgia (Aug. 1986).

(8) "A Spectral Navier-Stokes Solver for the Flow in a Spinning and Nutating Cylinder," 1986 U.S. Army CRDEC Scientific Conference on Chemical Defense Research, Aberdeen Proving Ground, Maryland (Nov. 1986).

(9) "Spectral Co[illegible]ation of the Viscous Flow in a Rotating and Nutating Cylinder," by R. Li and Th. Herbert, 39th Annual Meeting of the Division of Fluid Dynamics, American Physical Society, Columbus, Ohio (Nov. 1986).

(10) "Wavenumber Selection in Taylor-Vortex Flow," by Th. Herbert and R. Li, Fifth Taylor-Vortex Flow Working Party, Tempe, Arizona (March 1987).

(11) "Viscous Fluid Motion in a Spinning and Nutating Cylinder," by Th. Herbert, Department of Mechanical Engineering, Massachusetts Institute of Technology, Cambridge, Massachusetts (April 1987).

(12) "Numerical Study of the Flow in a Spinning and Nutating Cylinder," by Th. Herbert and R. Li, AIAA 19th Fluid Dynamics, Plasma Dynamics and Laser Conference, Honolulu, Hawaii (June 1987).

(13) "Computation of the Flow in a Spinning and Nutating Cylinder," by Th. Herbert, Department of Aeronautical and Astronautical Engineering, The Ohio State University, Columbus, Ohio (Oct. 1987).

(14) "Flight Simulation for Liquid-Filled Projectiles," by Th. Herbert, 1987 U.S. Army CRDEC Scientific Conference on Chemical Defense Research, Aberdeen Proving Ground, Maryland (Nov. 1987).

(15) "Analysis of Viscous Flows by Spectral Methods," by Th. Herbert, Seminars on Algorithms for Supercomputing, Ohio Supercomputer Center, Columbus, Ohio (September 1988).

(16) "High-Reynolds Number Flows in a Spinning and Nutating Cylinder," by Th. Herbert, Chemical Research Development Engineering Center, Aberdeen Proving Ground, Maryland (November 1988).

6. References

Th. Herbert (1986) "Viscous fluid motion in a spinning and nutating cylinder," *J. Fluid Mech.*, Vol 167, pp. 181-198.

H. R. Vaughn, W. L. Oberkampf, and W. P. Wolfe (1985a) "Fluid motion inside a spinning nutating cylinder," *J. Fluid Mech.*, Vol. 150, pp. 121-138.

J. C. Strikwerda and Y. M. Nagel (1985) "A numerical method for computing the flow in rotating and coning fluid-filled cylinders," in *Proc. 1984 Scientific Conf. on Chemical Defense Research, Aberdeen Proving Ground, Maryland*, ed. M. Rausa, pp. 523-527, CRDC-SP-85006.

Th. Herbert and R. Li (1987) "Numerical study of the flow in a spinning and nutating cylinder," AIAA Paper No. 87-1445. Submitted to AIAA Journal.

Th. Herbert (1988) "Flight Simulation for Liquid-Filled Projectiles," in *Proc. 1987 U.S. Army CRDEC Scientific Conference on Chemical Defense Research, Report CRDEC-CR-88013*, ed. M. Rausa, pp. 377-385.

H. R. Vaughn, W. P. Wolfe, and W. L. Oberkampf (1985b) "Six degree of freedom simulation of fluid payload projectiles using numerically computed fluid moments," Sandia Report SAND 85-1166.

P. Hall, R. Sedney, and N. Gerber (1987) "Fluid motion in a spinning, coning cylinder via spatial eigenfunction expansion," Ballistic Research Laboratory, Technical Report BRL-TR-

2813, Aberdeen Proving Ground, MD.

R. Li and Th. Herbert (1988) "High-Reynolds-number flows in a spinning and nutating cylinder," in *Proc. 1988 Scientific Conf. on Chemical Defense Research, Aberdeen Proving Ground, Maryland, 1988.*, ed. M. Rausa.

BLANK

APPENDIX A

VISUALIZATION OF THE FLOW IN A SPINNING AND NUTATING CYLINDER

By

Thorwald Herbert
David Pierpont

Visualization of the Flow in a Spinning and Nutating Cylinder

Thorwald Herbert

David Pierpont

Department of Engineering Science and Mechanics
Virginia Polytechnic Institute and State University
Blacksburg, Virginia 24061

Abstract

In the framework of a feasibility study, we have designed a small model test fixture for visualization of the flow in a spinning and nutating cylinder. We describe the apparatus and the visualization technique, and report some results. As the Reynolds number increases, we observe an axially almost uniform flow that turns at the ends, the development of two elongated cells in the plane of the spin and nutation axis, the formation of additional laminar cells, and ultimately unsteady and turbulent flow with a superposed large-scale cellular motion.

1. Introduction

It is well-known that spin-stabilized shells carrying liquid payloads can suffer dynamical instability. For cylindrical cavities and low viscosity of the liquid, the instability due to basically inviscid inertial waves is rather well understood[1]. The instability of certain shells like the XM761, however, is distinguished in character by the rapid loss in spin rate. Experiments[2] and subsequent field tests[3] establish that this flight instability is most pronounced for liquid fills of very high viscosity.

Theoretical analysis of a simple model of the internal flow[4] has provided some insight into the physical mechanisms of this instability, and rough information on flow velocity and despin moment. For sufficiently low Reynolds numbers, more detailed results for the velocity field have been obtained using computational methods for steady flows[5,6]. The flow phenomena at higher Reynolds numbers, however, are outside the scope of these methods, and it is not even clear whether the steady approach is justified.

Previous experiments at CRDC and BRL were carried out under full-scale conditions. These studies concentrated largely on global properties such as the moments exerted by the internal fluid motion. The yet most successful study of the field properties is Miller's observation of the void in a partially filled cylinder[7]. This study shows an axisymmetric void at low Reynolds numbers, a characteristic wavy distortion of the void at medium Reynolds numbers and an irregular (probably unsteady) liquid-air interface at high Reynolds number. Computational studies[5] indicate a cellular structure of the flow at a Reynolds number $Re = 45$, where $Re = \omega a^2/\nu$ is formed with the spin rate ω, the cylinder radius a and the kinematic viscosity ν. However, there is yet no link between numerical results and void observations. An attempt to trace buoyant beads with a movie camera[8] was very limited in revealing details of the velocity field. The limitations are due to distortion of the tracer path in the multi-media optical path involving curved surfaces, and to inevitable minute density differences in combination with high accelerations. Miller[8] used photochromic dye excited by a high-power pulsed laser in order to generate and record velocity profiles. Lighting problems in recording the pictures by a high-speed movie camera forced a reduction of the time scale, i.e. operation of the test fixture at lower spin rate, nutation rate, and kinematic

viscosity. Qualitative pictures of the small azimuthal velocity have been obtained. The efforts to provide more detailed data have been discontinued, however, due to continuing lighting problems, and the adverse off-design conditions at further reduced time scales.

In earlier work[9], we have proposed a drastic reduction of length and time scales for experimental studies, exploiting the principles of dynamical similarity. Following these considerations, we have designed and built a low-cost test fixture for flow visualization. In our qualitative approach, the length scale is reduced to 1/5, the time scale to 1/10, thus reducing moments by more than five orders of magnitude and velocities to 1/50. In spite of improvising and compromising in the interest of saving time and money, we have observed a wealth of phenomena from laminar, dominantly unidirectional flow through various stages of cellular motions to turbulent motions with a superposed cellular structure.

In the following we describe the principles underlying the design, the test fixture, the visualization technique, and some of our observations.

2. Dimensional Analysis

Evaluation of the experimental attempts to visualize the fluid flow clearly reveals the extreme full-scale conditions as evil. However, conclusive experiments can be conducted by exploiting the principles of dynamical similarity and appropriate scaling laws[3,4]. Between the three reference quantities, radius a, spin rate ω, and density ρ for length, time, and mass, respectively, the density of different fluids offers little variability. However, length scale and time scale can be easily changed. For dynamical similarity, the following dimensionless quantities must be kept fixed:

$\lambda = c/a$	aspect ratio
θ	nutation angle
$\tau = \Omega/\omega$	frequency
$Re = \rho\omega a^2/\mu$	Reynolds number

The nutation angle must remain the same in a scaled setup. Radius a and half-length c of the cylinder must be scaled by the same factor in order to keep the aspect ratio fixed. A second factor can be applied to both spin rate ω and nutation rate Ω, in order to preserve the frequency. Keeping Re fixed requires changing the kinematic viscosity $\nu = \mu/\rho$ by the same factor as ωa^2. Since the desired tendency is toward smaller radii and spin rates, we require less viscous fluids than those used in the full-scale experiments. Such fluids are easy to find.

It is obvious that the main thrust of an experiment may require specific optimum conditions. Flow visualization requires low velocities, i.e. low values of ωa. Measurements of moments require optimum values of $\omega^2 a^6$. Minimizing the rate of change of temperature requires a minimum of $\omega^3 a^2$. A good setup for flow visualization, therefore, may produce moments in a hardly measurable range.

3. The Test Fixture

The goal of our efforts was to show that a low-cost device ($\simeq$ \$500) can be designed for flow visualization. Details had to be kept simple. Accuracy and convenience had to compromise. Various preliminary concepts have been condensed into the design of a small apparatus that was built and explored as a senior student project[10]. The result of these efforts is shown in figure 1. A one-inch inner diameter cylinder of aspect ratio $\lambda = 4.3$ is used. The cylinder is cut from a pyrex glass tube with the inner diameter accurate within 1/5000 inch, but with varying wall thickness that affects the optical quality. The cylinder is filled with mixtures of water and glycerin. The mixing ratio is used to vary viscosity. On top, the cylinder is closed with a screwed-in plastic plug. A center hole allows access to the interior, especially for removing air bubbles. The hole can be closed using a toothpick.

The cylinder is glued to a drive plug and axis machined from a single piece of aluminum. The one-sided support allows easy (optical) access to the cylinder and permits using cylinders of different length. One-sided support is affordable due to the moments being approximately five orders of magnitude smaller than in the full-scale experiments. The axis is twice supported by ball bearings. The cylinder and shaft are driven via timing belts over exchangeable sets of pulleys by a $\leq$24V d.c. motor with sufficient torque in the range of 500 - 5000 rpm. Motor and cylinder support are mounted to an aluminum frame that can

be inclined to the vertical axis by approximately 5, 10, 15 and 20° using different support holes and struts.

The horizontal support plate is machined to leave the center position free for access and is screwed to a commercial record player (Garrard model 775). The plate can be offset in order to align the liquid's center of mass with the nutation axis. The record player provides nutation rates of 33, 45, and 78 rpm. The hollow axis is utilized to provide power to the spin motor. A nail with a smooth top and a brush fixed to the turntable proved sufficient for transmitting a single voltage to the motor. The remaining components of the experiment are: a Heathkit regulated power supply for the spin motor, a strobelight for controlled pulsed lighting, and suitable flow tracers. The strobelight (General Radio Strobotac) with adjustable frequency is used for lighting as well as for measuring the spin rate of the cylinder.

4. Visualization

As flow tracers we use Affair 100 Silver Pearl, kindly donated by EM Chemicals, Hawthorne, NY. The material consists of very fine and shiny plastic platelets commercially used for cosmetic purposes. Although their specific weight is different from that of the fluid, the low accelerations in the scale model permit practically buoyant behavior of the platelets over considerable time.

At the slow time scale of the experiment, the fluid motion can be visually inspected while running the apparatus. At high viscosities, the apparatus can also be suddenly stopped, with the flow tracers "frozen" in the resting fluid. The platelets align with surfaces of constant shear. Therefore, by manually rotating the cylinder forth and back, the three-dimensional structure of the field can be inspected. This crude observation is very helpful in developing the visualization technique. A detailed account of the technique (appropriate particle density, pitfalls such as the history of particle distribution and alignment) has been given elsewhere[10].

Visualization of the frozen pattern can be essentially improved by using a light sheet passing through the spin axis. Sheet lighting enhances the clarity of the flow pattern by showing only the reflecting particles in a cut through the fluid. It reduces the undesirable reflections from the cylindrical surfaces and also enables photographic recording of the flow structure while the apparatus is in operation. A continuous light sheet is produced by a Spectra Physics model 120 (15 mW) helium-neon laser and a cylinder lens. In order to avoid the need for accurately firing the camera (35 mm Pentax with 50 mm lens) at a certain time, a cylindrical card board screen with a vertical slot and a 90° offset opening is fixed to the circumference of the turntable. The shutter is manually opened and closed after the laser sheet of light flashed 3 to 5 times through the slot.

5. Results

Some photographs taken with the apparatus in motion are shown in Figures 2-7. The figures show the flow pattern in the plane spanned by spin axis and nutation axis for $\theta = 21.3°$, $\Omega = 78$ rpm and different Reynolds numbers. Figure 2 shows that at Reynolds numbers as low as $Re = 20$ a cellular pattern develops with a pronounced symmetry about the axis as well as the midplane of the cylinder. At the present time it is unclear whether this pattern reflects the instantaneous velocity field. Symmetry arguments support viewing this pattern as originating from a nonlinear streaming term. As Re increases to $Re = 40$ (Figure 3), the pattern and its symmetry become more pronounced. At $Re = 50$ (Figure 4), additional cells develop near the cylinder's midplane. Simultaneously, the symmetry with respect to the cylinder axis is broken. A characteristic wavy distortion of the pattern near the axis develops that is more clearly shown in Figure 5 at $Re = 105$. While the cells disappeared, virtually axisymmetric bubbles occur at the end plates. At $Re = 140$ (Figure 6) these bubbles still persist. The bright, wavy line near the axis has broken into segments that are very much aligned like the void in Miller's observations. This pattern occurs only in the plane of spin axis and nutation axis and is therefore considered to represent the instantaneous velocity field. From the wealth of increasingly complex phenomena, Figure 7 finally shows a visualization at high $Re = 8000$. The random distribution of the particles in the interior most likely indicates turbulent flow. Nevertheless, the faint line near the axis resembles the characteristic centerline distortion of Figure 6, indicating a superposed large scale structure. The presence of such a large scale motion is also supported by the regular bands of particles deposited at the cylinder wall.

Specification of accurate Reynolds numbers suffers from some uncertainty in monitoring and measuring the wide range of viscosities for the hygroscopic water-glycerin mixtures exposed to uncontrolled thermal conditions. To within this uncertainty, however, the figures clearly reveal the cellular structure of the flow and the changes of the structure as the Reynolds number increases. Perhaps the most striking result of this visual study of the flow structure is the manifold of pattern at higher Reynolds numbers. A systematic analysis of these patterns has not been conducted. Although we found numerous opportunities for improvements, the feasibility of flow visualization with relatively simple means by proper scaling has been clearly demonstrated.

ACKNOWLEDGMENT

This experimental study is a digression from theoretical work supported by the Army Research Office under Contract DAAG29-82-K-0129 and by the Army AMCCOM under Contracts DAAK11-83-K-0011 and DAAA15-85-K-0012.

REFERENCES

1 Sedney, R. 1985 "A Survey of the Fluid Dynamic Aspects of Liquid-Filled Projectiles," AIAA Paper No. AIAA-85-1822-CP

2 Miller, M. C. 1982 "Flight Instabilities of Spinning Projectiles Having Nonrigid Payloads," *Journal of Guidance, Control, and Dynamics*, Vol. 5, pp. 151-157.

3 D'Amico, W. P. & Miller, M. C. 1979 "Flight Instability Produced by a Rapidly Spinning, Highly Viscous Liquid," *Journal of Spacecraft and Rockets*, Vol. 16, pp. 62-64.

4 Herbert, Th. 1985 "Viscous Fluid Motion in a Spinning and Nutating Cylinder", to appear in Journal of Fluid Mechanics.

5 Vaughn, H. R., Oberkampf, W. L. & Wolfe, W. P. 1985 "Fluid Motion Inside a Spinning Nutating Cylinder," Journal of Fluid Mechanics, Vol. 150, pp. 121-138.

6 Nagel, Y. & Strikwerda, J. 1985 "A Numerical Study of Flow in Spinning and Coning Cylinders," in these Proceedings.

7 Miller, M. C. 1981 "Void Characteristics of a Liquid Filled Cylinder Undergoing Spinning and Coning Motion," J. of Spacecraft and Rockets, Vol. 18, pp. 286-288.

8 Miller, M. C. 1984 "Visualization Studies of Viscous Liquid Flow in a Spinning and Coning Cylinder," Proc. 1984 Scientific Conference on Chemical Defense Research, (Ed. M. Rausa), Report CRDC-SP-85006, pp. 541-546.

9 Herbert, Th. 1982 "Fluid Motion in a Rotating and Nutating Cylinder - Part I," Report prepared under the Scientific Services Program. Published as Report CRDC-CR-84087, 1984

10 Pierpont, D. 1985 "Design of an Experiment for Visualization of the Flow in a Spinning and Nutating Cylinder," Senior Project Report, VPI & SU.

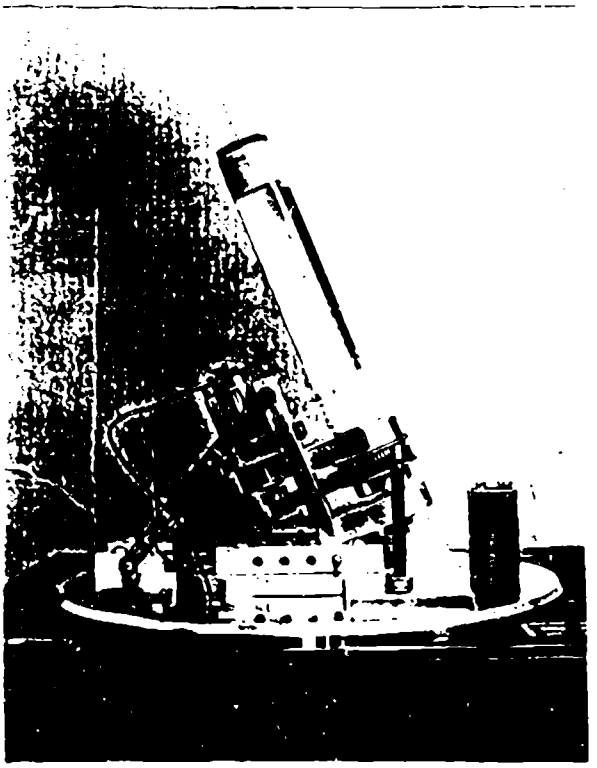

Figure 1

The miniature test fixture. The inner radius of the cylinder is $a = 1.27$ cm, the aspect ratio 4.3.

Figure 2

$\theta = 21.3°$
$\Omega = 78$ rpm
$\nu = 240$ cSt
$\omega = 300$ rpm
$Re = 20$

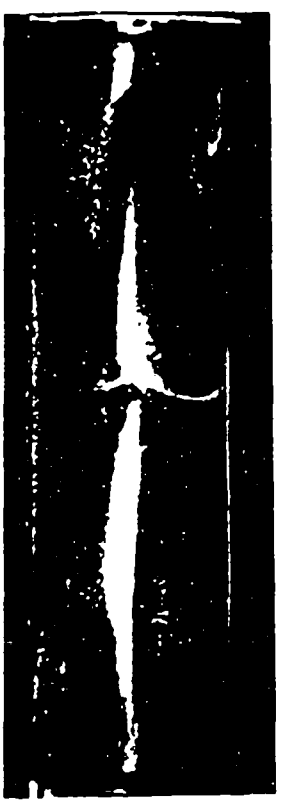

Figure 3

$\theta = 21.3°$
$\Omega = 78$ rpm
$\nu = 240$ cSt
$\omega = 600$ rpm
$Re = 40$

Figure 4

$\theta = 21.3°$
$\Omega = 78$ rpm
$\nu = 240$ cSt
$\omega = 750$ rpm
$Re = 50$

Figure 5

$\theta = 21.3°$
$\Omega = 78$ rpm
$\nu = 70$ cSt
$\omega = 450$ rpm
$Re = 105$

Figure 6

$\theta = 21.3°$
$\Omega = 78$ rpm
$\nu = 70$ cSt
$\omega = 600$ rpm
$Re = 140$

Figure 7

$\theta = 21.3°$
$\Omega = 78$ rpm
$\nu = 0.95$ cSt
$\omega = 450$ rpm
$Re = 8000$

BLANK

APPENDIX B

ANALYTICAL AND COMPUTATIONAL STUDIES OF THE FLUID MOTION IN LIQUID-FILLED SHELLS

By

Thorwald Herbert

Analytical and Computational Studies of the Fluid Motion in Liquid-Filled Shells

Thorwald Herbert

Department of Engineering Science and Mechanics
Virginia Polytechnic Institute and State University
Blacksburg, Virginia 24061

ABSTRACT

Spin-stabilized projectiles with liquid payloads can experience a severe flight instability characterized by a rapid yaw-angle growth and a simultaneous loss in spin rate. Laboratory experiments and field tests have shown that this instability originates from the internal fluid motion in the range of small Reynolds numbers. In earlier work, we developed a simple model of this flow based on linearized equations for the deviation from solid-body rotation in an infinite cylinder. Here, we perform a perturbation analysis in order to estimate the effect of nonlinear terms. Beyond a small correction of the axial velocity component, we obtain radial and azimuthal components of the velocity field in agreement with computational results for the core region of a finite-length cylinder. The analytical results are exploited in the design of a spectral Navier-Stokes solver for the steady motion in a finite cylinder. A first raw version of this spectral code provides flow field and pressure distribution in a small fraction of the computer time required by existing codes. We report some results and discuss possible refinements of this code.

1. Introduction

It is well-known that spin-stabilized shells carrying liquid payloads can suffer a dynamical instability which results in an increased coning (or yaw) angle and a simultaneous loss in spin rate. Laboratory experiments, computational results, and field tests indicate that these phenomena arise from the coning-induced fluid motion in a limited range of small Reynolds numbers. Although in special cases this instability has been removed by trial and error, future design of reliable projectiles would profit from the opportunity to estimate the liquid moments, and to include these moments in flight simulators. The empirical data base [1, 2] is sparse, however, and computational methods in use [3, 4, 5] are rather demanding.

Our theoretical analysis of this problem serves on one hand to gain insight into the anatomy of the flow phenomena and to support the ongoing experiments. On the other hand, it promotes our efforts to develop a more efficient code for the numerical simulation of the flow in a finite container. While the analytical work aims at the velocity field in the core region of a sufficiently long cylinder and on the viscous components of the moments, in particular the viscous despin (negative roll) moment, the computational work also captures the flow near the end walls and the pressure contributions to yaw and pitch moments.

Our previous work [6] shows that the deviation from solid body rotation is governed by a small parameter $\epsilon = \Omega \sin\theta/\omega$ involving the nutation rate Ω, the nutation angle θ, and the spin rate ω. The solution of the linearized equations consists of

only an axial component of order $O(\epsilon)$. This axial flow is the dominating feature of the fluid motion and produces a negative roll moment of order $O(\epsilon^2)$ owing to Coriolis forces. Although these results are in reasonable agreement with experimental and computational data, one may anticipate modifications of velocity field and roll moment if nonlinear terms are taken into account. Estimates of these nonlinear effects are desired in order to support previous results and to verify our conclusion that the three-dimensional flow field in a finite-length cylinder is essentially given by the solution of linearized momentum equations. In the following, we perform a straightforward perturbation expansion for the nonlinear problem. We develop and solve the equations for the flow in an infinitely long cylinder up to order $O(\epsilon^3)$. A closed-form solution is given for the radial and azimuthal velocity components at second order. The third-order equations are solved numerically.

The perturbation solution also provides estimates for the number of expansion functions required for accurate spectral representation of the radial (r) and azimuthal (ϕ) structure of the solution. A spectral code appears as an attractive alternative to the existing Navier-Stokes solvers. The finite-difference code developed at Sandia Laboratories [3, 4] exploits Chorin's method of artificial compressibility. The steady solution at $11 \times 24 \times 21$ grid points in r, ϕ, z-direction is obtained by integrating over typically 10^4 time steps, a task that requires 68 minutes of CPU time on an IBM 3090. The result consists of 22,000 plus values for the velocity components v_r, v_ϕ, v_z and the pressure p that can be utilized for a calculation of the moments. Strikwerda & Nagel [5] describe a code using finite differences in radial and axial direction and pseudospectral differencing in the azimuthal direction. Nonuniform grids are introduced for increased resolution near the walls. The difference equations are solved by an iterative method based on successive over-relaxation. The computer time required is comparable to that of the Sandia code (Nusca, BRL, personal communication). Although the relative merits of the two codes, especially with respect to the captured range of Reynolds numbers are yet in the dark, it seems well possible to beat both of these codes in two respects: computer time and adaptability to the unsteady problem.

For a feasibility study, we have pursued a simple concept that is open to numerous refinements. We use Chebyshev-Fourier-Chebyshev expansions in r, ϕ, z, respectively, and convert the linearized equations into a linear algebraic system for the expansion coefficients. The solution of this system (or any other solution at neighboring parameters) is used as initial approximation for iterative improvement by the modified Newton method. The experience with this code is encouraging with respect to accuracy, efficiency, and robustness.

2. Governing Equations

We consider the motion of a fluid of density ρ and viscosity μ in a cylinder of radius a and length $2c$ that rotates with the spin rate ω about its axis of symmetry, the z-axis. We consider the motion with respect to the nutating coordinate system x, y, z. This system is obtained from the inertial system X, Y, Z by a rotation with the nutation angle θ about the axis $Y = y$. Therefore, x is in the Z, z-plane, and this plane rotates about the Z-axis with the nutation rate Ω. The two axes of rotation intersect in the center of mass of the cylinder. We consider $\omega > 0$, Ω, and $0 \leq \theta \leq \pi/2$ as constant.

The fluid motion is governed by the Navier-Stokes equations written in the nutating coordinate system:

$$\rho\left\{\frac{D\mathbf{V}_n}{Dt} + 2\Omega \times \mathbf{V}_n + \mathbf{\Omega} \times (\mathbf{\Omega} \times \mathbf{r})\right\} = -\nabla P_n + \mu\nabla^2\mathbf{V}_n , \tag{1a}$$

$$\nabla \cdot \mathbf{V}_n = 0 . \tag{1b}$$

$\mathbf{V}_n$ is the velocity measured in the nutating frame, P_n the pressure, and $\mathbf{r}$ the position vector. Equations (1) are subject to the no-slip and no-penetration conditions at the cylinder walls.

It is convenient [6] to split the velocity and pressure fields according to

$$\mathbf{V}_n = \mathbf{V}_s + \mathbf{V}_d , \quad P_n = P_s + P_d , \tag{2}$$

where $\mathbf{V}_s$, P_s describe the state of pure solid-body rotation, whereas $\mathbf{V}_d$, P_d represent the deviation from solid-body rotation. The deviation $\mathbf{V}_d$ and the reduced pressure P_d are ultimately responsible for the observed flight instability.

The equations for $\mathbf{V}_d$, P_d are written in terms of nondimensional quantities $\mathbf{v}_d$, p_d using a, ω, and ρ for scaling length, time, and mass, respectively. The solution then depends on four nondimensional parameters: aspect ratio $\lambda = c/a$, nutation angle θ, frequency $\tau = \Omega/\omega$, and Reynolds number $R = \rho\omega a^2/\mu$. The aspect ratio enters the solution only through the boundary conditions at the end walls of the cylinder. The boundary conditions on $\mathbf{v}_d$ are homogeneous.

In cylindrical coordinates r, ϕ, z, the equations for the nondimensional deviation velocity $\mathbf{v}_d = (v_r, v_\phi, v_z)$ and pressure p_d take the form

$$\frac{1}{r}\frac{\partial}{\partial r}(rv_r) + \frac{1}{r}\frac{\partial v_\phi}{\partial \phi} + \frac{\partial v_z}{\partial z} = 0 , \tag{3a}$$

$$D'v_r - \frac{v_\phi^2}{r} - 2(1+\tau_z)v_\phi + 2\tau_\phi v_z = -\frac{\partial p_d}{\partial r} + \frac{1}{R}\left[D''v_r - \frac{v_r}{r^2} - \frac{2}{r^2}\frac{\partial v_\phi}{\partial \phi}\right] , \tag{3b}$$

$$D'v_\phi + \frac{v_r v_\phi}{r} + 2(1+\tau_z)v_r - 2\tau_r v_z = -\frac{1}{r}\frac{\partial p_d}{\partial \phi} + \frac{1}{R}\left[D''v_\phi - \frac{v_\phi}{r^2} + \frac{2}{r^2}\frac{\partial v_r}{\partial \phi}\right] , \tag{3c}$$

$$D'v_z + 2\tau_r v_\phi - 2\tau_\phi v_r = -\frac{\partial p_d}{\partial z} - 2r\tau_r + \frac{1}{R}D''v_z , \tag{3d}$$

where

$$D' = \frac{\partial}{\partial t} + \frac{\partial}{\partial \phi} + v_r\frac{\partial}{\partial r} + \frac{v_\phi}{r}\frac{\partial}{\partial \phi} + v_z\frac{\partial}{\partial z} ,$$

$$D'' = \frac{\partial^2}{\partial r^2} + \frac{1}{r}\frac{\partial}{\partial r} + \frac{1}{r^2}\frac{\partial^2}{\partial \phi^2} + \frac{\partial^2}{\partial z^2} ,$$

and

$$\tau_r = -\epsilon\cos\phi\ ,\quad \tau_\phi = \epsilon\sin\phi\ ,\quad \tau_z = \tau\cos\theta\ ,\quad \epsilon = \tau\sin\theta\ . \tag{4}$$

The primary effect of nutation is contained in the ϕ-periodic force term $-2r\tau_r = 2\epsilon r\cos\phi$ in the z-momentum equation (3d). For $\epsilon = 0$, equations (3) support the trivial solution $\mathbf{v}_d \equiv 0$, $p_d \equiv 0$. The system also supports the following symmetries:

$$v_r(r, \phi+\pi, -z) = v_r(r, \phi, z) \tag{5a}$$

$$v_\phi(r, \phi+\pi, -z) = v_\phi(r, \phi, z) \tag{5b}$$

$$v_z(r, \phi+\pi, -z) = -v_z(r, \phi, z) \tag{5c}$$

$$p_d(r, \phi+\pi, -z) = p_d(r, \phi, z) \tag{5d}$$

3. Perturbation analysis for an infinite cylinder

The steady flow in a relatively long cylinder (aspect ratio $\lambda > 4$) at low Reynolds number is expected to have a rather simple structure and to provide a roll moment proportional to Re. In fact, the flow is expected to exhibit little axial variation over much of the cylinder length. Previous work [6] has therefore relaxed the boundary conditions at the end walls. In this way, one seeks the steady flow in a finite segment of an infinitely long cylinder.

In the physical situations of interest, $\epsilon = (\Omega/\omega)\sin\theta$ is a small parameter, $\epsilon \leq 0.06$. Consequently, it seems reasonable to pursue a straightforward perturbation expansion in ϵ. This provides $\mathbf{v}_d$ in the form

$$\mathbf{v}_d = \sum_{n=1}^{\infty} \epsilon^n \mathbf{v}^{(n)}(r, \phi) \tag{6}$$

and similar expressions for p_d.

The development of general expressions for the expansion coefficients $\mathbf{v}^{(n)}$ from equations (3) indicates an alternating pattern: Odd-order terms contain odd multiples of ϕ and contribute only to the axial velocity v_z, while even-order terms contain even multiples of the azimuthal coordinate ϕ and contribute only to the radial velocity v_r and azimuthal velocity v_ϕ. Therefore,

$$\mathbf{v}^{(n)} = \begin{cases} (0, 0, v_z^{(n)}), & n \text{ odd}, \\ (v_r^{(n)}, v_\phi^{(n)}, 0), & n \text{ even}, \end{cases} \tag{7}$$

and the components of $\mathbf{v}^{(n)}$ take the form

$$v_r^{(n)} = \sum_{m=1}^{n/2} \left(u_{nm}(r)\, e^{i2m\phi} + \tilde{u}_{nm}(r)\, e^{-i2m\phi}\right), \tag{8a}$$

$$v_\phi^{(n)} = v_{no}(r) + \sum_{m=1}^{n/2} \left(v_{nm}(r)\, e^{i2m\phi} + \tilde{v}_{nm}(r)\, e^{-i2m\phi}\right), \tag{8b}$$

$$v_z^{(n)} = \sum_{m=1}^{(n+1)/2} \left(w_{nm}(r)\, e^{i(2m-1)\phi} + \tilde{w}_{nm}(r)\, e^{-i(2m-1)\phi}\right), \tag{8c}$$

where the tilde denotes the complex conjugate. The aperiodic term in $v_r^{(n)}$ is suppressed

by the continuity equation. The r-dependent coefficient functions in eqs. (8) are required to satisfy homogeneous boundary conditions at $r = 1$ and to be finite at the axis $r = 0$ for a physically meaningful solution.

At the lowest order $O(\epsilon)$, the z-independent force term in eq. (3d) can be balanced only by an axial component of the deviation velocity. This component is the dominating feature of the flow in a long cylinder. The axial velocity at order $0(\epsilon)$ can be found in analytical form,

$$w_{11}(r) = i\left(\frac{I_1(\alpha r)}{I_1(\alpha)} - r\right), \tag{10}$$

where I_1 is the modified Bessel function, and $\alpha = (1 + i)(R/2)^{1/2}$. This solution is valid for arbitrary Reynolds number but may be unstable as R exceeds some critical value. The properties of the resulting flow field are discussed by Herbert [6].

At higher order, it is convenient to eliminate the pressure for the periodic components by using the vorticity form of eqs. (3). At order $O(\epsilon^2)$, comparison of the equation for v_{20} with the imaginary part of the equation for w_{11} immediately shows that the aperiodic component of the azimuthal velocity is

$$v_{20}(r) = -2\,\mathrm{Im}(w_{11}(r)). \tag{11}$$

This relation can be exploited to show that the despin moment of order $O(\epsilon^2)$ due to shear forces on the cylinder wall is identical with our former result.

The ϕ-periodic components are governed by a coupled set of inhomogeneous differential equations with variable coefficients. Essential simplification at the expense of increasing the order of differentiation results from eliminating v_{21} by use of the continuity equation. With some effort, the radial velocity component of $O(\epsilon^2)$ can be found in closed form,

$$u_{21}(s) = \frac{1}{s}[c_1 J_2(s) + c_2 Y_2(s)] + c_3 s + \frac{c_4}{s^3} + \frac{2i\sqrt{2}}{s}\frac{J_2(s/\sqrt{2})}{J_1(\beta/\sqrt{2})} \tag{12}$$

where $s = \beta r$, $\beta = (i - 1)R^{1/2}$, and J_1, J_2, and Y_2 are Bessel functions. The coefficients c_1, c_2, c_3, and c_4 can be determined numerically.

The velocity components at order $O(\epsilon^3)$ are of interest primarily since w_{31} provides the first nonlinear correction to the despin moment. In view of the effort involved in deriving the closed form solution for u_{21} and the ultimate need to determine the coefficients in eq. (12) numerically, we decided to solve the differential equations for the third-order components by means of a spectral collocation method.

4. Results of the Perturbation Analysis

Detailed equations, results, and graphs of the various functions at relevant Reynolds numbers will be published elsewhere [7]. Here we give only a summary of the main results. The motion is governed by the axial component w_{11} at order $O(\epsilon)$. Of the higher order terms, only the aperiodic term v_{20} is substantial. In the cylinders center section, these terms are in good agreement with results obtained from the Sandia code, and in excellent agreement with our own computations. All the other terms are not only of order $O(1)$ but in fact less than unity, assuring rapid convergence of the perturbation

series. The contribution of w_{31} to the despin moment is negligible. The ϕ-periodic terms oscillate about zero as r varies between $0 \leq r \leq 1$. Accurate representation of single high-order terms by radial Chebyshev series may require numerous expansion functions. For the total velocity field, however, the error in representing these terms is of little importance. At Reynolds numbers in the range of maximum despin moment, reasonably accurate approximations can be obtained with as few as five polynomials in radial direction. In the azimuthal direction, the solution is governed by terms periodic in ϕ, and by the aperiodic term v_{20}. Fourier series with three or five modes, therefore, provide approximations of sufficient accuracy for practical purpose.

5. Spectral Approximations for a Finite-Length Cylinder

The results of the perturbation analysis suggest that a good approximation to the flow in a finite cylinder can be obtained by solving the linearized version of equations (3). Linearization can be performed in different ways. The first is a linearization in ϵ, as in the perturbation analysis. The resulting equations support strong symmetries. Beyond equations (5), the solution satisfies

$$\mathbf{v}_d(r, \phi+\pi, z) = -\mathbf{v}_d(r, \phi, z), \tag{13a}$$

$$p_d(r, \phi+\pi, z) = -p_d(r, \phi, z). \tag{13b}$$

These relations provide a useful check on the results of the spectral code. A second linear system can be obtained by linearization in the components of $\mathbf{v}_d$. This linearization retains coupling terms such as $2\tau_\phi v_z$ in eq. (3b) which destroy the symmetries (13). The second system can be considered a special case of a third linearization about some known solution $\mathbf{v}_d^{(0)}$, $p_d^{(0)}$. The third procedure is very efficient if the solution is sought for a densely spaced sequence of parameter combinations as in flight simulations. The second system is equivalent with the third one for $\mathbf{v}_d^{(0)} = p_d^{(0)} = 0$.

The algebraic form of the equations is obtained by use of spectral collocation. The velocity components are expressed in the form

$$v_r = \sum_{k=1}^{K} \sum_{l=1}^{L} \sum_{m=1}^{M} u_{klm} R_{kl}^{u}(r) F_l(\phi) Z_m(z/\lambda) \tag{14}$$

with similar expressions for v_ϕ, v_z, and p_d. The azimuthal functions are $F_l = \cos[(l-1)\phi/2]$ for odd l, $F_l = \sin[l\phi/2]$ for even l, where $l = 1, 2, \cdots L$, and L is odd. The azimuthal collocation points are equidistant, $\phi_l = 2\pi(l-1)/L$. If no use of the symmetries (5) is made, the axial expansion functions are the Chebyshev polynomials $Z_m = T_{m-1}(z/\lambda)$, $m = 1, 2, \cdots M$. The collocation points are $z_m/\lambda = \cos[(m-1)\pi/(M-1)]$. In radial direction, even or odd Chebyshev polynomials are used, depending on the quantity under consideration and the periodicity in ϕ. The proper choice is dictated by the requirement of a unique value of all quantities on the axis $r = 0$. For example, the axial velocity component must assume a unique value independent of ϕ as $r \to 0$. Therefore, even polynomials are to be used if $l = 1$ while odd polynomials are to be used if $l > 1$. The radial collocation points are $r_k = \cos[(k-1)\pi/(2K-1)]$, $k = 1, 2, \cdots K$. Consequently, $0 < r_k \leq 1$, and no difficulty can arise from points on the axis. The collocation points in radial and axial direction are concentrated near the boundary such that high resolution in this region is obtained without additional coordinate transformations.

Our implementation of the spectral method uses precalculated and stored matrices containing the values of the expansion functions and their derivatives at the collocation points. It is a straightforward matter to convert the linear system of partial differential equations derived from eqs. (3) into an algebraic system of dimension $N = 4\,K\,L\,M$ for the coefficients u_{klm}, v_{klm}, w_{klm}, and p_{klm} for v_r, v_ϕ, v_z, and p_d, respectively. It is not straightforward, however, to implement the homogeneous boundary conditions for the velocities at the cylinder wall and the condition on the pressure that is only determined to within an additive constant. In principle, the boundary conditions are implemented by replacing three of the four differential equations in the boundary points. The question then is which equation should be retained and where the condition on the pressure, e.g. $p_d = 0$, should be applied. Trial-and-error leads to numerous cases with ill-determined matrices or zero determinant. In other cases, a correct solution for the velocity field is obtained, but the pressure contains a non-physical spurious term. With the velocity field given, we attempted to calculate the pressure by solving a Poisson equation with von Neumann boundary conditions, but we encountered the same difficulties. Problems with calculating the pressure in closed domains with spectral methods are well-known, e.g. [8]. However, the reports of negative results are rather unspecific, and neither the origin nor methods for removal of this spurious term seem to be known.

We have therefore performed a detailed analysis of the flow in a square driven by an internal force field. This simpler two-dimensional problem exhibits all characteristics - including the spurious pressure term - of the original problem. Detailed results of this study will be reported elsewhere [9]. The study reveals that the spurious term is associated with the corners of the domain. The term vanishes in all collocation points except the corners, where it may assume arbitrary values. The term can be suppressed by retaining in the corners one of the momentum equations that contain the derivative of the pressure in the direction of the boundary. In the cylinder problem, the z-momentum must be retained in order to suppress even as well as odd spurious terms. The condition on the pressure can be applied anywhere except in the corner points.

We solve the linear algebraic system for the expansion coefficients with a special subroutine based on Gauss elimination with partial pivoting. The subroutine stores all data required to solve the same system with a new right-hand side without repeating the costly ($O(N^3)$ operations) reduction of the matrix to upper triangular form. Once the solution is obtained, a new right-hand side is formed taking the nonlinear terms into account and the system is solved again. This procedure is iteratively repeated until sufficient accuracy is obtained. The procedure is equivalent to the modified Newton iteration (without updating the Jacobian in every step) and converges rapidly since the nonlinear corrections to the velocity are small while the pressure appears linear in equations (3).

6. Results on the Spectral Code

In the following, we present some preliminary results of a test run for $R = 14.95$, $\theta = 20^\circ$, $\tau = 0.1667$, and $\lambda = 4.368$ which results in $\epsilon = 0.057$. The results are for $K = 4$, $L = M = 5$, and consequently $N = 400$. Detailed convergence tests will be performed with later versions of the spectral code. Figure 1 shows the axial and radial velocity in the x, z-plane. Only the upper half, $z \geq 0$, of the cylinder is shown; the lower half is governed by the symmetries (5). The velocity distribution at $z = 0$ agrees

well with the results of the perturbation analysis and computations with the Sandia code. Near the walls, the solution seems to be more realistic and more accurate than the Sandia results. The figure also verifies the existence of a predominantly axial flow over most of the cylinder length, except within a region of the order of the radius near the end wall. Linear and nonlinear velocity distributions are hardly distinguishable. Clearly visible is the turning of the flow near the end wall. The radial and azimuthal velocities at $z = 0.9\lambda$ are shown in figure 2. The right tick mark indicates the x-direction, $\phi = 0$. At Re = 14.95, the maximum of the axial velocity occurs at $\phi \approx 45°$.

Pressure distributions in the x, z-plane are given in figures 3 and 4 with the heavy lines indicating positive values. The pressure in figure 3 is obtained simultaneously with $\mathbf{v}_d$ from equations linearized in ϵ, and clearly shows the symmetry (13b). Figure 4 gives the result from the nonlinear equations. It is interesting to note that a very similar pressure field can be obtained by solving the Poisson equation for the pressure with the linear velocity field. The inhomogeneous term in the Poisson equation is inherently nonlinear in the velocities. Figure 5 gives the pressure distribution across the cylinder near the end wall at $z = 0.9\lambda$. Remarkable is the formation of a high-pressure region in the corner near $\phi = 0$, which produces a large moment about the y-axis. Looking at a series of plots like figures 4 and 5, one may wonder whether the details of the pressure variation near the cylinder wall can be resolved with a finite difference approximation with a step size of $\Delta r = 0.1$.

The azimuthal mean velocity at $z = 0$ is shown in figure 6. The shear exerted by this component on the cylinder wall opposes the spinning motion and is the ultimate cause of the despin moment. The axial and radial mean velocity field is given in figure 7. This streaming term exhibits a toroidal motion stretched over each half of the cylinder. It is this mean velocity that causes the symmetric pattern in flow visualizations [10]. Figure 8 shows the observed pattern of the flow at $R \approx 30$ which is typical for the range of low Reynolds numbers.

7. Discussion

The experience with the first version of the spectral code shows that high performance can be achieved. The reported run with $N = 400$ requires 1.3 minutes CPU time on an IBM 3090, 48 minutes on an Apollo DN300 desktop computer. The solution is obtained in semi-analytical form with only $N = 400$ numerical coefficients. This low data volume is especially attractive for communication with remote supercomputers. The code is very well suited for vectorization, since practically all CPU time is spent on constructing and solving an algebraic system. However, the code demands larger memory than other codes [3, 5]. Since 64-bit arithmetic is highly recommended for spectral methods in general, and the algebraic system requires $N(N+1)$ words of storage, the above test requires 1.3 Mbyte of memory. Nowadays, the memory requirement appears acceptable even if higher resolution is desired.

Finally, there are various ways to improve the performance and lessen the demands. The first step is to exploit symmetry which reduces N by a factor of 1/2, storage by 1/4, and time by $\approx 1/8$. Second, the solution process can be split into two levels, the first of which calculates only the velocity components while the pressure is obtained a posteriori by solving the Poisson equation. After these changes, the above test run will require less than 1 minute on an MC68020/68881 based desktop computer

Alternatively, runs with higher resolution can be executed within a short time on supercomputers. One may also consider reducing the storage requirement by line iteration. However, the ability to obtain a reasonably acurate solution by direct solution of the (large) algebraic system bears valuable potential to answer the question whether the steady solution is stable, and allows for analysis of unsteady motions. The design of a reliable code for the unsteady problem can take profit from the kowledge of the eigenvalue spectrum for small unsteady disturbances of the steady flow.

ACKNOWLEDGMENT

The assistance of Ri-Hua Li and Steven D. Greco in the analytical and numerical work is greatly appreciated. Earlier work has been supported by the Army Research Office under Contract DAAG29-82-K-0129 and by the Army AMCCOM under Contract DAAK11-83-K-0011. The current efforts are supported by the Army AMCCOM under Contract DAAA15-85-K-0012.

REFERENCES

1. M. C. Miller 1982 "Flight instabilities of spinning projectiles having nonrigid payloads," *J. Guidance, Control, and Dynamics*, vol. 5, pp. 151-157.
2. R. Sedney 1985 "A Survey of the fluid dynamic aspects of liquid-filled projectiles," AIAA Paper No. 85-1822-CP.
3. H. R. Vaughn, W. L. Oberkampf, and W. P. Wolfe 1983 "Numerical solution for a spinning nutating fluid-filled cylinder," Sandia Report SAND 83-1789.
4. H. R. Vaughn, W. L. Oberkampf, and W. P. Wolfe 1985 "Fluid motion inside a spinning nutating cylinder," *J. Fluid Mech.*, vol. 150, pp. 121-138.
5. J. C. Strikwerda and Y. M. Nagel 1985 "A numerical method for computing the flow in rotating and coning fluid-filled cylinders," in *Proc. 1984 Scientific Conf. on Chemical Defense Research, Aberdeen Proving Ground, Maryland*, ed. M. Rausa, pp. 523-527, CRDC-SP-85006.
6. Th. Herbert 1986 "Viscous fluid motion in a spinning and nutating cylinder," *J. Fluid Mech.*, vol. 167, pp. 181-198.
7. Th. Herbert and S. D. Greco 1986 "Higher approximations for the viscous flow in a spinning and nutating cylinder," *J. Fluid Mech.* To be submitted.
8. R. Peyret and T. D. Taylor 1983 *Computational Methods for Fluid Flow*, p. 236, Springer-Verlag.
9. Th. Herbert 1986 "On the spurious pressure in spectral computations of flows in closed domains," *J. Comp. Phys.* To be submitted.
10. Th. Herbert and D. Pierpont 1986 "Visualization of the flow in a spinning and nutating cylinder," in *Proc. 1985 Scientific Conf. on Chemical Defense Research*, ed. M. Rausa, pp. 989-994, Aberdeen Proving Ground, Maryland.

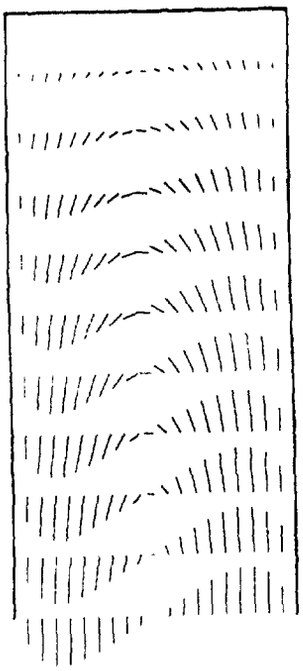

Figure 1. Vector plot of the velocity field in the x, z-plane for $z \geq 0$.

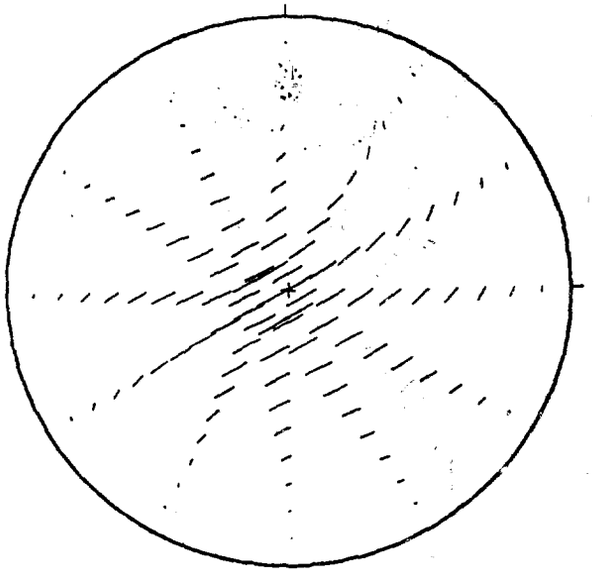

Figure 2. Vector plot of the velocity field across the cylinder at $z/\lambda = 0.9$.

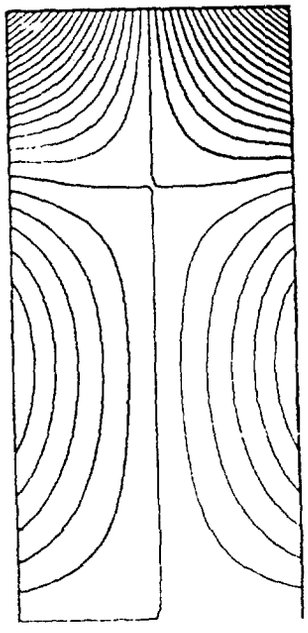

Figure 3. Contour plot of the linear pressure field in the x, z-plane for $z \geq 0$.

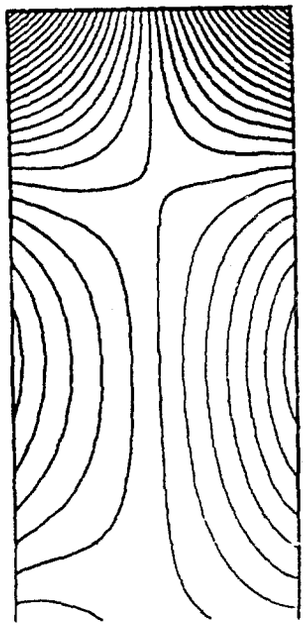

Figure 4. Contour plot of the nonlinear pressure field in the x, z-plane for $z \geq 0$.

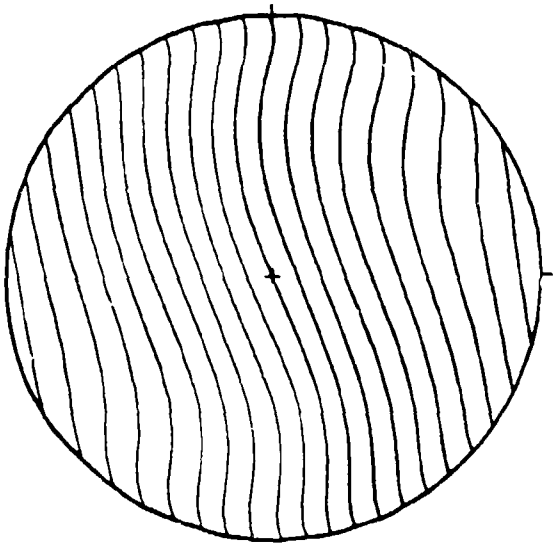

Figure 5. Contour plot of the pressure field across the cylinder at $z/\lambda = 0.9$.

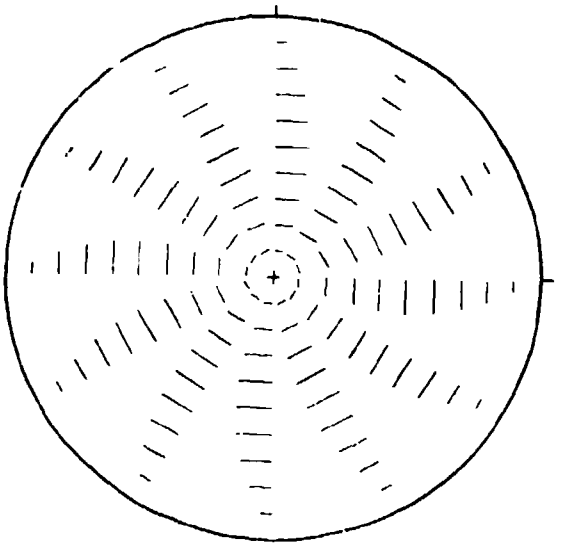

Figure 6. Vector plot of the mean velocity field across the cylinder at $z/\lambda = 0$.

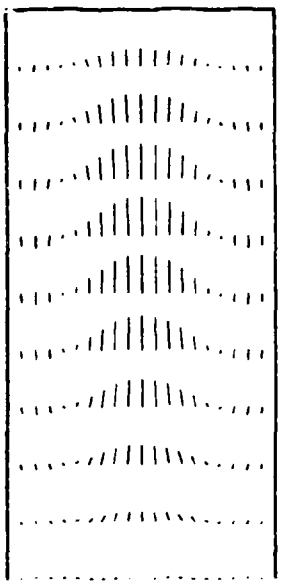

Figure 7. Vector plot of the mean velocity field in the x, z-plane for $z \geq 0$.

Figure 8. Pattern of the fluid motion at low Reynolds numbers ($R \approx 30$) in the x, z-plane.

APPENDIX C

A SPECTRAL NAVIER-STOKES SOLVER FOR THE FLOW IN A SPINNING AND NUTATING CYLINDER

By

Thorwald Herbert

A SPECTRAL NAVIER-STOKES SOLVER FOR THE FLOW IN A SPINNING AND NUTATING CYLINDER

Thorwald Herbert

Department of Engineering Science and Mechanics
Virginia Polytechnic Institute and State University
Blacksburg, Virginia 24061

ABSTRACT

Artillery shells with liquid payloads may experience a severe flight instability owing to the viscous fluid motion in the cylindrical payload container. Analytical studies of this fluid motion suggest that the velocity field in the aeroballistic coordinate system can be obtained from a linearized system of equations, with a small correction for nonlinear terms. Moreover, the smooth solution of the Navier-Stokes equations at the relevant low Reynolds numbers can be accurately approximated by relatively few terms of spectral expansions. We describe a spectral collocation method for calculating velocity and pressure field and the associated moments for liquid-filled cylinders embedded in spinning and nutating projectiles. The design goals are high efficiency, robustness, and the opportunity of extending the method to unsteady problems. The method uses Chebyshev-Fourier-Chebyshev expansions in the radial, azimuthal, and axial direction and exploits the symmetries of the problem. We present solutions for the steady motion and compare with experimental data. We also evaluate the performance of our code in comparison with other computer codes.

1. Introduction

It is well known that spin-stabilized shells carrying liquid payloads can suffer a dynamical instability which results in an increased nutation (or yaw) angle and a simultaneous loss in spin rate. Laboratory experiments, computational results, and field tests indicate that these phenomena arise from the nutation-induced fluid motion in a certain range of small Reynolds numbers. Although in special cases this instability has been overcome by trial and error, future design of reliable projectiles would profit from the opportunity to calculate the liquid moments and to account for these moments in flight simulators. The empirical data base [1, 2] is sparse, however, and computational methods in use [3, 4, 5] are rather demanding.

In previous work,[6] we conducted a theoretical analysis which aimed at the origin of the viscous despin (negative roll) moment. This analysis showed that the deviation from solid body rotation is governed by a small parameter $\epsilon = \Omega \sin\theta/\omega$ involving the nutation rate Ω, the nutation angle θ, and the spin rate ω. A solution of the linearized equations was developed for a finite-length segment of an

infinitely long cylinder, i. e. disregarding the end walls of the cylinder. Velocity field and the viscous components of the moments were obtained in closed form. The velocity field consists only of an axial component of order $O(\epsilon)$ which is the dominating feature of the fluid motion and produces a negative roll moment of order $O(\epsilon^2)$ owing to Coriolis forces. Although these results are in reasonable agreement with experimental and computational data, one may anticipate modifications of velocity field and roll moment if nonlinear terms are taken into account. Moreover, yaw and pitch moments contain essential contributions of the pressure [4] that originate from the turning of the flow near the end walls. The effect of nonlinearity was studied [7] by using perturbation expansions in ϵ and was found to be small. The flow in a finite-length cylinder, however, can only be captured by a computational approach.

The existing computer codes may serve for establishing some basic results but are too inefficient and insufficiently verified for routine applications. Our analytical work suggests the use of a code that exploits (i) the near-linearity of the governing equations and (ii) the smoothness of the solution in the relevant range of Reynolds numbers. Therefore, we have pursued a simple concept that is open to numerous refinements. We use Chebyshev-Fourier-Chebyshev expansions in r, ϕ, z, respectively, and convert the linearized equations into a linear algebraic system for the expansion coefficients. The solution of this system (or any other solution at neighboring parameters) is used as initial approximation for iterative improvement by the modified Newton method. The feasibility of this approach has been demonstrated [8] with a crude spectral approximation to the solution. The version of the code reported here exploits the diametral symmetry of the flow and allows for higher resolution at modest CPU times. This version can also be adapted to a time-accurate analysis of the unsteady problem.

2. Governing Equations

We consider the deviation $\mathbf{v}_d$, p_d from solid-body rotation in a nutating coordinate system x, y, z where z is the cylinder axis and x is coplanar with the two axes of rotation. (For a detailed discussion of the governing equations, see the article by Herbert.[6]) All quantities are made nondimensional using a, ω, and ρ for scaling length, time, and mass, respectively. The solution depends on four nondimensional parameters: aspect ratio $\lambda = c/a$, nutation angle θ, frequency $\tau = \Omega/\omega$, and Reynolds number $R = \rho\omega a^2/\mu$, where $2c$ is the length of the cylinder, ρ is the density, and μ the viscosity of the fluid. The aspect ratio enters the solution only through the boundary conditions at the end walls of the cylinder. The motion is subject to the no-slip and no-penetration conditions at the cylinder walls. Therefore, the boundary conditions on the deviation velocity are homogeneous.

In cylindrical coordinates r, ϕ, z, the equations for the velocity components $\mathbf{v}_d = (v_r, v_\phi, v_z)$ and pressure p_d take the form

$$\frac{1}{r}\frac{\partial}{\partial r}(rv_r) + \frac{1}{r}\frac{\partial v_\phi}{\partial \phi} + \frac{\partial v_z}{\partial z} = 0\,, \tag{1a}$$

$$D'v_r - \frac{v_\phi^2}{r} - 2(1+\tau_z)v_\phi + 2\tau_\phi v_z = -\frac{\partial p_d}{\partial r} + \frac{1}{R}\left[D''v_r - \frac{v_r}{r^2} - \frac{2}{r^2}\frac{\partial v_\phi}{\partial \phi}\right], \tag{1b}$$

$$D'v_\phi + \frac{v_r v_\phi}{r} + 2(1+\tau_z)v_r - 2\tau_r v_z = -\frac{1}{r}\frac{\partial p_d}{\partial \phi} + \frac{1}{R}\left[D''v_\phi - \frac{v_\phi}{r^2} + \frac{2}{r^2}\frac{\partial v_r}{\partial \phi}\right], \tag{1c}$$

$$D'v_z + 2\tau_r v_\phi - 2\tau_\phi v_r = -\frac{\partial p_d}{\partial z} - 2r\tau_r + \frac{1}{R}D''v_z\,, \tag{1d}$$

where

$$D' = \frac{\partial}{\partial t} + \frac{\partial}{\partial \phi} + v_r \frac{\partial}{\partial r} + \frac{v_\phi}{r}\frac{\partial}{\partial \phi} + v_z \frac{\partial}{\partial z} , \quad D'' = \frac{\partial^2}{\partial r^2} + \frac{1}{r}\frac{\partial}{\partial r} + \frac{1}{r^2}\frac{\partial^2}{\partial \phi^2} + \frac{\partial^2}{\partial z^2} ,$$

and

$$\tau_r = -\epsilon \cos\phi , \quad \tau_\phi = \epsilon \sin\phi , \quad \tau_z = \tau \cos\theta , \quad \epsilon = \tau \sin\theta . \tag{2}$$

The effect of nutation is comprised in the ϕ-periodic force term $-2r\tau_r = 2\epsilon r\cos\phi$ in the z-momentum equation (1d). For $\epsilon = 0$, equations (1) support the trivial solution $\mathbf{v}_d \equiv 0$, $p_d \equiv 0$. The system supports the following symmetries:

$$v_r(r, \phi+\pi, -z) = v_r(r, \phi, z) , \quad v_\phi(r, \phi+\pi, -z) = v_\phi(r, \phi, z) , \tag{3a,b}$$

$$v_z(r, \phi+\pi, -z) = -v_z(r, \phi, z) , \quad p_d(r, \phi+\pi, -z) = p_d(r, \phi, z) . \tag{3c,d}$$

3. Spectral Approximations for a Finite-Length Cylinder

The results of the analytical work suggest that a good approximation to the flow in a finite cylinder can be obtained by solving linearized versions of equations (1). Linearization can be performed in different ways. The first is a linearization in ϵ. Beyond eqs. (3), the resulting equations support the additional symmetries

$$\mathbf{v}_d(r, \phi+\pi, z) = -\mathbf{v}_d(r, \phi, z) , \quad p_d(r, \phi+\pi, z) = -p_d(r, \phi, z) . \tag{4}$$

These relations permit useful checks on the results of the spectral code. A second linear system can be obtained by linearization in the components of $\mathbf{v}_d$. This linearization retains coupling terms such as $2\tau_\phi v_z$ in eq. (1b) which destroy the symmetries (4). The second system can be considered a special case with $\mathbf{v}_d^{(0)} = p_d^{(0)} = 0$ of a third linearization about some known solution $\mathbf{v}_d^{(0)}$, $p_d^{(0)}$. This third procedure is very efficient if the solution is sought for a densely spaced sequence of parameter combinations as in flight simulations.

The algebraic form of the equations is obtained by use of spectral collocation. The velocity components are expressed in the form

$$v_r = \sum_{k=1}^{K} \sum_{l=1}^{L} \sum_{m=1}^{M} u_{klm} R_{kl}^u(r) F_l(\phi) Z_{ml}^u(z/\lambda) , \tag{5}$$

with similar expressions for v_ϕ, v_z, and p_d. The azimuthal functions are $F_l = \cos[(l-1)\phi/2]$ for odd l, $F_l = \sin[l\phi/2]$ for even l, where $l = 1, 2, \cdots L$, and L is odd. The azimuthal collocation points are equidistant, $\phi_l = 2\pi(l-1)/L$. The expansion functions in radial and axial direction depend on the index l and may be different for the variables v_r, v_ϕ, v_z, and p_d. They are combinations of even or odd Chebyshev polynomials such that (i) the homogeneous boundary conditions are implicitly satisfied, (ii) the symmetry conditions (3) are satisfied, and (iii) the limit values of the variables for $r \to 0$ (i. e. the values on the axis) are independent of ϕ. The collocation points are $r_k = \cos[(2k-1)\pi/4K]$, $k = 1, 2, \cdots K$, and $z_m/\lambda = \cos[(2m-1)\pi/4M]$, $m = 1, 2, \cdots M$, Consequently, $0 < r_k$, and no points are located on the axis. Also, $r_k < 1$, $z_m < \lambda$, such that no points are located on the surface. This choice prevents the occurrence of spurious pressure terms and avoids the difficulties associated with corners and axis. The points are concentrated near the boundary such that higher resolution in this region is obtained without additional coordinate stretching.

The spectral collocation method converts the linear system of partial differential equations derived from eqs. (1) into an algebraic system of dimension $N = 4 \cdot K \cdot L \cdot M$ for the coefficients u_{klm}, v_{klm}, w_{klm}, and p_{klm} of v_r, v_ϕ, v_z, and p_d, respectively. The linear algebraic system for the expansion coefficients is solved by Gauss elimination with partial pivoting. The subroutine used retains all data

required to solve the same system with a new right-hand side without repeating the costly reduction of the matrix to upper triangular form. Once the solution is obtained, a new right-hand side is formed taking the nonlinear terms into account and the system is iteratively solved until sufficient accuracy is achieved. The procedure is equivalent to the modified Newton iteration (without updating the Jacobian in every step) and converges rapidly since the nonlinear corrections to the velocity are small while the pressure appears linear in equations (1).

4. Results of the Spectral Code

In the following, we present some results for $R = 14.95$, $\theta = 20°$, $\tau = -0.1667$, and $\lambda = 4.368$ which results in $\epsilon = 0.057$. The results are for $K = L = M = 5$, and consequently $N = 500$. Figure 1 shows the axial and radial velocities in the planes $\phi = 45°$ and $135°$. Only the upper half, $z \geq 0$, of the cylinder is shown; the lower half is governed by the symmetries (3). The velocity distribution at $z = 0$ agrees well with the results of the perturbation analysis and computations with the Sandia code. Near the end walls, the solution seems to be more realistic and more accurate than the Sandia results. Good resolution of the velocity gradients and pressure at the boundary is important for accurate calculations of the moments. The figure also verifies the existence of a predominantly axial flow over most of the cylinder length, except within a region of the order of the radius near the end wall. Linear and nonlinear velocity distributions are hardly distinguishable. Clearly visible is the turning of the flow near the end wall.

The pressure distribution in the plane $\phi = 45°$ is shown in figure 2 with the heavy lines marking positive values. Remarkable are the regions of high and low pressure in the corners near $\phi \approx 45°$ and $\phi \approx 225°$, respectively, which produce large pressure contributions to the moments about x-axis and y-axis.

The dominant components of velocity and pressure fields are azimuthally periodic with period 2π. The harmonics are small, indicating the small effect of nonlinearity. The only important nonlinear term is the aperiodic mean flow. The axial and radial mean velocity field is given in figure 3. This streaming term produces a toroidal mean motion near the end wall.

The despin moment about the z-axis is largely governed by the shear stress at the side wall caused by the azimuthal mean velocity. This component shows little variation over about 90% of the cylinder length. This result explains the good agreement of our earlier analytical results for the despin moment [6] with experimental and computational data. Besides the calculation of the moments from local velocity gradients and pressures at the surface, we have also obtained these moments from volume integrals involving the velocity only. This second method provides accurate values of the moments from low-resolution spectral approximations that would be insufficient when using the surface values. Reasonable accuracy of the moments can be obtained with $K = M = 4$, $L = 3$. This approximation has been used to obtain the data shown in figure 4 together with results of the Sandia code [4] and the analytical results. [6] The region of maximum despin moment will be subject to further study with higher resolution.

5. Discussion

The finite-difference code developed at Sandia Laboratories [3,4] provides the steady solution at $11 \times 24 \times 21$ grid points in r, ϕ, z-direction by integrating over typically 10^4 to $8 \cdot 10^4$ time steps, a task that requires 6 to 48 minutes CPU time on a Cray-1S. This requirement translates into 6 to 48 days on the MC68010 based Apollo DN300 work station used for our studies. The result consists of over 22,000 values for velocities and pressure. Strikwerda & Nagel [5] briefly describe a code using finite differences in radial and axial directions and pseudospectral differencing in the azimuthal direction.

Nonuniform grids are introduced for increased resolution near the walls. The difference equations are solved by an iterative method based on successive over-relaxation. The computer time required is comparable to that of the Sandia code (Nusca, BRL, personal communication). The relative merits of the two codes, especially with respect to the captured range of Reynolds numbers are yet concealed.

The experience with the present version of the spectral code shows that high performance can be achieved. The reported run with $N = 500$ requires about 3 hours on an Apollo DN300 work station. The solution is obtained in semi-analytical form with only $N = 500$ numerical coefficients. This low data volume is very attractive for communication with remote supercomputers. The code is well suited for vectorization, since practically all CPU time is spent on constructing and solving an algebraic system. The code demands larger memory than other codes because 64-bit arithmetic is highly recommended for spectral methods in general, and the algebraic system requires $N(N + 1)$ words of storage. Nowadays, this memory requirement appears acceptable even if higher resolution is desired. Calculation of the moments for figure 4 ($N = 192$) requires less than 12 minutes per point.

Finally, there are still ways to improve the performance. The solution process can be split into two levels, the first of which calculates only the velocity components from vorticity equations while the pressure is obtained a posteriori by solving the Poisson equation. For calculating the moments by volume integrals, only the first step is required. We expect that the next version of our code will provide accurate solutions for the moments in less than 1 minute on an MC68020/68881 based work station and can be used as an efficient subroutine in flight simulators.

ACKNOWLEDGMENT

The assistance of Ri-Hua Li in the analytical and numerical work is greatly appreciated. This work is supported by the U. S. Army AMCCOM under Contract DAAA15-85-K-0012.

REFERENCES

1. M. C. Miller 1982 "Flight instabilities of spinning projectiles having nonrigid payloads," *J. Guidance, Control, and Dynamics*, vol. 5, pp. 151-157.

2. R. Sedney 1985 "A Survey of the fluid dynamic aspects of liquid-filled projectiles," AIAA Paper No. 85-1822-CP.

3. H. R. Vaughn, W. L. Oberkampf, and W. P. Wolfe 1983 "Numerical solution for a spinning nutating fluid-filled cylinder," Sandia Report SAND 83-1789.

4. H. R. Vaughn, W. L. Oberkampf, and W. P. Wolfe 1985 "Fluid motion inside a spinning nutating cylinder," *J. Fluid Mech.*, vol. 150, pp. 121-138.

5. J. C. Strikwerda and Y. M. Nagel 1985 "A numerical method for computing the flow in rotating and coning fluid-filled cylinders," in *Proc. 1984 Scientific Conf. on Chemical Defense Research, Aberdeen Proving Ground, Maryland*, ed. M. Rausa, pp. 523-527, CRDC-SP-85006.

6. Th. Herbert 1986 "Viscous fluid motion in a spinning and nutating cylinder," *J. Fluid Mech.*, vol. 167, pp. 181-198.

7. Th. Herbert and S. D. Greco 1987 "Higher approximations for the viscous flow in a spinning and nutating cylinder," *J. Fluid Mech.* To be submitted.

8. Th. Herbert 1986 "Analytical and computational studies of the fluid motion in liquid-filled shells," in *Proc. 4th Army Conf. on Appl. Math. and Computing, Ithaca, New York, 1986.* To appear.

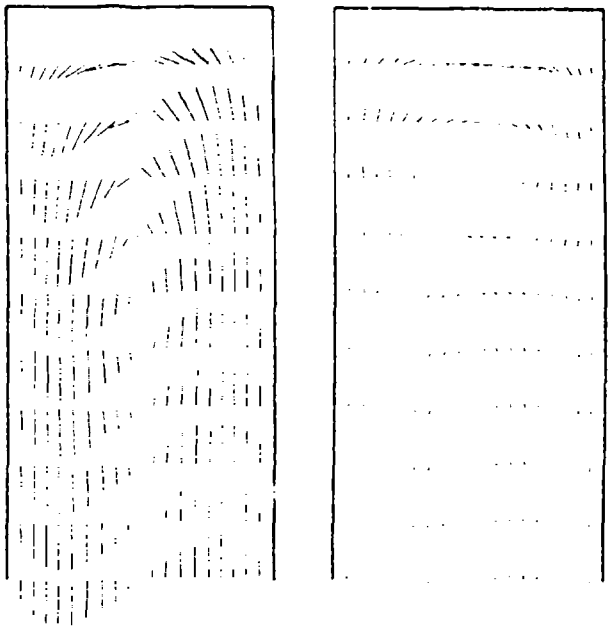

Figure 1. Vector plot of the velocity field in the planes $\phi = 45°$ (left) and $\phi = 135°$ for $z \geq 0$. The maximum velocity is 0.0616.

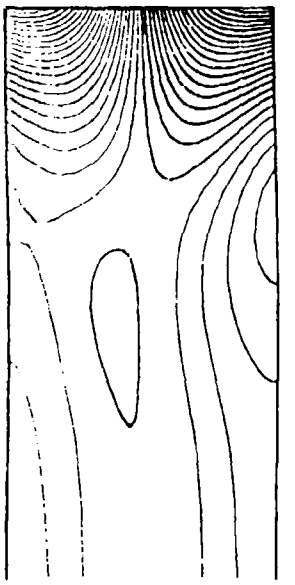

Figure 2. Contour plot of the pressure field in the plane $\phi = 45°$ for $z \geq 0$. Levels every 0.0025.

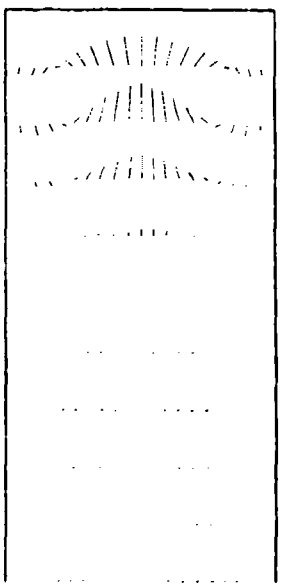

Figure 3. Vector plot of the mean velocity field for $z \geq 0$. The maximum velocity is 0.00143.

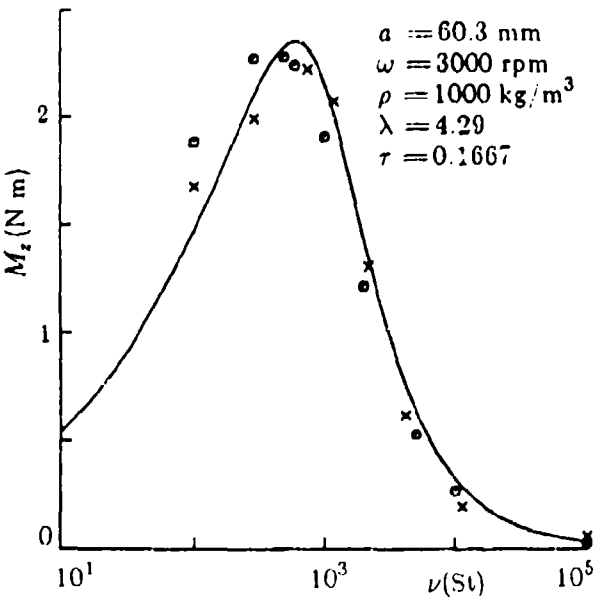

Figure 4. Despin moment M_z as a function of the kinematic viscosity ν: ○ spectral code, × Sandia code,[4] (——) theory.[6]

BLANK

APPENDIX D

NUMERICAL STUDY OF THE FLOW IN A SPINNING AND NUTATING CYLINDER

By

Thorwald Herbert
Rihua Li

NUMERICAL STUDY OF THE FLOW IN A SPINNING AND NUTATING CYLINDER

Thorwald Herbert *
Ruhua Li **

Department of Engineering Science and Mechanics
Virginia Polytechnic Institute and State University
Blacksburg, Virginia 24061

ABSTRACT

Artillery shells with liquid payloads may experience a severe flight instability owing to the moments exerted by the viscous fluid motion in the cylindrical payload container. Incorporation of these moments into flight simulators as a routine design tool requires a highly efficient code for solving the Navier-Stokes equations. We describe a spectral collocation method which is based on Chebyshev-Fourier-Chebyshev expansions in the radial, azimuthal, and axial direction. The method exploits the symmetries of the problem. Using a volume approach and an analytical result by Rosenblat, accurate moments are obtained in small fractions of the time required by other codes. Solutions for the steady motion are presented and compared with numerical and experimental data. The performance of our code is evaluated in comparison with other computer codes.

Introduction

Gyros and rotating fluids often exhibit unexpected behavior. In the past, it has been recognized that spin-stabilized shells with liquid payloads can suffer a dynamical instability originating from resonance with inertial waves.[1] Since this phenomenon is basically inviscid and is routinely avoided by proper design, it was surprising to observe in some cases another type of instability which is characterized by an increase in nutation (or yaw) angle and a simultaneous loss in spin rate. The rapid drop in spin rate is clearly a viscous phenomenon, and laboratory experiments, computational results, and field tests have meanwhile shown that this instability is caused by the nutation-induced fluid motion in a certain range of relatively small Reynolds numbers. Although in special cases this instability has been overcome by trial and error, future design of reliable projectiles would take profit from the opportunity to calculate the liquid moments and to account for these moments in flight simulators. The empirical data base [2] is sparse, however, and computational methods in use [3,4,5,6] are rather demanding. An evaluation and verification of the codes by Vaughn et al. [4] and Strikwerda & Nagel [5] is currently conducted at BRL.[7] Typical computer times for a single case are in the range of 6-12 hours on VAX-class machines. Six-degree-of-freedom flight simulators [8] typically use $2 \cdot 10^6$ time steps over the flight time of the order of 30 seconds. Study of the interaction of the interior fluid motion with the exterior aeroballistics consequently requires either a very fast subroutine for calculating the liquid moments or interpolation in a multi-dimensional table of 500-1000 [8] precalculated values. Hence, flight simulations for liquid-filled shells are currently a very expensive tool and are not ready for routine applications.

In previous work [9] we conducted a theoretical analysis which aimed at the origin of the viscous despin (negative roll) moment in cylinders of large aspect ratio. This analysis showed that the deviation from solid body rotation is governed by a small parameter, $\epsilon = (\Omega/\omega)\sin\theta$, involving the nutation rate Ω, the nutation angle θ, and the spin rate ω. A solution of the linearized equations was developed for a finite-length segment of an infinitely long cylinder, i. e. disregarding the end walls of the cylinder. Velocity field and the viscous components of the moments were obtained in closed form. The velocity field consists only of an axial component of order $O(\epsilon)$ which is the prominent feature of the fluid motion and produces a negative roll moment of order $O(\epsilon^2)$ owing to Coriolis forces. Although this roll moment is in reasonable agreement with experimental and computational data, the original analysis accounted only for the viscous part of the yaw and pitch moment. These latter moments contain essential contributions of the pressure [4] that originate from the turning of the flow near the end walls and were not captured by the linear analysis. The effect of nonlinearity was studied [10] by using perturbation expansions in ϵ and was found to be small except for an aperiodic stream-

---

* Professor, Engineering Science and Mechanics
Member AIAA

** Research Associate

ing term in the azimuthal direction.

Athough the perturbation approach cannot capture the pressure field, it provides valuable insight into the structure of both equations and solution. The analytical work suggests the use of a numerical method that exploits (i) the near-linearity of the governing equations and (ii) the smoothness of the solution in the relevant range of Reynolds numbers. We have therefore pursued a simple concept that is open to further refinements. We use Chebyshev-Fourier-Chebyshev expansions in r, ϕ, z, respectively, and convert the linearized equations into an algebraic system for the expansion coefficients. Linearization can be performed about the trivial solution or any other known solution, e. g. at neighboring parameters. The solution of the linear algebraic system is used as initial approximation for iterative improvement by the modified Newton method. The feasibility of this approach has been demonstrated [11] with a crude spectral approximation to the solution. Problems in calculating the pressure that arise from the invalidity of the basic equations in the corners joining the flat end walls to the cylindrical side wall have meanwhile been overcome.[12] The present version of the code exploits the diametral symmetry of the flow about the center of the cylinder and allows for higher resolution at modest CPU times. This version can also be adapted for the analysis of unsteady problems. Dramatic increase in efficiency has recently been achieved [13] by combining an analytical result of Rosenblat et al. [6] with a volume formulation for calculating the liquid moments. The moments can be obtained from only the simply periodic components of the axial velocity and the azimuthal streaming term. A fast subroutine for flight simulations exploits the analytical results. For more accurate studies, complete tables of moments can be calculated in a few hours on a VAX-type computer.

Governing Equations

We consider the steady motion of a fluid of density ρ and viscosity μ in a cylinder of radius a and length $2c$ in an aeroballistic coordinate system x, y, z, where z is the axis of the cylinder, as shown in Figure 1. The inertial axis Z in flight direction and the z-axis enclose the nutation angle θ. The cylinder rotates with the spin rate ω about z while the x, z-plane rotates with the nutation rate Ω about the Z-axis. Spin rate ω and nutation rate Ω are constant. All quantities are made nondimensional using a, ω, and ρ for scaling length, time, and mass, respectively. The solution depends on four nondimensional parameters: aspect ratio $\eta = c/a$, nutation angle θ, frequency $\tau = \Omega/\omega$, and Reynolds number $Re = \rho\omega a^2/\mu$. The aspect ratio enters the solution only through the boundary conditions at the end walls of the cylinder. The motion is subject to the no-slip and no-penetration conditions at the cylinder walls. Since the velocity field degenerates for either $\omega = 0$, $\Omega = 0$, $\theta = 0$, or $\mu \to \infty$ to rigid-body rotation of the fluid, it is appropriate to concentrate on the deviation $\mathbf{v}^d$ of the velocity from rigid-body rotation $\mathbf{v}^r$,

$$\mathbf{v} = \mathbf{v}^r + \mathbf{v}^d \ , \quad \mathbf{v}^r = r\mathbf{e}_\phi \ , \tag{1}$$

where $\mathbf{e}_\phi$ is the azimuthal unit vector. The boundary conditions on $\mathbf{v}^d$ are homogeneous. The pressure field is split according to

$$p = p^r + p^d \ , \tag{2a}$$

$$p^r = r^2(1+\tau_z)^2 + r^2\tau_\phi^2 + z^2\epsilon^2 - 2rz\epsilon\tau_r \ , \tag{2b}$$

where $\tau_r = -\epsilon\cos\phi$, $\tau_\phi = \epsilon\sin\phi$, $\tau_z = \tau\cos\theta$, $\epsilon = \tau\sin\theta$. The pressure p^r differs from the pressure in rigid-body rotation. The form of p^r is chosen such that the reduced pressure p^d appears only in the z-momentum equation.

In cylindrical coordinates r, ϕ, z, the equations for the velocity components $\mathbf{v}^d = (v_r, v_\phi, v_z)$ and pressure p^d take the form

$$\frac{1}{r}\frac{\partial}{\partial r}(rv_r) + \frac{1}{r}\frac{\partial v_\phi}{\partial \phi} + \frac{\partial v_z}{\partial z} = 0 \ , \tag{3a}$$

$$D'v_r - \frac{v_\phi^2}{r} - 2(1+\tau_z)v_\phi + 2\tau_\phi v_z =$$

$$-\frac{\partial p^d}{\partial r} + \frac{1}{Re}\left[D''v_r - \frac{v_r}{r^2} - \frac{2}{r^2}\frac{\partial v_\phi}{\partial \phi}\right] , \tag{3b}$$

$$D'v_\phi + \frac{v_r v_\phi}{r} + 2(1+\tau_z)v_r - 2\tau_r v_z =$$

$$-\frac{1}{r}\frac{\partial p^d}{\partial \phi} + \frac{1}{Re}\left[D''v_\phi - \frac{v_\phi}{r^2} + \frac{2}{r^2}\frac{\partial v_r}{\partial \phi}\right] , \tag{3c}$$

$$D'v_z + 2\tau_r v_\phi - 2\tau_\phi v_r =$$

$$-\frac{\partial p^d}{\partial z} - 2r\tau_r + \frac{1}{Re}D''v_z \ , \tag{3d}$$

where

$$D' = \frac{\partial}{\partial t} + \frac{\partial}{\partial \phi} + v_r\frac{\partial}{\partial r} + \frac{v_\phi}{r}\frac{\partial}{\partial \phi} + v_z\frac{\partial}{\partial z} \ ,$$

$$D'' = \frac{\partial^2}{\partial r^2} + \frac{1}{r}\frac{\partial}{\partial r} + \frac{1}{r^2}\frac{\partial^2}{\partial \phi^2} + \frac{\partial^2}{\partial z^2} \ .$$

The primary effect of nutation is the ϕ-periodic force term $-2r\tau_r = 2\epsilon r\cos\phi$ in the z-momentum equation (3d). For $\epsilon = 0$, equations (3) have the trivial solution $\mathbf{v}^d \equiv 0$, $p^d \equiv 0$. The system supports the following symmetries:

$$v_r(r, \phi+\pi, -z) = v_r(r, \phi, z), \quad (4a)$$

$$v_\phi(r, \phi-\pi, -z) = v_\phi(r, \phi, z), \quad (4b)$$

$$v_z(r, \phi+\pi, z) = -v_z(r, \phi, z), \quad (4c)$$

$$p^*(r, \phi+\pi, -z) = p^*(r, \phi, z). \quad (4d)$$

Some Analytical Results

The steady flow in a relatively long cylinder (aspect ratio $\eta > 4$) at low Reynolds number is expected to exhibit little axial variation over most of the cylinder length. Previous work [9] has therefore relaxed the boundary conditions at the end walls and studied the steady flow in a finite segment of an infinitely long cylinder.

In the physical situations of interest, $\epsilon = (\Omega/\omega)\sin\theta$ is a small parameter, and consequently, it is reasonable to pursue a perturbation expansion in ϵ. This provides $\mathbf{v}^*$ in the form

$$\mathbf{v}^* = \sum_{n=1}^{\infty} \epsilon^n \mathbf{v}^{(n)}(r, \phi) \quad (5)$$

and similar expressions for p^*. The development of expressions for the expansion coefficients $\mathbf{v}^{(n)}$ from equations (3) leads to an alternating pattern:

$$\mathbf{v}^{(n)} = \begin{cases} (0, 0, v_z^{(n)}), & n \text{ odd}, \\ (v_r^{(n)}, v_\phi^{(n)}, 0), & n \text{ even}. \end{cases} \quad (6)$$

and the components of $\mathbf{v}^{(n)}$ take the form

$$v_r^{(n)} = \sum_{m=1}^{n/2} (u_{nm} e^{i2m\phi} + \tilde{u}_{nm} e^{-i2m\phi}), \quad (7a)$$

$$v_\phi^{(n)} = v_{n0} + \sum_{m=1}^{n/2} (v_{nm} e^{i2m\phi} + \tilde{v}_{nm} e^{-i2m\phi}), \quad (7b)$$

$$v_z^{(n)} = \sum_{m=1}^{(n+1)/2} (w_{nm} e^{i(2m-1)\phi} + \tilde{w}_{nm} e^{-i(2m-1)\phi}), \quad (7c)$$

where the tilde denotes the complex conjugate. The aperiodic term in $v_r^{(n)}$ is suppressed by the continuity equation. The r-dependent coefficient functions in Eqs. (7) are required to satisfy homogeneous boundary conditions at $r = 1$ and to be finite at the axis $r = 0$.

The axial velocity at order $O(\epsilon)$ can be found in analytical form,

$$w_{11}(r) = i\left[\frac{I_1(\alpha r)}{I_1(\alpha)} - r\right], \quad (8)$$

where I_1 denotes the modified Bessel function, and $\alpha = (1+i)(Re/2)^{1/2}$. This solution is valid for arbitrary Reynolds number but may be unstable as Re exceeds some critical value. This component is the dominating feature of the flow in a long cylinder. The interesting properties of the associated flow field are discussed by Herbert.[9]

At order $O(\epsilon^2)$, comparison of the equation for v_{20} with the imaginary part of the equation for w_{11} immediately shows that the aperiodic component of the azimuthal velocity is

$$v_{20}(r) = -2\,\mathrm{Im}[w_{11}(r)]. \quad (9)$$

The ϕ-periodic components are governed by a coupled set of inhomogeneous differential equations with variable coefficients. Essential simplification at the expense of increasing the order of differentiation results from eliminating v_{21} by use of the continuity equation. With some effort, the radial velocity component of $O(\epsilon^2)$ can be found in closed form,

$$u_{21}(s) = \frac{1}{s}[c_1 J_2(s) + c_2 Y_2(s)] + c_3 s + \frac{c_4}{s^3} + \frac{2i\sqrt{2}}{s} \frac{J_2(s/\sqrt{2})}{J_1(\beta/\sqrt{2})}, \quad (10)$$

where $s = \beta r$, $\beta = (i-1)\,Re^{1/2}$, and J_1, J_2, and Y_2 are Bessel functions. The coefficients c_1, c_2, c_3, and c_4 can be determined numerically.[10] In view of the effort involved in deriving the closed form solution for u_{21} and the ultimate need to determine the coefficients numerically, the differential equations for the third-order components were solved by means of a spectral collocation method.

The motion is governed by the axial component w_{11} at order $O(\epsilon)$. Of the higher order terms, only the aperiodic term v_{20} is substantial. In the cylinder's center section, these terms are in good agreement with computational results. All the other terms are not only of order $O(1)$ but in fact less than unity, assuring rapid convergence of the perturbation series. The contribution of w_{31} to the despin moment is negligible. The ϕ-periodic terms oscillate about zero as r varies between $0 \le r \le 1$. Accurate representation of single high-order terms by radial Chebyshev series may require numerous expansion functions. For the total velocity field, however, the error in representing these terms is of little importance. At Reynolds numbers in the range of maximum despin moment, reasonably accurate approximations can be obtained with only a few polynomials in radial direction. In the azimuthal direction, the solution is governed by terms periodic in ϕ, and by the aperiodic term v_{20}. Fourier series with three or five modes, therefore, provide approximations of sufficient accuracy for practical purpose. The perturbation analysis clearly shows that the main features of the flow are governed by the linear $O(\epsilon)$ part of equations (3) with small corrections for nonlinearity. This property will not change for a finite-length cylinder.

Spectral Approximations

The results of the analytical work suggest that a good approximation to the flow in a finite cylinder can be obtained by solving linearized versions of equations (3). Linearization can be performed in different ways. The first is a linearization in ϵ. Besides Eqs. (4), the resulting equations support additional symmetries:

$$\mathbf{v}^{\epsilon}(r, \phi+\pi, z) = -\mathbf{v}^{\epsilon}(r, \phi, z), \quad (11a)$$

$$p^{\epsilon}(r, \phi+\pi, z) = -p^{\epsilon}(r, \phi, z). \quad (11b)$$

These relations permit useful checks on the results of the spectral code. A second linear system can be obtained by linearization in the components of $\mathbf{v}^{\epsilon}$. This linearization retains coupling terms such as $2r_{\phi}v_r$ in Eq. (3b) which destroy the symmetries (11). The second system can be considered a special case with $\hat{\mathbf{v}}^{\epsilon} = 0$ of a linearization about some known solution $\hat{\mathbf{v}}^{\epsilon}$. The latter procedure is very efficient if the solution is sought for a densely spaced sequence of parameter combinations as in flight simulations.

The algebraic form of the equations is obtained by use of a spectral collocation method. The velocity components are expressed in the form

$$v_r = \sum_{k=1}^{K} \sum_{l=1}^{L} \sum_{m=1}^{M} u_{klm} R_k(r) F_l(\phi) Z_m(\frac{z}{\eta}), \quad (12)$$

with similar expressions for v_{ϕ}, v_z, and p^{ϵ}. The azimuthal functions are

$$F_l = \begin{cases} \cos \frac{l-1}{2}\phi, & l \text{ odd}, \\ \sin \frac{l}{2}\phi, & l \text{ even}. \end{cases} \quad (13)$$

The azimuthal collocation points are equidistant.

$$\phi_l = 2\pi(l-1)/L, \quad l = 1, 2, \cdots L, \quad (14)$$

and L is odd.

In a first version of the code, radial and axial collocation points are located at the maxima of the highest Chebyshev polynomials. The boundary conditions are implemented by replacing three of the four differential equations in the boundary points. The question then is which equation should be retained and where the condition on the pressure, e.g. $p^{\epsilon} = 0$, should be applied. Trial-and-error leads to numerous cases with ill-determined matrices or zero determinant. In other cases, a correct solution for the velocity field is obtained, but the pressure contains a non-physical spurious term. Problems with spectral calculations of the pressure in closed domains with corners are well-known but the reports on their origin and methods for solution are rather unspecific. We have therefore performed a detailed analysis of the flow in a square driven by an internal force field. This simpler two-dimensional problem exhibits all characteristics - including the spurious pressure term - of the original problem. Detailed results of this study will be reported elsewhere.[14] The study reveals that the spurious term vanishes in all collocation points except the corners, where it may assume arbitrary values. The term can be suppressed by retaining in the corners one of the momentum equations that contain the derivative of the pressure in the direction of the boundary.

In a second version of the spectral code, the problems of the pressure calculation have been avoided by using a different set of collocation points. The expansion functions in radial and axial direction depend on the index l and may be different for the variables v_r, v_{ϕ}, v_z, and p^{ϵ}. They are combinations of even or odd Chebyshev polynomials such that

(i) the homogeneous boundary conditions are implicitly satisfied,

(ii) the symmetry conditions (4) are satisfied, and

(iii) the limit value of the variables for $r \to 0$ (i. e. the value on the axis) is independent of ϕ.

The collocation points are

$$r_k = \sin \frac{k-1}{2K}\pi, \quad k = 1, 2, \cdots K, \quad (15a)$$

$$\frac{z_m}{\eta} = \sin \frac{m-1}{2M}\pi, \quad m = 1, 2, \cdots M. \quad (15b)$$

Consequently $0 < r_k$, and no points are located on the axis. Also, $r_k < 1$, $z_m < \eta$ such that no points are located on the surface. The points in radial and axial direction are concentrated near the boundary such that high resolution in this region is obtained without additional coordinate stretching. Thus the boundary layers forming at higher Reynolds number can be resolved by slightly increasing K and M.

The spectral collocation method converts the linear system of partial differential equations derived from Eqs. (3) into an algebraic system of dimension $N = 4 \cdot K \cdot L \cdot M$ for the coefficients u_{klm}, v_{klm}, w_{klm}, and p_{klm} of v_r, v_{ϕ}, v_z, and p^{ϵ}, respectively. The linear system for the expansion coefficients is solved by Gauss elimination with partial pivoting. The subroutine used retains all data required to solve the same system with a new right-hand side without repeating the costly reduction of the matrix to upper triangular form. Once the solution is obtained, a new right-hand side is formed by taking the nonlinear terms into account and the system is iteratively solved until sufficient accuracy is achieved. The procedure is equivalent to the modified Newton

iteration (without updating the Jacobian in every step) and converges rapidly since the nonlinear corrections to the velocity are small while the pressure appears linear in equations (3).

Results for Velocity and Pressure

In the following, we present some results for the velocity and pressure fields at $\theta = 20°$, $\tau = 0.16667$, and $\eta = 4.368$ which results in $\epsilon = 0.057$. The results are for $K = 6$, $L = 5$, and $M = 8$, and consequently $N = 960$. Calculation of a single solution with this high resolution requires about 2 minutes on a Cray-1S. Figure 2 shows the axial and radial velocities in the planes $\phi = 45°$ and $\phi = 135°$ at $Re = 20$. Only the upper half, $z \geq 0$, of the cylinder is shown; the lower half is governed by the symmetries (4). The scale values give the velocity per unit length where the diameter is six units. The velocity distribution at $z = 0$ agrees well with the results of the perturbation analysis and computations with the Sandia code.[3] Near the end walls, the solution is more realistic and more accurate than the Sandia results. The figure also verifies the existence of a predominantly axial flow over most of the cylinder length, except within a region of the order of the radius near the end wall. Linear and nonlinear velocity distributions are hardly distinguishable. Clearly visible is the turning of the flow near the end wall. While the flow appears steady in the coordinate system chosen, the velocity field describes in fact an oscillatory motion of fluid elements about their near-circular orbit.

The pressure distributions for the same case are shown in Figure 3 with the heavy lines indicating positive values. Remarkable is the formation of regions of high and low pressure in the corner near $\phi \approx 45°$ and $\phi \approx 135°$, respectively, which produce large contributions to the moments about x axis and y-axis. Except in this region near the end walls, the variation of the pressure is relatively weak. The azimuthal position of extremum pressure changes from $\phi = 0$ for small values of Re to $\phi \approx 90°$ at $Re = 1000$.

The dominant components of velocity and pressure fields are azimuthally periodic with period 2π. The harmonics are small, indicating the small effect of nonlinearity in the range of low Reynolds numbers. The only important nonlinear term is the aperiodic mean flow. This is clearly shown by Figure 4 which gives the azimuthal velocity in the center plane $z = 0$. The aperiodic component is opposite to the rigid-body rotation and exerts a negative roll moment through the wall shear stress $\tau_{r\phi}$. The axial and radial mean velocity field is given in Figure 5. This streaming term exhibits a toroidal motion near the end in each half of the cylinder and causes a slow drift of fluid elements with respect to circular orbits. This mean velocity produces the symmetric pattern in flow visualizations [15] at low Reynolds numbers.

At the higher Reynolds number $Re = 300$, the maximum axial velocity appears at $\phi \approx 90°$. As shown in Figure 6, the flow in the plane $\phi = 90°$ breaks up into two swirls, one in each half of the cylinder, with little flow across the plane $z = 0$. Three weak swirls develop in the plane $\phi = 0$ such that the velocity field is reminiscent of a chain with five links. Notably, the break-up into cells is restricted to an inner region of the cylinder. The motion in the pronounced boundary layer visible in the plane $\phi = 0$ does not follow the cellular structure and may have a direction opposite to the core flow. The pressure variation is characteristically different from that at low Reynolds number. Figure 7 shows the strong variation and the formation of an almost symmetric pattern along the cylinder in the plane $\phi = 0$, while the variation at $\phi = 90°$ is rather weak. This pressure field explains the void observations of Miller [16] which show a wavy distortion of the void in the plane $\phi = 0$ at high Reynolds numbers. The steep and opposite pressure gradients across the cylinder axis near $z/\eta = 0.25$ and $z/\eta = 0.75$ displace the void near these positions in opposite directions along the diameter at $\phi \approx -15°$.

Calculation of the Liquid Moments

Conservation of angular momentum for the steady flow in a control volume V with surface S rotating with constant rate Ω about a fixed axis requires

$$\mathbf{M} = \int_S (\mathbf{r} \times \mathbf{F}) dS = \int_V \mathbf{r} \times (2\Omega \times \mathbf{v}) \rho \, dV + \int_V \mathbf{r} \times [\Omega \times (\Omega \times \mathbf{r})] \rho \, dV + \int_S (\mathbf{r} \times \mathbf{v}) \rho (\mathbf{v} \cdot d\mathbf{S}) \qquad (16)$$

where the velocity $\mathbf{v}$ is measured relative to the aeroballistic frame. On the left-hand side, $\mathbf{M}$ is the resultant torque on the control volume, $\mathbf{r}$ is the position vector, and $\mathbf{F}$ the stress acting on the cylinder. The presence and meaning of certain terms depend on the choice of the control volume. The surface integral on the right-hand side of Eq. (16) vanishes if the surface of the control volume is closed.

For ease of practical application, we express the moment $\mathbf{M} = (M_x, M_y, M_z)$ in terms of cartesian

... which provide yaw, pitch, and roll moment, respectively. Analogue to Eq. (1) we decompose the moments into

$$\mathbf{M} = \mathbf{M}^r + \mathbf{M}^d \ , \qquad (17)$$

where $\mathbf{M}^r$ corresponds to the pure rigid-body motion while $\mathbf{M}^d$ originates from the deviation velocity and pressure. For the cylindrical control volume, the rigid-body rotation causes only a pitch component

$$M_y^r = 2\pi\epsilon\eta[1 + \frac{\epsilon}{\tan\theta}(\frac{1}{2} - \frac{2}{3}\eta^2)] \ , \qquad (18)$$

while $M_x^r = M_z^r = 0$. Note that $\mathbf{M}$ is dimensionless; the reference moment is $\rho a^5\omega^2$.

The evaluation of the components of $\mathbf{M}^d$ bears some ambiguity that can be exploited for advantages. Previous computational work [3, 4, 5, 6] employed a control volume consisting of an "empty" closed cylinder with only the pressure and stresses acting on the inside surface. In this "surface approach," the right hand side of Eq. (16) vanishes and the moments are obtained from the stresses $\mathbf{F}$ at the inside wall of the control volume. Here, we choose a "volume approach" that bears great advantages especially for computational work.

We consider a control volume consisting of a solid cylindrical surface completely enclosing the liquid. The moment calculation for this "full" control volume rests on the relation

$$\mathbf{M}^d = \int_V \mathbf{r} \times (2\Omega \times \mathbf{v}^d)\rho dV \qquad (19)$$

Using analytical relations derived by Rosenblat et al.,[6] the components of $\mathbf{M}^d$ can be shown to take the form

$$M_x^d = -I_1\cos\theta \qquad (20a)$$

$$M_y^d = I_2\sin\theta - I_3\cos\theta \qquad (20b)$$

$$M_z^d = I_4\sin\theta \qquad (20c)$$

where

$$I_1 = \int_V z(v_r\cos\phi - v_\phi\sin\phi)r dr d\phi dz \ , \qquad (21a)$$

$$I_2 = \frac{1}{2}\int_V v_\phi r^2 dr d\phi dz \ , \qquad (21b)$$

$$I_3 = -\int_V v_z\sin\phi\, r^2 dr d\phi dz \ , \qquad (21c)$$

$$I_4 = -I_1 \ . \qquad (21d)$$

Finally, we obtain the moments in the form

$$M_x^d = \frac{2\epsilon}{\tan\theta}\int_{-\eta}^{\eta}\int_0^{2\pi}\int_0^1 v_z r^2\cos\phi\, dr d\phi dz \ , \qquad (22a)$$

$$M_y^d = \epsilon\int_{-\eta}^{\eta}\int_0^{2\pi}\int_0^1 v_\phi r^2 dr d\phi dz$$

$$+ \frac{2\epsilon}{\tan\theta}\int_{-\eta}^{\eta}\int_0^{2\pi}\int_0^1 v_z r^2\sin\phi\, dr d\phi dz \ , \qquad (22b)$$

$$M_z^d = M_x^d\tan\theta \ . \qquad (22c)$$

The volume integral approach leads to handy expressions which involve only the radial and azimuthal velocity components. Integration over ϕ reduces the requirements in fact to the knowledge of the aperiodic component of v_ϕ and the simply periodic components of v_z. Therefore, the volume approach can also be applied to the analytical results given above and provides yaw and pitch moments without explicit knowledge of the pressure.

Results for the Liquid Moments

While velocity and pressure fields are primarily of basic fluid mechanical interest, the practical need for the moments dictates the measure for efficiency of the code. The moments derived from the volume approach and the surface approach applied to the same spectral solutions is shown in Tables 1 and 2, respectively. The Reynolds number $Re = 20$ is in the range of maximum despin moment M_z.

Table 1. Volume Approach

$\eta = 4.368$			$\tau = .1667$	$\theta = 20$	Re = 20
K	L	M	M_x	M_y	M_z
3	3	3	0.08305	0.07475	0.03023
4	3	4	0.08260	0.07334	0.03006
5	3	5	0.08300	0.07332	0.03021
5	3	6	0.08317	0.07353	0.03027
6	3	5	0.08300	0.07332	0.03021
6	3	6	0.08317	0.07353	0.03027
4	5	4	0.08280	0.07353	0.03014
5	5	5	0.08322	0.07355	0.03029
6	5	6	0.08340	0.07374	0.03035
6	5	8	0.08335	0.07385	0.03034

It is obvious that the volume approach provides results of superior quality and more rapid convergence. The required (absolute) accuracy of 10^{-3} for engineering applications can be achieved with the low truncation $K = 4$, $L = 3$, $M = 4$. This accuracy has to be seen in the light of considerable uncertainty in the moments governing the exterior aerodynamics of the projectile. We note, however, that an increase in the aspect ratio may require additional expansion functions in axial direction while increasing Reynolds number requires higher resolution in both radial and axial direction. Figure 9 gives the

Table 2. Surface Approach

$\eta = 4.368$			$\tau = .1667$	$\theta = 20$	$Re = 20$
K	L	M	M_x	M_y	M_z
3	3	3	0.07394	0.09396	0.03308
4	3	4	0.07247	0.08133	0.02992
5	3	5	0.07904	0.07291	0.03024
5	3	6	0.08178	0.07039	0.03028
6	3	5	0.07864	0.07354	0.03023
6	3	6	0.08137	0.07115	0.03027
4	5	4	0.07289	0.08354	0.02999
5	5	5	0.07894	0.07703	0.03032
6	5	6	0.08152	0.07491	0.03036
6	5	8	0.08289	0.07415	0.03034

comparison of the roll moments for a wide range of Reynolds numbers with the experimental results of Miller [2] and with computational results.[4, 6] The deviation of the results of the Sandia code[4] is due to using inappropriate formulas for the moments in the nutating coordinate system.[7] The agreement with the other computational data is good. Test runs with high resolution up to $Re = 300$ indicate that the small errors are due to insufficient resolution of the finite-element code [6] in combination with the surface approach for the moments. The experiments were made in a range of spin rates ω between 2000 and 4000 rpm. While $\omega = 3000$ rpm has been used in figure 9, assumption of a lower value would improve the comparison with respect to the maximum values. Figure 10 shows a similar comparison for the yaw and pitch moments. The results of the Sandia code are suppressed since they suffer from a dimensional inconsistency.[7] While the agreement for the yaw moment at high Reynolds numbers is surprisingly good, the deviation in the pitch moment is likely to originate from insufficient resolution of the steep pressure gradients. This source of discretization errors has been eliminated in the results of the spectral code.

The effect of nonlinearity in ϵ on the yaw and pitch moments is shown in Figure 11 for different nutation angles θ at fixed $\tau = 1$ and different values of τ at $\theta = 20°$. The figure shows the ratio of the nonlinear to the linear solution. In absence of nonlinearity all points should be located on the horizontal lines. Yaw and roll moments are largely independent of ϵ. However, the nonlinear effect on the pitch moment is only negligible at small nutation angles θ as they may occur for soft launch conditions and stable projectile flight.

Figure 12 shows the dependence of the yaw and pitch moments per unit length (the roll moment is proportional to M_z) on the aspect ratio of the cylinder and compares with results of the code written by Strikwerda & Nagel.[5, 7] and the analytical results for $\eta \to \infty$. This diagram indicates that a reduction in the overall liquid moments for a given fluid mass can be achieved by splitting the cylindrical volume into slices of low aspect ratio.

Discussion

The codes previously in use may serve for establishing some basic results but are too inefficient (and insufficiently verified) for routine applications. The finite-difference code developed at Sandia Laboratories [3, 4] rests on Chorin's method of artificial compressibility and provides the steady solution at $11 \times 24 \times 21$ grid points in r, ϕ, z-direction by integrating over typically 10^4 to $8 \cdot 10^4$ time steps, a task that requires 6 to 48 minutes of CPU time on a Cray-1S. The result consists of over 22,000 values of the velocities v_r, v_ϕ, v_z and the pressure p.

Strikwerda & Nagel [5] briefly describe a code using finite differences in radial and axial direction and pseudospectral differencing in the azimuthal direction. Nonuniform grids are introduced for increased resolution near the walls. The difference equations are solved by an iterative method based on successive over-relaxation. The computer time required is comparable to that of the Sandia code. A thorough evaluation of the two codes is currently conducted at BRL.[7]

The experience with the present version of the spectral code shows that high performance can be achieved. The solution is obtained in semi-analytical form with only $N = 4 \cdot K \cdot L \cdot M$ (typically less than 500) numerical coefficients. This low data volume is especially attractive for storage and for communication with remote supercomputers. The code is very well suited for vectorization, since practically all CPU time is spent on constructing and solving an algebraic system. The code demands larger memory than other codes, because 64-bit arithmetic is highly recommended for spectral methods in general, and the algebraic system requires $N(N+1)$ words of storage. A run with $N = 500$ requires about 2 Mbyte of memory and can easily be carried out on nowadays engineering workstations within a few minutes. (Most of our work was done on an MC68010-based Apollo DN300 workstation. Runs with $N = 500$ require 160 minutes, while moment calculations with $N = 192$ require less than 3

minutes per point.) Since the memory requirement is acceptable even if higher resolution is desired, the method applied here is a viable alternative in numerous other fluid mechanical problems. The ability to obtain accurate solutions for the steady problem directly from (large) algebraic system bears valuable potential to answer the question whether the steady solution is stable, and allows analysis of unsteady motions with implicit time-stepping. The design of a reliable code for the unsteady problem can take profit from the knowledge of the eigenvalue spectrum for small unsteady disturbances of the steady flow.

While the calculation of velocity and pressure fields provides insight into the physics of the flow, the practical interest in the moments for the quasi-steadily changing parameters in flight simulations can be satisfied with modest amounts of computer time. This is due to using the modified Newton method which updates the Jacobian only when demanded by deteriorating convergence.

In general, the volume approach provides much more accurate results than the surface approach. This is due to the additional smoothing of fluctuating data by integrating over three instead of two space directions and to using fewer, less fluctuating, and more accurate input data. The absence of v_r in the volume formulation is welcome. This velocity component is small over most of the cylinder length but oscillatory in the radial direction (Herbert et al. 1987) with considerable gradients near the wall. Near the end walls, v_r is of the same order as v_z with steep gradients toward the end wall. Inspection of the velocity plots of Vaughn et al.[4] indicates that these gradients were difficult to resolve by the finite difference method. The aperiodic component of v_ϕ is a relatively small streaming term of smooth and almost uniform behavior along the cylinder axis. The large azimuthally periodic components of v_ϕ near the end walls do not affect the moment calculation.

Probably the greatest advantage of the volume formulation is the absence of the pressure from the moment equations. This property favors the use of pressure-free sets of basic equations, e. g. in terms of vorticity or vector potential. The smaller number of dependent variables can be exploited for further increasing the efficiency. Even in natural variable formulations, the pressure is difficult to obtain with high accuracy because of the invalidity of the equations in the corners joining the flat end walls to the cylindrical side wall. As shown in Figure 3, the pressure may assume extrema and vary strongly near the corners and, therefore, inaccuracies in this region may influence yaw and pitch moments. In this context, it is instructive to evaluate the convergence history of the artificially time-dependent method implemented in the Sandia code.[3] While the velocity rapidly reaches a quasi-steady state, about 75% of the iterations are spent on improving the pressure field. We estimate that by use of the volume approach equivalent or superior values for the moments could be obtained with less than 20% of the iterations. It is worthwhile to note that the analytical results of Rosenblat et al.,[6] and equations (21) for the moments are valid for closed containers of more general shape and thus can be used for other interior flow problems.

ACKNOWLEDGMENT

The discussions with S. Rosenblat and M. Nusca are greatly appreciated. Both made results available prior to publication. The technical monitor of this project, M. C. Miller deserves our gratitude for his sustained interest and the support of this work by the U. S. Army AMCCOM under Contract DAAA15-85-K-0012.

REFERENCES

1. R. Sedney 1985 "A Survey of the fluid dynamic aspects of liquid-filled projectiles," AIAA Paper No. 85-1822-CP.

2. M. C. Miller 1982 "Flight instabilities of spinning projectiles having nonrigid payloads," *J. Guidance, Control, and Dynamics*, vol. 5, pp. 151-157.

3. H. R. Vaughn, W. L. Oberkampf, and W. P. Wolfe 1983 "Numerical solution for a spinning nutating fluid-filled cylinder," Sandia Report SAND 83-1789.

4. H. R. Vaughn, W. L. Oberkampf, and W. P. Wolfe 1985 "Fluid motion inside a spinning nutating cylinder," *J. Fluid Mech.*, vol. 150, pp. 121-138.

5. J. C. Strikwerda and Y. M. Nagel 1985 "A numerical method for computing the flow in rotating and coning fluid-filled cylinders," in *Proc. 1984 Scientific Conf. on Chemical Defense Research, Aberdeen Proving Ground, Maryland*, ed. M. Rausa, pp. 523-527, CRDC-SP-85006.

6. S. Rosenblat, A. Gooding, and M. S. Engleman 1986 "Finite-element calculations of viscoelastic fluid flow in a spinning and nutating cylinder," Chemical Research, Development &

Engineering Center, Report CRDEC-CR-87021.

7. M. J. Nusca and W. P. D'Amico 1986 "Parametric Study of Low Reynolds number processing/spinning incompressible flow," Ballistic Research Laboratory, Interim Memorandum Report BRL-IMR-881.

8. H. R. Vaughn, W. P. Wolfe, and W. J. Oberkampf 1985 "Six degree of freedom simulation of fluid payload projectiles using numerically computed fluid moments," Sandia Report SAND 85-1166.

9. Th. Herbert 1986 "Viscous fluid motion in a spinning and nutating cylinder," *J. Fluid Mech.*, vol. 167, pp. 181-198.

10. Th. Herbert, R. H. Li, and S. D. Greco 1987 "Perturbation analysis of the viscous flow in a spinning and nutating cylinder of large aspect ratio," *J. Fluid Mech.* In preparation.

11. Th. Herbert 1986 "Analytical and computational studies of the fluid motion in liquid-filled shells," in *Proc. 4th Army Conf. on Appl. Math. and Computing, Ithaca, New York, 1986.* To appear.

12. Th. Herbert 1986 "A spectral Navier-Stokes solver for the flow in a spinning and nutating cylinder," Proc. 1986 Scientific Conf. on Chemical Defense Research, Aberdeen Proving Ground, Maryland. To appear.

13. R. H. Li and Th. Herbert 1987 "Calculation of the liquid moments in a spinning and nutating cylinder," *Int. J. Num. Meth. Fluids.* In preparation.

14. Th. Herbert 1987 "On the spurious pressure in spectral solutions of the Navier-Stokes equations in domains with corners," *Computers & Fluids.* In preparation.

15. Th. Herbert and D. Pierpont 1986 "Visualization of the flow in a spinning and nutating cylinder," in *Proc. 1985 Scientific Conf. on Chemical Defense Research*, ed. M. Rausa, pp. 989-994, Aberdeen Proving Ground, MD.

16. M. C. Miller 1981 "Void characteristics of a liquid filled cylinder undergoing spinning and nutating motion," *J. Spacecraft Rockets*, vol. 18, pp. 286-288.

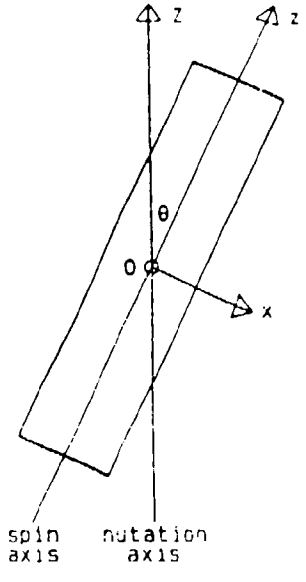

Figure 1. Definition sketch.

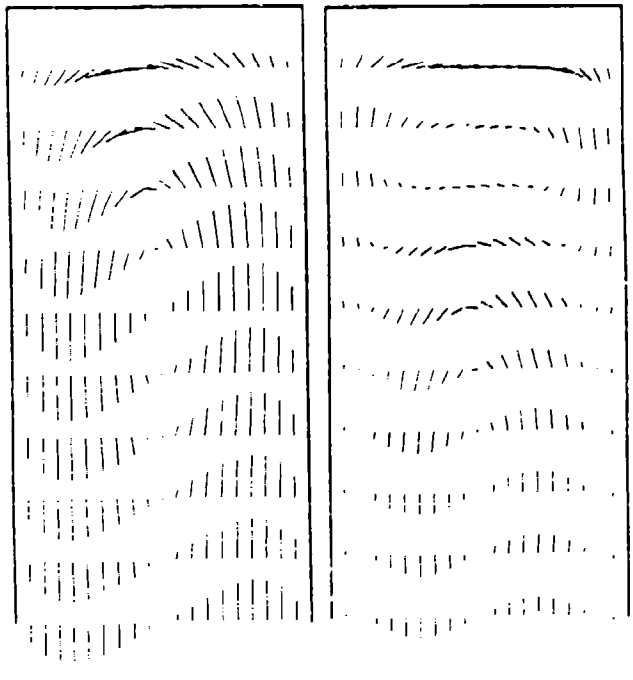

Figure 2. Vector plot of the axial and radial velocities in the planes $\phi = 45°$ (left, scale 0.0375) and $\phi = 135°$ (right, scale 0.0375) at $Re = 20$ for $z \geq 0$.

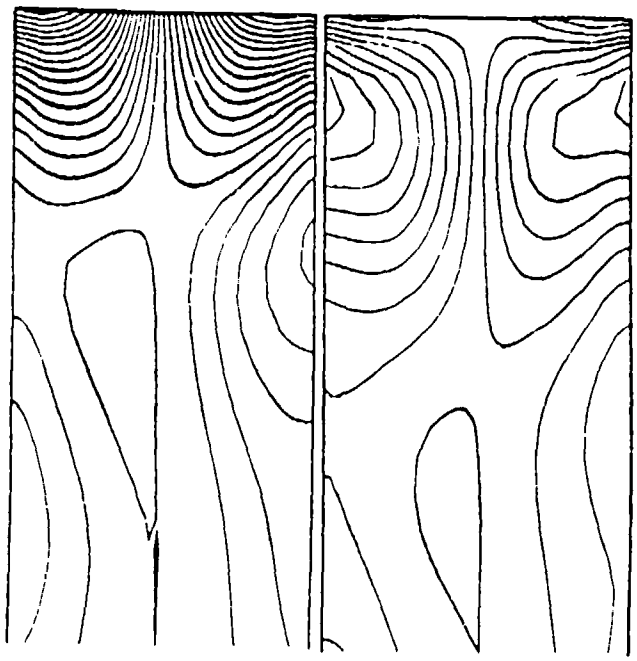

Figure 3. Contour plot of the pressure field in the planes $\phi = 45°$ (left) and and $\phi = 135°$ (right) at $Re = 20$ for $z \geq 0$. Levels every 0.0025.

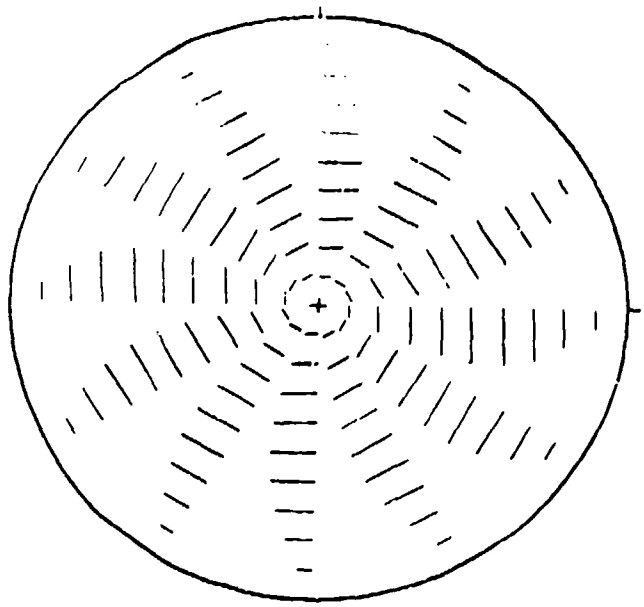

Figure 4. Vector plot of the azimuthal velocity v_ϕ in the center plane at $z = 0$, $Re = 20$. Scale 0.003.

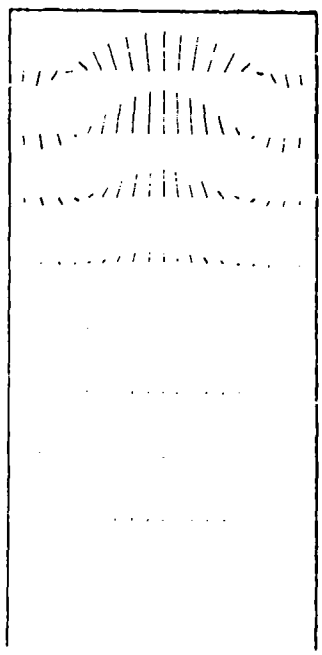

Figure 5. Vector plot of the axial and radial mean velocity v_ϕ for $Re = 20$. Scale 0.002.

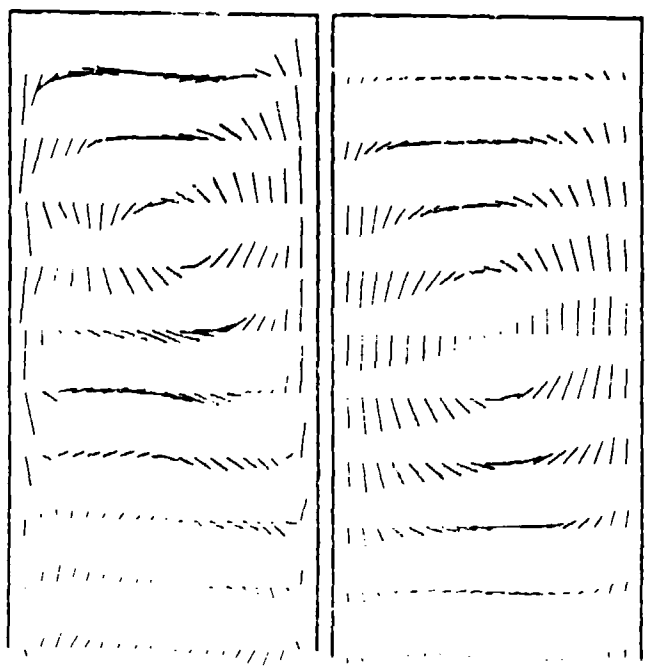

Figure 6. Vector plot of the axial and radial velocities in the planes $\phi = 0°$ (left, scale 0.05) and $\phi = 90°$ (right, scale 0.2) at $Re = 300$ for $z \geq 0$.

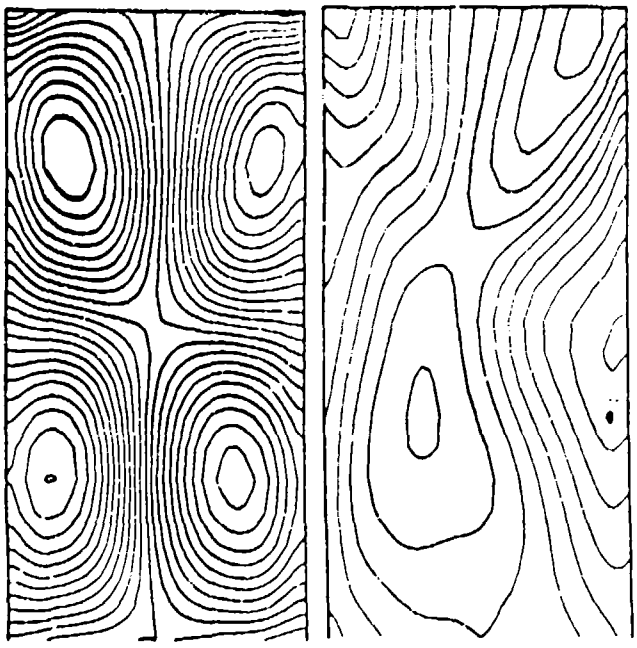

Figure 7. Contour plot of the pressure field in the planes $\phi = 0°$ (left) and and $\phi = 90°$ (right) at $Re = 300$ for $z \geq 0$. Levels every 0.005.

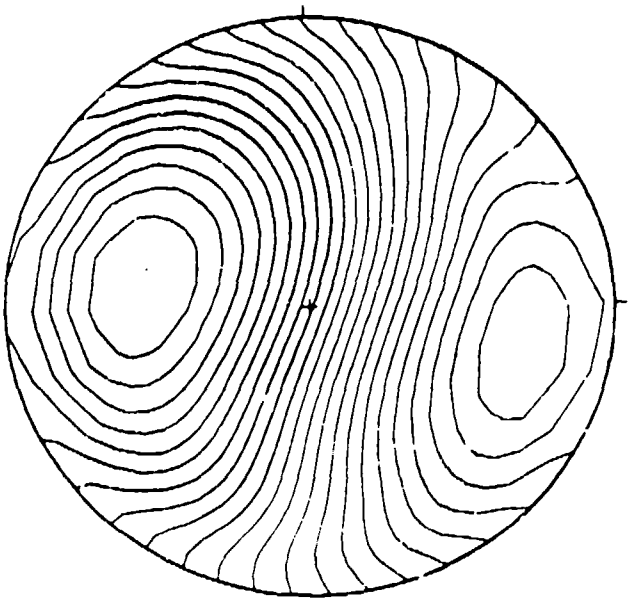

Figure 8. Contour plot of the pressure filled in the plane $z = 0.25$ at Re $= 300$. Levels every 0.005.

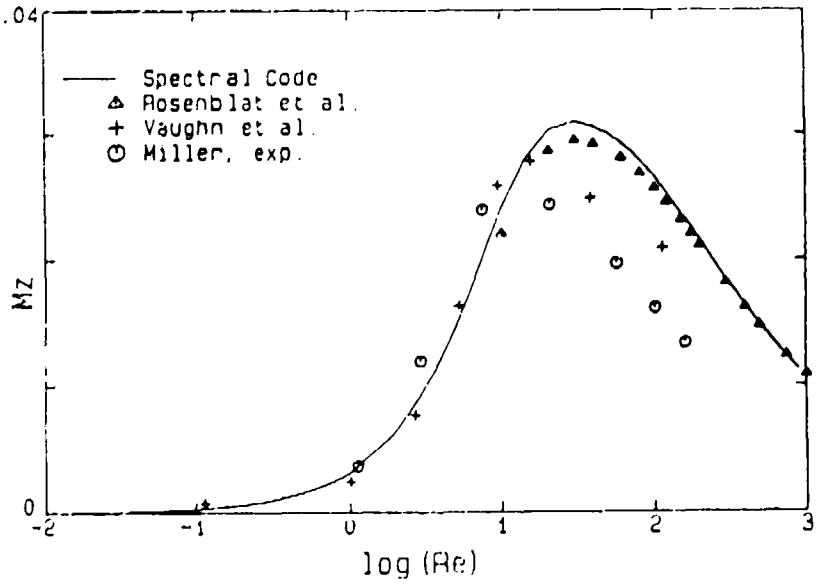

Figure 9. Roll moment M_z vs Reynolds number Re for $\eta = 4.368$, $\tau = 0.16667$, and $\theta = 20°$. Comparison with numerical and experimental data.

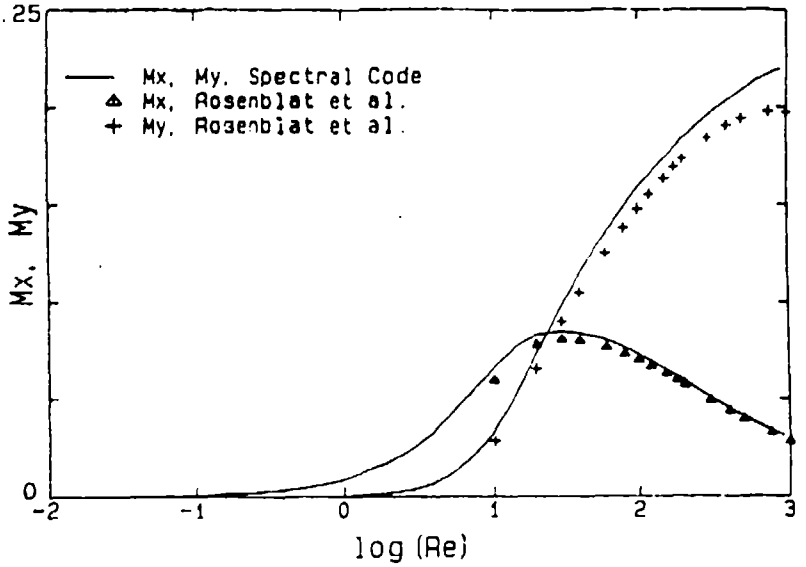

Figure 10. Yaw moment M_z and pitch moment M_y vs. Reynolds number Re for $\eta = 4.368$, $\tau = 0.16667$, and $\theta = 20°$. Comparison with numerical data.

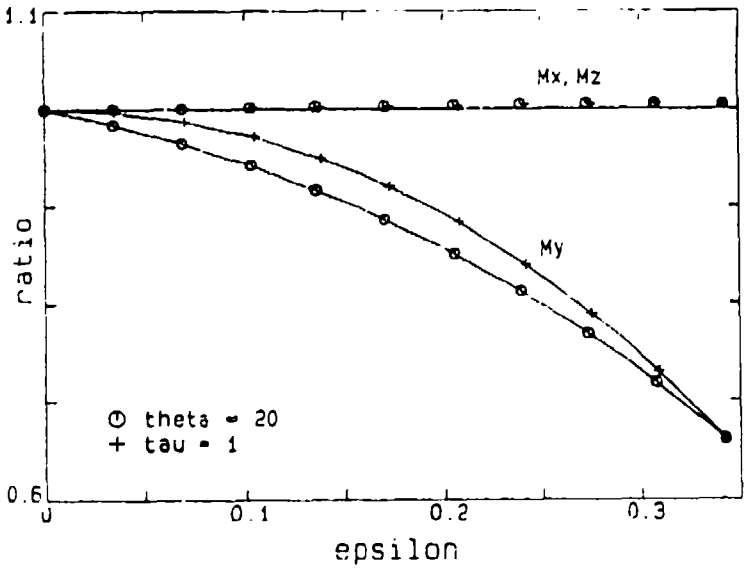

Figure 11. Ratios of nonlinear to linear solutions for the moments at $Re = 20$, $\eta = 4.368$.

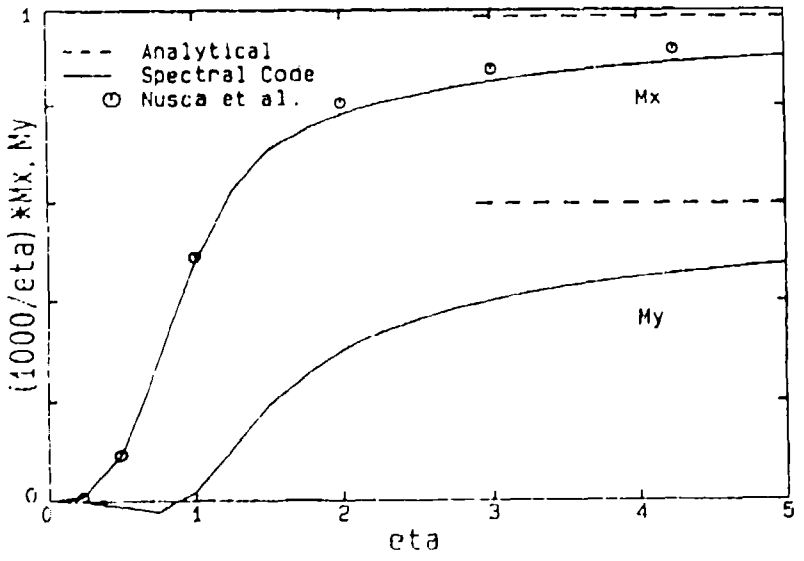

Figure 12. Yaw moment M_z and pitch moment M_y per unit length vs. aspect ratio η at $Re = 10$, $\tau = 0.123$, and $\theta = 2°$. Comparison of present numerical results with analytical results for $\eta \to \infty$ and data obtained by Nusca with Strikwerda's code.

BLANK

APPENDIX E

FLIGHT SIMULATION FOR LIQUID-FILLED PROJECTILES

By

Thorwald Herbert

FLIGHT SIMULATION FOR LIQUID-FILLED PROJECTILES

Thorwald Herbert

Department of Mechanical Engineering
Department of Aeronautics and Astronautics
The Ohio State University,
Columbus, Ohio 43210

ABSTRACT

The fluid motion in a liquid-filled payload container can jeopardize the stable flight of spin-stabilized projectiles. We have developed analytical solutions to obtain estimates and an efficient numerical (spectral) method to calculate accurate values of the moments exerted by the liquid on the projectile. These moments have been incorporated into a modified version of the numerical flight simulator suggested by Vaughn, Oberkampf & Wolfe. Prototype flights with liquid versus solid payload verify the destabilizing effect of the liquid payload and are consistent with field tests. Moreover, we demonstrate that such flight simulations can be expedited on today's engineering work stations.

1. Introduction

Well-designed spin-stabilized projectiles can exhibit a severe flight instability if they carry a liquid payload. Two types of such instability can be excited by the coning motion of the projectile about the trajectory.[1] The first type originates from resonance with inertial waves at critical frequencies (ratios of coning rate Ω to spin rate ω). This resonance is most pronounced for low-viscosity liquid fills, i.e. at high Reynolds numbers, and depends sensitively on the cylinder's aspect ratio. Theoretical analysis involving the boundary-layer approximation provides design criteria for sufficiently large Reynolds numbers, $R > 1000$, say. We define the Reynolds number by $R = \rho\omega a^2/\mu$, where ρ is the density, a the radius of the cylindrical cavity, and μ the viscosity. The second type of instability is of essentially viscous nature and occurs at low and medium Reynolds numbers for a wide range of aspect ratios and frequencies. Theoretical analysis must be based on the Navier-Stokes equations. For a wide range of Reynolds numbers, both types of instability may appear simultaneously.

To enable the design of reliable projectiles, the effects of the liquid payload must be analyzed and incorporated into the design tools such as the numerical flight simulators. A prototype flight simulator (FFS6DOF) has been developed by Vaughn et al.[2] by integrating a table of liquid moments into a six-degree-of-freedom code. The moments were computed with a Navier-Stokes solver (FFS6).[3,4] The computational demands of this two-level code prevent application in practice.

In the following we describe two more efficient procedures to obtain the liquid moments for integration into flight simulations. The first method rests on quick estimates of the moments from analytical solutions, the second efficiently calculates accurate moments in a

wide range of Reynolds numbers by means of a spectral Navier-Stokes code. The development of a new method for calculating the moments was essential in achieving these goals. One of the flights studied by Vaughn et al.[2] is used as an example to show some shortcomings of the earlier approach and to demonstrate the feasibility of flight simulations for liquid-filled shells on engineering work stations.

2. Approximate Solutions

In earlier work,[5,6] we have reported results of a perturbation analysis of the nonlinear problem for the deviation of the velocity from rigid-body rotation in a finite segment of an infinite cylinder. The expansion parameter is $\epsilon = (\Omega/\omega)\sin\theta$, where θ is the coning angle. At the linear level, $O(\epsilon)$, we obtain a purely axial flow in the form $v_{z1} = -2\epsilon\,\mathrm{Im}\{[I_1(\alpha r)/I_1(\alpha) - r]e^{i\phi}\}$ where I_1 denotes the modified Bessel function, $\alpha = (1-i)(R/2)^{1/2}$, and the azimuthal angle ϕ is measured from the plane of the two axes of rotation. This component v_{z1} is the dominating feature of the flow in a long cylinder. The second order terms, $O(\epsilon^2)$, were also obtained in analytical form. Of these terms, only the aperiodic component of the azimuthal velocity is relevant to the moments. This component turns out to be proportional to the component of v_{z1} in the plane $\phi = \pi/2$, $v_{\phi 0} = -2\epsilon^2\,\mathrm{Re}\{I_1(\alpha r)I_1(\alpha) - r\}$. This solution is valid for arbitrary Reynolds number. Owing to the neglect of the end walls, however, this analytical result is expected to be a reasonable approximation only for cylinders of sufficiently large aspect ratio.

3. Spectral Navier-Stokes Code

To calculate the deviation of velocity field, pressure field, and moments from solid-body motion in a wide range of parameters for finite-length cylinders, we have developed a fully spectral code [7] for solving the Navier-Stokes equations. The code uses Fourier series in the azimuthal direction and combinations of Chebyshev polynomials in the radial and axial directions. The combinations are chosen such that the no-penetration and no-slip boundary conditions are implicitly satisfied. By appropriate choice of even or odd polynomials, we avoid singularities on the axis and implement the symmetries of the solution in the upper and lower half cylinder. Gauss-Lobatto points are used for collocation such that no points are located on the surface nor the axis. This choice avoids the occurrence of spurious pressure terms associated with the corners of the domain and solves the axis problem in an elegant way.

The solution procedure consists of two basic elements, the first of which rests on a linearization of the Navier-Stokes equations about some known solution $\hat{\mathbf{v}}^d$. This 'known' solution may be $\hat{\mathbf{v}}^d \equiv 0$, or in general, a solution previously obtained for neighboring parameters. The collocation method converts the linear partial differential equations into a linear algebraic system of dimension $N = 4KLM$ for the coefficients of the natural variables v_r^d, v_ϕ^d, v_z^d, and p^d. The numbers K, L, M of expansion functions in radial, azimuthal, and axial direction, respectively, govern the accuracy of the approximation.

The second element of the procedure utilizes the modified Newton method for solving the nonlinear problem. In the modified form, the Jacobian is not updated in every step but only when necessary. The need to recalculate the Jacobian is detected by a simple algorithm that monitors the rate of convergence. This strategy is especially suited for flight simulations where the parameters vary slowly with the flight time.

4. Volume Integrals for the Moments

In earlier work,[3, 2, 8, 9] the moments are calculated by integration of normal and tangential stresses acting at the inside wall of the cylinder. This 'surface approach' derives the moments from the pressure and the velocity gradients at the wall. These values are difficult to obtain with good accuracy. Li & Herbert [10] have developed a new formulation for the moments which rests on volume integrals. The nondimensional moment coefficients can be shown to take the form

$$M_z^d = \frac{2\epsilon}{\tan\theta} \int_{-\eta}^{\eta} \int_0^{2\pi} \int_0^1 v_z\, r^2 \cos\phi \, dr d\phi \, dz \;, \quad M_z^d = M_z^d \tan\theta \;,$$

$$M_y^d = \epsilon \int_{-\eta}^{\eta} \int_0^{2\pi} \int_0^1 v_\phi r^2 dr d\phi \, dz + \frac{2\epsilon}{\tan\theta} \int_{-\eta}^{\eta} \int_0^{2\pi} \int_0^1 v_z\, r^2 \sin\phi \, dr d\phi \, dz \;,$$

where η is the cylinder's aspect ratio. The reference moment is $\rho\omega^2 a^5$. The volume integral approach involves only the radial and azimuthal velocity components. Integration over $d\phi$ reduces the requirements to the knowledge of the aperiodic component $v_{\phi 0}$ of v_ϕ and the simply periodic component v_{z1} of v_z. Therefore, the volume approach can also be applied to the analytical results given above and provides yaw and pitch moments without explicit knowledge of the pressure.

5. Results for the Liquid Moments

While the accurate description of velocity and pressure at higher Reynolds numbers requires many expansion functions, the smoothing of small oscillations by the volume approach allows calculation of the moments from crude approximations. The (absolute) accuracy of 10^{-3} for engineering applications can be achieved with spectral approximations as low as $K = 4$, $L = 3$, $M = 4$. The accuracy has to be seen in the light of considerable uncertainty in the moments governing the exterior aerodynamics of the projectile. We note, however, that large aspect ratios may require additional expansion functions in axial direction while increasing Reynolds number in general requires higher resolution in both radial and axial direction.

Figure 1 shows the comparison of numerical results for the yaw and pitch moments. The roll moment is proportional to the yaw moment. While the agreement for the yaw moment at high Reynolds numbers is surprisingly good, the deviation in the pitch moment is likely to originate from insufficient resolution of the steep pressure gradients in the finite-element code.[9] The effect of discretization errors has been reduced in the results of the spectral code by use of the volume integrals for the moments. Figure 2 compares the analytical estimates for yaw and pitch moments with the numerical results of the spectral code. Some systematic deviations exist, but the quantitative and qualitative features are very similar. The computational effort for the analytical results is negligible.

6. A Prototype Flight

We have used the flight of an M483 projectile as described by Vaughn et al.[2] as a test case for verifying the function of our version of the flight simulator, for studying the effect of the improved moments in comparison with earlier work, and for evaluating the different concepts of incorporating the fluid moments. Some erratic behavior of the original code FFS6DOF under extreme flight conditions will be cultivated in a future version.

Two options have been considered for incorporating the liquid moments. The first way utilizes a table of moments and linear interpolation, as the original code. Alternatively, the moments are calculated by a subroutine which is called whenever the parameters vary beyond some threshold. The latter approach avoids the error introduced by linear interpolation on a coarse grid and is especially efficient for stable flights after an initial transient period after launch. For systematic studies of different launch conditions for a given shell, however, the precalculated table seems more appropriate and the efficiency of the spectral code permits use of finer grids. Some accuracy can also be gained by improving the interpolation.

Our computational work has been performed on a Sun 3/140 work station with floating point accelerator. Simulation of a typical flight (32 seconds flight time) requires 12 minutes if the liquid-moment table is precalculated. Generation of this table from the analytical solution requires less than 10 seconds. Incorporation of the analytical estimates by subroutine contributes a negligible increase in the simulation time. Precalculation of the $9 \times 8 \times 8$ moment table with $K = 4$, $L = 3$, and $M = 4$ requires less than 2 hours, although the sequence of the calculations has not yet been optimized. This sequence is relevant when using the modified Newton method.

In the following cases, we keep all parameters at the values specified by Vaughn et al.[2] except the pitch rate at launch. The initial data for the flight simulation - angle and pitch rate at the muzzle - are difficult to determine and may vary between flights. An initial pitch rate of -1.946 rad/s was chosen by Vaughn et al. to match the observed flight behavior,[11] in particular the truncated flight time of approximately 26 seconds. Figure 3a shows the history of the aeroballistic angle of attack for a solid payload (with all liquid moments set to zero) that represents the 'normal' flight of a projectile of this type. The results of Vaughn et al. (ref. 2, figure 3) for a liquid payload are reproduced with our version of the code in Figure 3b. Figure 3c shows the result for the same initial conditions with the liquid moments calculated by the spectral code. Use of the analytical estimates leads to an almost identical picture. With the correct moments, the flight is essentially stable, with some high-frequency motion over the whole flight time. The liquid payload does not prevent the shell from achieving the full flight time or distance.

When using the correct moments, we observe the flight time reported by Vaughn et al.[2] and observed in the field tests [11] with initial pitch rates in excess of -3.5 rad/s as shown in Figure 4a. Under the given transonic launch conditions, this pitch rate appears very realistic (D'Amico, personal communication). Simulation of the same flight using the analytical estimates for the moments leads to earlier onset of the instability, as shown in Figure 4b. A flight time of 26 seconds is obtained with the lower initial pitch rate of -3.2 rad/s. Since the use of the analytical estimates predicts less stable behavior, the estimates can be used for a first conservative check of the design.

7. Summary

We have developed analytical solutions for the liquid moments which allow quick and conservative estimates on the flight instability of liquid-filled shells. For more accurate studies, the liquid moments can be generated with a spectral Navier-Stokes solver for Reynolds numbers in the range $R \leq 1000$. While the analytical results predict only the viscous flight instability, the Navier-Stokes solutions incorporate both, viscous flight instability and instability due to resonance with inertial waves.

The computation of the table of liquid moments in the most critical range of Reynolds numbers, $R \leq 100$, requires less than two hours on an engineering work station Sun 3/140 FPA. The flight simulation runs at approximately 25 times real time, typically 12 minutes. These data clearly show that the liquid moments can be incorporated into the flight simulations for practical applications.

ACKNOWLEDGMENT

The assistance of Dr. Rihua Li in the analytical and numerical work is greatly appreciated. Dr. Walter Wolfe of Sandia National Laboratories provided the code FFS6DOF, data, and assistance in porting the flight simulator to our computer environment. I am grateful for his cooperation. This work is supported by the U. S. Army AMCCOM under Contract DAAA15-85-K-0012.

References

1. R. Sedney, "A Survey of the fluid dynamic aspects of liquid-filled projectiles," AIAA Paper No. 85-1822-CP, 1985.
2. H. R. Vaughn, W. P. Wolfe, and W. L. Oberkampf, "Six degree of freedom simulation of fluid payload projectiles using numerically computed fluid moments," Sandia Report SAND 85-1166, 1985.
3. H. R. Vaughn, W. L. Oberkampf, and W. P. Wolfe, "Numerical solution for a spinning nutating fluid-filled cylinder," Sandia Report SAND 83-1789, 1983.
4. H. R. Vaughn, W. L. Oberkampf, and W. P Wolfe, "Fluid motion inside a spinning nutating cylinder," *J. Fluid Mech.*, vol. 150, pp. 121-138, 1985.
5. Th. Herbert, "Viscous fluid motion in a spinning and nutating cylinder," *J. Fluid Mech.*, vol. 167, pp. 181-198, 1986.
6. Th. Herbert, R. H. Li, and S. D. Greco, "Perturbation analysis of the viscous flow in a spinning and nutating cylinder of large aspect ratio," *J. Fluid Mech.*, 1987. In preparation
7. Th. Herbert and R. H. Li, "Numerical study of the flow in a spinning and nutating cylinder," AIAA Paper No. 87-1445, 1987.
8. J. C. Strikwerda and Y. M. Nagel, "A numerical method for computing the flow in rotating and coning fluid-filled cylinders," in *Proc. 1984 Scientific Conf. on Chemical Defense Research, Aberdeen Proving Ground, Maryland*, ed. M. Rausa, pp. 523-527, CRDC-SP-85006, 1985.
9. S. Rosenblat, A. Gooding, and M. S. Engleman, "Finite-elemet calculations of viscoelastic fluid flow in a spinning and nutating cylinder," Chemical Research, Development & Engineering Center, Report CRDEC-CR-87021, 1986.
10. R. H. Li and Th. Herbert, "Calculation of the liquid moments in a spinning and nutating cylinder," *Int. J. Num. Meth. Fluids*, 1987. In preparation.
11. W. P. D'Amico and W. H. Clay, "High viscosity liquid payload yawsonde data for small launch yaws," Ballistic Research Laboratory, Memorandum Report ARBRL-MR-03029, 1980.

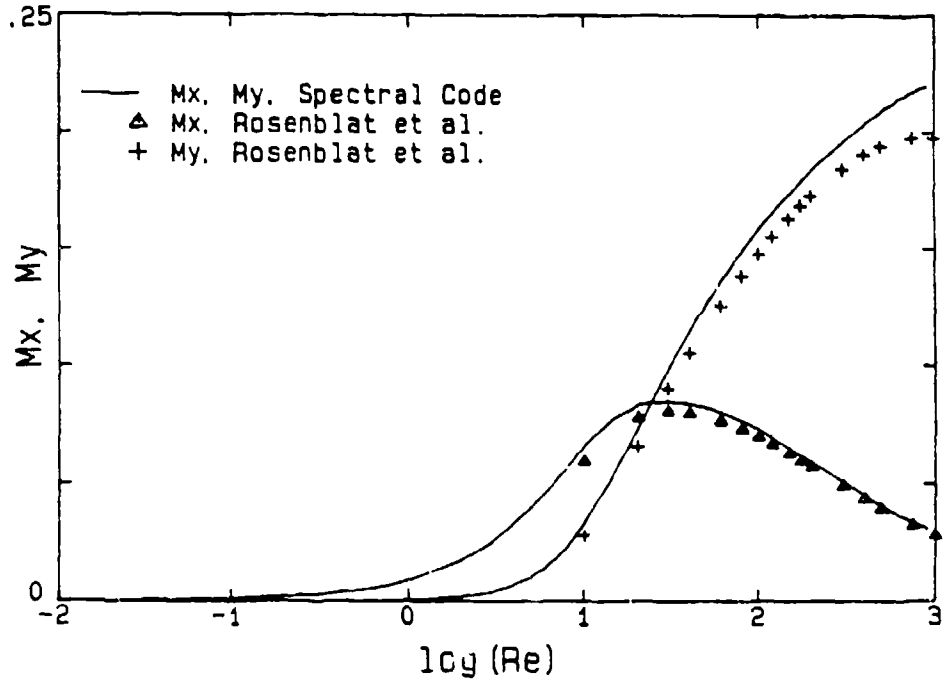

Figure 1. Yaw moment M_x and pitch moment M_y vs. Reynolds number R for $\eta = 4.368$, $\tau = 0.16667$, and $\theta = 20^\circ$. Comparison between numerical data.

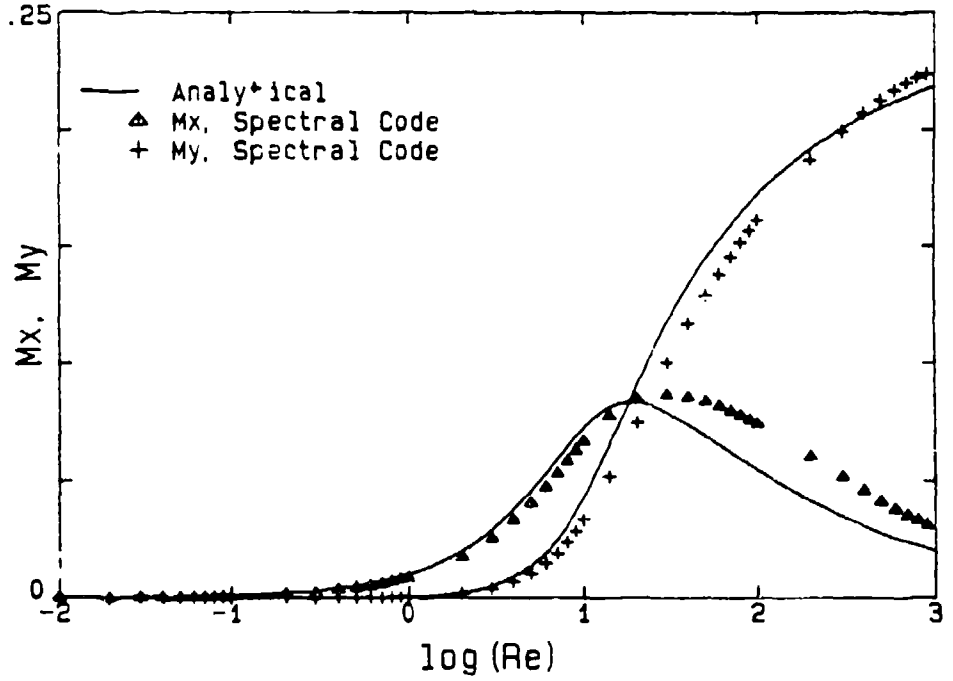

Figure 2. Yaw moment M_x and pitch moment M_y vs. Reynolds number R for $\eta = 4.368$, $\tau = 0.16667$, and $\theta = 20^\circ$. Comparison between analytical and numerical data.

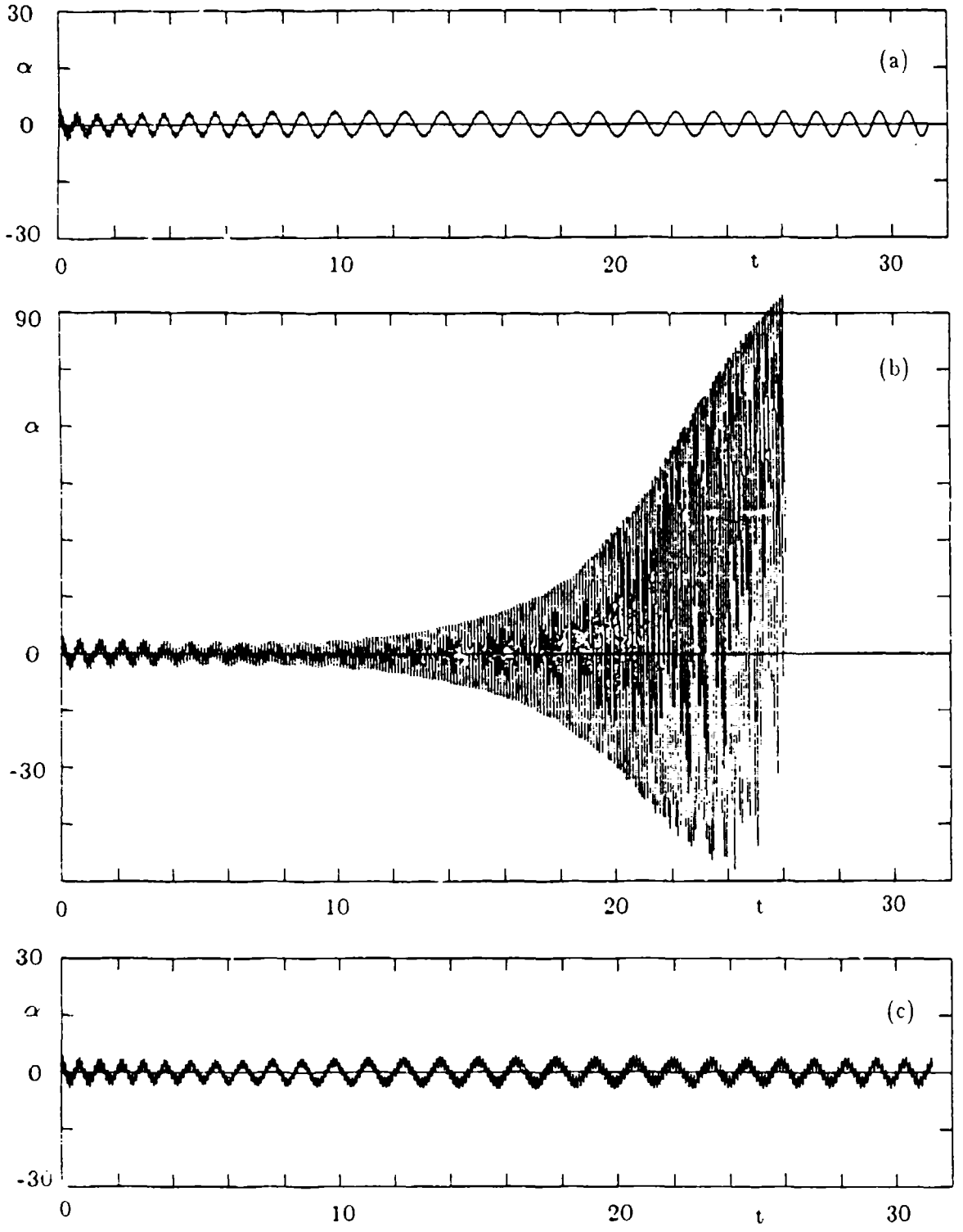

Figure 3. Aeroballistic angle of attack as a function of the time of flight. Initial pitch rate -1.946 rad/s. (a) Solid payload. (b) Liquid payload. Table of liquid moments produced by the code FFS6 of Vaughn et al. (c) Liquid payload. Table of liquid moments from spectral code.

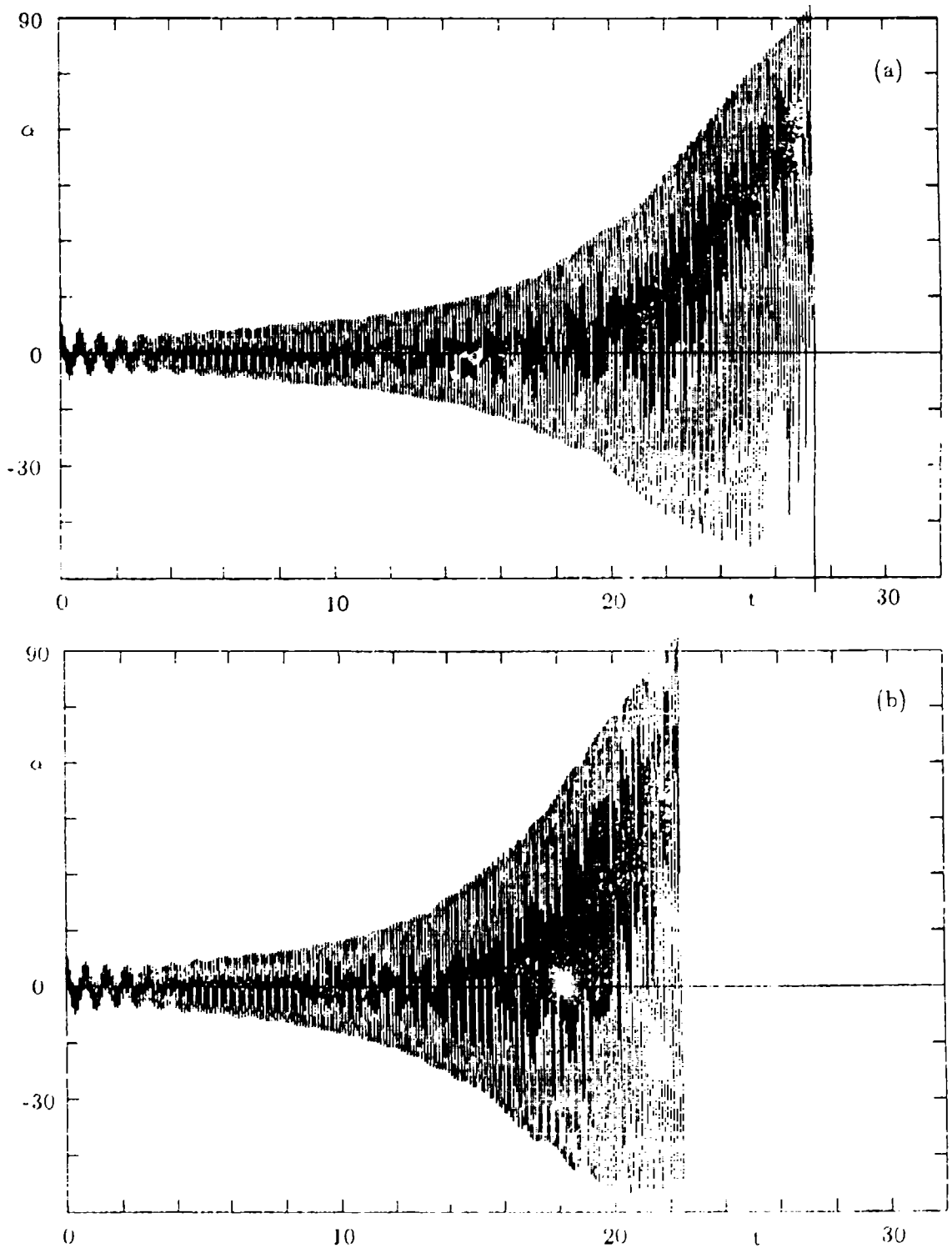

Figure 4. Aeroballistic angle of attack as a function of the time of flight. Liquid payload. Initial pitch rate -3.5 rad/s. (a) Table of liquid moments from spectral code. (b) Table of liquid moments from analytical estimates.

BLANK

APPENDIX F

COMPUTATIONAL STUDY OF THE FLOW IN A SPINNING AND NUTATING CYLINDER

By

Thorwald Herbert
Rihua Li

ABSTRACT

Artillery shells with liquid payloads may experience a severe flight instability owing to the moments exerted by the viscous fluid motion in the cylindrical payload container. Incorporation of these moments into flight simulations as a routine design tool requires a highly efficient code for solving the Navier-Stokes equations. We describe a spectral collocation method which is based on Chebyshev-Fourier-Chebyshev expansions in the radial, azimuthal, and axial direction. The method exploits the symmetries of the problem. Using a volume approach and an analytical result by Rosenblat, accurate moments are obtained in small fractions of the time required by other codes. Solutions for the steady motion are presented and compared with numerical and experimental data.

Introduction

Gyros and rotating fluids often exhibit unexpected behavior. In the past, it has been recognized that spin-stabilized shells with liquid payloads can suffer a dynamical instability originating from resonance with inertial waves.[1] Since this phenomenon is basically inviscid and is routinely avoided by proper design, it was surprising to observe in some cases another type of instability which is characterized by an increase in nutation (or yaw) angle and a simultaneous loss in spin rate. The rapid drop in spin rate is clearly a viscous phenomenon, and laboratory experiments, computational results, and field tests have meanwhile shown that this instability is caused by the nutation-induced fluid motion in a certain range of relatively small Reynolds numbers. Although in special cases this instability has been overcome by trial and error, future design of reliable projectiles would take profit from the opportunity to calculate the liquid moments and to account for these moments in flight simulations. The empirical data base [2] is sparse, however, and the computational methods in use [3, 4, 5, 6] are rather demanding. An evaluation and verification of the codes by Vaughn et al.[4] and Strikwerda & Nagel [5] is currently conducted at BRL.[7] Typical computer times for a single case are in the range of 6-12 hours on VAX-class machines. Six-degree-of-freedom flight simulations [8] typically use $2 \cdot 10^5$ time steps over the

flight time of the order of 30 seconds. Study of the interaction of the interior fluid motion with the exterior aeroballistics consequently requires either a very fast subroutine for calculating the liquid moments or interpolation in a multi-dimensional table of 500 - 1000 [8] precalculated values. Hence, flight simulations for liquid-filled shells are currently a very expensive tool and are not ready for routine applications.

In previous work,[9] we conducted a theoretical analysis which aimed at the origin of the viscous despin (negative roll) moment in cylinders of large aspect ratio. This analysis showed that the deviation from solid-body rotation is governed by a small parameter, $\epsilon = (\Omega/\omega)\sin\theta$, involving the nutation rate Ω, the nutation angle θ, and the spin rate ω. A solution of the linearized equations was developed for a finite-length segment of an infinitely long cylinder, i. e. disregarding the end walls of the cylinder. Velocity field and the viscous components of the moments were obtained in closed form. The velocity field consists only of an axial component of order $O(\epsilon)$ which is the prominent feature of the fluid motion in slender cylinders and produces a negative roll moment of order $O(\epsilon^2)$ owing to Coriolis forces. Although this roll moment is in reasonable agreement with experimental and computational data, the original analysis accounted only for the viscous part of the yaw and pitch moments. These latter moments contain essential contributions of the pressure [4] that originate from the turning of the flow near the end walls and were not captured by the linear analysis. The effect of nonlinearity was studied [10] by using perturbation expansions in ϵ and was found to be small except for an aperiodic streaming term in the azimuthal direction.

Whereas the pressure field cannot be captured by the perturbation approach, it provided valuable insight into the structure of equations and solution. The analytical work suggests the use of a numerical method that exploits (i) the near-linearity of the governing equations and (ii) the smoothness of the solution in the relevant range of Reynolds numbers. We have therefore pursued a simple concept that is open to further refinements. We use Chebyshev-Fourier-Chebyshev expansions in r, ϕ, z, respectively, and convert the linearized

equations into an algebraic system for the expansion coefficients. Linearization can be performed about the trivial solution or any other known solution, e. g. at neighboring parameters. The solution of the linear algebraic system is used as initial approximation for iterative improvement by the modified Newton method. The feasibility of this approach has been demonstrated [11] with a crude spectral approximation to the solution. Problems in calculating the pressure that arise from the invalidity of the basic equations along the joint of the flat end walls to the cylindrical side wall have meanwhile been overcome.[12] The present version of the code exploits the diametral symmetry of the flow about the center of the cylinder and allows for higher resolution at modest CPU times. This version can also be adapted for the analysis of unsteady problems. Dramatic increase in efficiency has recently been achieved [13] by combining an analytical result of Rosenblat et al.[6] with a volume formulation for calculating the liquid moments. The moments can be obtained from only the simply periodic components of the axial velocity and the azimuthal streaming term. A fast subroutine for flight simulations exploits the analytical results. For more accurate studies, complete tables of moments can be calculated in a few hours on an engineering workstation.

Governing Equations

We consider the steady motion of a fluid of density ρ and viscosity μ in a cylinder of radius a and length $2c$ in an aeroballistic coordinate system x, y, z, where z is the axis of the cylinder, as shown in Figure 1. The inertial axis Z in flight direction and the z-axis enclose the nutation angle θ. The cylinder rotates with the spin rate ω about z while the x, z-plane rotates with the nutation rate Ω about the Z-axis. Spin rate ω and nutation rate Ω are constant. All quantities are made nondimensional using a, ω, and ρ for scaling length, time, and mass, respectively. The solution depends on four nondimensional parameters: aspect ratio $\eta = c/a$, nutation angle θ, frequency $\tau = \Omega/\omega$, and Reynolds number $Re = \rho\omega a^2/\mu$. The aspect ratio enters the solution only through the boundary conditions at the end walls of the cylinder. The motion is subject to

the no-slip and no-penetration conditions at the cylinder walls. Since the velocity field degenerates for either $\omega = 0$, $\Omega = 0$, $\theta = 0$, or $\mu \to \infty$ to rigid-body rotation of the fluid, it is appropriate to concentrate on the deviation $\mathbf{v}^d$ of the velocity from rigid-body rotation,

$$\mathbf{v} = \mathbf{v}^r + \mathbf{v}^d \ , \ \mathbf{v}^r = r\,\mathbf{e}_\phi \tag{1a,b}$$

where $\mathbf{e}_\phi$ is the azimuthal unit vector. The boundary conditions on $\mathbf{v}^d$ are homogeneous. The pressure field is split according to

$$p = p^r + p^d \ , \ p^r = r^2(1+\tau_z)^2 + r^2\tau_\phi^2 + z^2\epsilon^2 - 2rz\,\epsilon\tau_r \tag{2a,b}$$

where $\tau_r = -\epsilon\cos\phi$, $\tau_\phi = \epsilon\sin\phi$, $\tau_z = \tau\cos\theta$, $\epsilon = \tau\sin\theta$. The pressure p^r differs from the pressure in rigid-body rotation. The form of p^r is chosen such that the reduced pressure p^d appears only in the z-momentum equation.

In cylindrical coordinates r, ϕ, z, the equations for the velocity components $\mathbf{v}^d = (v_r, v_\phi, v_z)$ and pressure p^d take the form

$$\frac{1}{r}\frac{\partial}{\partial r}(rv_r) + \frac{1}{r}\frac{\partial v_\phi}{\partial \phi} + \frac{\partial v_z}{\partial z} = 0 \tag{3a}$$

$$D'v_r - \frac{v_\phi^2}{r} - 2(1+\tau_z)v_\phi + 2\tau_\phi v_z$$

$$= -\frac{\partial p^d}{\partial r} + \frac{1}{Re}\left[D''v_r - \frac{v_r}{r^2} - \frac{2}{r^2}\frac{\partial v_\phi}{\partial \phi}\right] \tag{3b}$$

$$D'v_\phi + \frac{v_r v_\phi}{r} + 2(1+\tau_z)v_r - 2\tau_r v_z$$

$$= -\frac{1}{r}\frac{\partial p^d}{\partial \phi} + \frac{1}{Re}\left[D''v_\phi - \frac{v_\phi}{r^2} + \frac{2}{r^2}\frac{\partial v_r}{\partial \phi}\right] \tag{3c}$$

$$D'v_z + 2\tau_r v_\phi - 2\tau_\phi v_r = -\frac{\partial p^d}{\partial z} - 2r\tau_r + \frac{1}{Re}D''v_z \tag{3d}$$

where

$$D' = \frac{\partial}{\partial t} + \frac{\partial}{\partial \phi} + v_r\frac{\partial}{\partial r} + \frac{v_\phi}{r}\frac{\partial}{\partial \phi} + v_z\frac{\partial}{\partial z}$$

$$D'' = \frac{\partial^2}{\partial r^2} + \frac{1}{r}\frac{\partial}{\partial r} + \frac{1}{r^2}\frac{\partial^2}{\partial \phi^2} + \frac{\partial^2}{\partial z^2}$$

The primary effect of nutation is the ϕ-periodic force term $-2r\tau_r = 2\epsilon r\cos\phi$ in the z-momentum equation (3d). For $\epsilon = 0$, equations (3) have the trivial solution $\mathbf{v}^d \equiv 0$, $p^d \equiv 0$. The system supports the following symmetries:

$$v_r(r, \phi+\pi, -z) = v_r(r, \phi, z), \quad v_\phi(r, \phi+\pi, -z) = v_\phi(r, \phi, z) \qquad (4a,b)$$

$$v_z(r, \phi+\pi, -z) = -v_z(r, \phi, z), \quad p^d(r, \phi+\pi, -z) = p^d(r, \phi, z) \qquad (4c,d)$$

Therefore it is sufficient to obtain a solution in the half-cylinder, $z \geq 0$, with appropriate symmetry conditions at $z = 0$.

Some Analytical Results

The steady flow in a relatively long cylinder (aspect ratio $\eta > 4$) at low Reynolds number is expected to exhibit little axial variation over most of the cylinder length. Previous work [9] has therefore relaxed the boundary conditions at the end walls and studied the steady flow in a finite segment of an infinitely long cylinder.

In the physical situations of interest, $\epsilon = (\Omega/\omega)\sin\theta$ is a small parameter, and consequently, it is reasonable to pursue a perturbation expansion in ϵ. This provides $\mathbf{v}_d$ in the form

$$\mathbf{v}^d = \sum_{n=1}^{\infty} \epsilon^n \mathbf{v}^{(n)}(r, \phi) \qquad (5)$$

and similar expressions for p^d. The development of expressions for the expansion coefficients $\mathbf{v}^{(n)}$ from equations (3) leads to an alternating pattern:

$$\mathbf{v}^{(n)} = \begin{cases} (0, 0, v_z^{(n)}), & n \text{ odd} \\ (v_r^{(n)}, v_\phi^{(n)}, 0), & n \text{ even} \end{cases} \qquad (6)$$

and the components of $\mathbf{v}^{(n)}$ take the form

$$v_r^{(n)} = \sum_{m=1}^{n/2} (u_{nm} e^{i2m\phi} + \tilde{u}_{nm} e^{-i2m\phi}) \qquad (7a)$$

$$v_\phi^{(n)} = v_{no} + \sum_{m=1}^{n/2} (v_{nm} e^{i2m\phi} + \tilde{v}_{nm} e^{-i2m\phi}) \qquad (7b)$$

$$v_z^{(n)} = \sum_{m=1}^{(n+1)/2} (w_{nm}\, e^{i(2m-1)\phi} + \tilde{w}_{nm}\, e^{-i(2m-1)\phi}) \tag{7c}$$

where the tilde denotes the complex conjugate. The aperiodic term in $v_r^{(n)}$ is suppressed by the continuity equation. The r-dependent coefficient functions in Eqs. (7) are required to satisfy homogeneous boundary conditions at $r = 1$ and to be finite at the axis $r = 0$.

The axial velocity at order $0(\epsilon)$ can be found in analytical form,

$$w_{11}(r) = i\,[\frac{I_1(\alpha r)}{I_1(\alpha)} - r] \tag{8}$$

where I_1 denotes the modified Bessel function, and $\alpha = (1 + i)(Re/2)^{1/2}$. This solution is valid for arbitrary Reynolds number but may be unstable as Re exceeds some critical value. This component is the dominating feature of the flow in a long cylinder. The interesting properties of the associated flow field are discussed by Herbert.[9]

At order $O(\epsilon^2)$, comparison of the equation for v_{20} with the imaginary part of the equation for w_{11} immediately shows that the aperiodic component of the azimuthal velocity is

$$v_{20}(r) = -2\,\mathrm{Im}[w_{11}(r)] \tag{9}$$

The ϕ-periodic components are governed by a coupled set of inhomogeneous differential equations with variable coefficients. With some effort, the radial velocity component of $O(\epsilon^2)$ can be found in closed form.[10] In view of the effort involved in deriving the analytical result and the ultimate need to determine certain coefficients numerically, the differential equations for the third-order components were solved by means of a spectral collocation method.

The motion is governed by the axial component w_{11} at order $O(\epsilon)$. Of the higher order terms, only the aperiodic term v_{20} is substantial. In the cylinder's center section, these terms are in good agreement with computational results. All the other terms are not only of order $O(1)$ but in fact less than unity, assuring rapid convergence of the perturbation series. The contribution of w_{31} to the

despin moment is negligible. The ϕ-periodic terms oscillate about zero as r varies between $0 \leq r \leq 1$. Accurate representation of single high-order terms by radial Chebyshev series may require numerous expansion functions. For the total velocity field, however, the error in representing these terms is of little importance. At Reynolds numbers in the range of maximum despin moment, reasonably accurate approximations can be obtained with only a few polynomials in radial direction. In the azimuthal direction, the solution is governed by terms periodic in ϕ, and by the aperiodic term v_{20}. Fourier series with three or five modes, therefore, provide approximations of sufficient accuracy for practical purpose. The perturbation analysis clearly shows that the main features of the flow are governed by the linear $O(\epsilon)$ part of equations (3) with small corrections for nonlinearity. This property will not change for a finite-length cylinder.

Spectral Approximations

The results of the analytical work suggest that a good approximation to the flow in a finite cylinder can be obtained by solving linearized versions of equations (3). Linearization can be performed in different ways. The first is a linearization in ϵ. Besides Eqs. (4), the resulting equations support the additional symmetries

$$\mathbf{v}^d(r, \phi+\pi, z) = -\mathbf{v}^d(r, \phi, z), \quad p^d(r, \phi+\pi, z) = -p^d(r, \phi, z) \quad (10a,b)$$

These relations permit useful checks on the results of the spectral code. A second linear system can be obtained by linearization in the components of $\mathbf{v}^d$. This linearization retains coupling terms such as $2r_\phi v_z$ in Eq. (3b) which destroy the symmetries (10). The second system can be considered a special case with $\hat{\mathbf{v}}^d = 0$ of a linearization about some known solution $\hat{\mathbf{v}}^d$. The latter procedure is very efficient if the solution is sought for a densely spaced sequence of parameter combinations as in flight simulations.

The algebraic form of the equations is obtained by use of spectral collocation. The velocity components are expressed in the form

$$v_r = \sum_{k=1}^{K} \sum_{l=1}^{L} \sum_{m=1}^{M} u_{klm} R^u_{kl}(r) F_l(\phi) Z^u_{ml}(\frac{z}{\eta}) \qquad (11)$$

with similar expressions for v_ϕ, v_z, and p^d. The azimuthal functions are

$$F_l = \begin{cases} \cos \frac{l-1}{2}\phi \ , & l \text{ odd} \\ \sin \frac{l}{2}\phi \ , & l \text{ even} \end{cases} \tag{12}$$

The azimuthal collocation points are equidistant,

$$\phi_l = 2\pi(l-1)/L \ , \ l = 1, 2, \cdots L \tag{13}$$

and L is odd.

In a first version of the code, radial and axial collocation points are located at the maxima of the highest Chebyshev polynomials. The boundary conditions are implemented by replacing three of the four differential equations in the boundary points. The question then is which equation should be retained and where the condition on the pressure, e.g. $p^d = 0$, should be applied. Trial-and-error leads to numerous cases with ill-determined matrices or zero determinant. In other cases, a correct solution for the velocity field is obtained, but the pressure contains a non-physical spurious term. Problems with spectral calculations of the pressure in closed domains with corners are well-known but the reports on their origin and methods for solution are rather unspecific. We have therefore performed a detailed analysis of the flow in a square driven by an internal force field. This simpler two-dimensional problem exhibits all characteristics - including the spurious pressure term - of the original problem. The study reveals that the spurious term vanishes in all collocation points except the corners, where it may assume arbitrary values. The term can be suppressed by retaining in the corners one of the momentum equations that contain the derivative of the pressure in the direction of the boundary.

In a second version of the spectral code, the problems of the pressure calculation have been avoided by using a different set of collocation points. The expansion functions in radial and axial direction depend on the index l and may be different for the variables v_r, v_ϕ, v_z, and p^d. They are combinations of even or odd Chebyshev polynomials such that

(i) the homogeneous boundary conditions are implicitly satisfied,

(ii) the symmetry conditions (4) are satisfied, and

(iii) the limit value of the variables for $r \to 0$ (i. e. the value on the axis) is independent of ϕ.

The collocation points are

$$r_k = \sin \frac{2k - 1}{4K}\pi \ , \ k = 1, 2, \cdots K \tag{14a}$$

$$\frac{z_m}{\eta} = \sin \frac{2m - 1}{4M}\pi \ , \ m = 1, 2, \cdots M \tag{14b}$$

Since $0 < r_k$, no points are located on the axis. Also, $r_k < 1$, $z_m < \eta$, such that no points are located on the surface. The points in radial and axial direction are concentrated near the boundary such that high resolution in this region is obtained without additional coordinate stretching. Thus the boundary layers forming at higher Reynolds number can be resolved by slightly increasing K and M.

The spectral collocation method converts the linear system of partial differential equations derived from Eqs. (3) into an algebraic system of dimension $N = 4 \cdot K \cdot L \cdot M$ for the coefficients u_{klm}, v_{klm}, w_{klm}, and p_{klm} of v_r, v_ϕ, v_z, and p^d, respectively. The linear system for the expansion coefficients is solved by Gauss elimination with partial pivoting. The subroutine used retains all data required to solve the same system with a new right-hand side without repeating the costly reduction of the matrix to upper triangular form. Once the solution is obtained, a new right-hand side is formed taking the nonlinear terms into account and the system is iteratively solved until sufficient accuracy is achieved. The procedure is equivalent to the modified Newton iteration (without updating the Jacobian in every step) and converges rapidly since the nonlinear corrections to the velocity are small while the pressure appears linear in equations (3).

Results for Velocity and Pressure

In the following, we present some results for the velocity and pressure fields at $\theta = 20^o$, $\tau = 0.16667$, and $\eta = 4.368$ which results in $\epsilon = 0.057$. The results are for $K = 6$, $L = 5$, and $M = 8$, and consequently $N = 960$. Calculation of a single solution with this high resolution requires about 2 minutes on a Cray-1S. Figure 2 shows the axial and radial velocities in the planes $\phi = 45^o$ and $\phi = 135^o$ at $Re = 20$. Only the upper half, $z \geq 0$, of the cylinder is shown; the lower half is governed by the symmetries (4). The scale values give the velocity per unit length where the diameter is four units. The velocity distribution at $z = 0$ agrees well with the results of the perturbation analysis and computations with the Sandia code.[3] Near the end walls, the solution is more realistic and more accurate than the Sandia results. The Figure also verifies the existence of a predominantly axial flow over most of the cylinder length, except within a region of the order of the radius near the end wall. Linear and nonlinear velocity distributions are hardly distinguishable. Clearly visible is the turning of the flow near the end wall. While the flow appears steady in the coordinate system chosen, the velocity field describes in fact an oscillatory motion of fluid elements about their near-circular orbit.

The pressure distributions for the same case are shown in Figure 3 with the heavy lines indicating positive values. Remarkable is the formation of regions of high and low pressure in the corner near $\phi \approx 45^o$ and $\phi \approx 135^o$, respectively, which produce large contributions to the moments about x-axis and y-axis. Except in this region near the end walls, the variation of the pressure is relatively weak. The azimuthal position of extremum pressure changes from $\phi = 0$ for small values of Re to $\phi = 90^o$ as $Re \rightarrow \infty$.

The dominant components of velocity and pressure fields are azimuthally periodic with period 2π. The harmonics are small, indicating the small effect of nonlinearity in the range of low Reynolds numbers. The only important nonlinear term is the aperiodic mean flow. This is clearly shown by Figure 4 which gives the azimuthal velocity in the center plane $z = 0$. The aperiodic component is opposite to the rigid-body rotation and exerts a negative roll moment

through the wall-shear stress $\tau_{r,\phi}$. The axial and radial mean velocity field is given in Figure 5. This streaming term exhibits a toroidal motion near the end in each half of the cylinder and causes a slow drift of fluid elements with respect to circular orbits. This mean velocity produces the symmetric pattern in flow visualizations [14] at low Reynolds numbers.

At the higher Reynolds number $Re = 300$, the maximum axial velocity appears at $\phi \approx 90^o$. As shown in Figure 6, the flow in the plane $\phi = 90^o$ breaks up into two swirls, one in each half of the cylinder, with little flow across the plane $z = 0$. Three weak swirls develop in the plane $\phi = 0$ such that the velocity field is reminiscent of a chain with five links. Notably, the break-up into cells is restricted to an inner region of the cylinder. The motion in the pronounced boundary layer visible in the plane $\phi = 0$ does not follow the cellular structure and may have a direction opposite to the core flow. The pressure variation is characteristically different from that at low Reynolds number. Figure 7 shows the strong variation and the formation of an almost symmetric pattern along the cylinder in the plane $\phi = 0$, while the variation at $\phi = 90^o$ is rather weak. This pressure field explains the void observations of Miller [15] which show a wavy distortion of the void in the plane $\phi = 0$ at high Reynolds numbers. The free surface in these observations can be interpreted as a surface of constant total pressure. The steep and opposite pressure gradients across the cylinder axis near $z/\eta = 0.25$ and $z/\eta = 0.75$ displace the void near these positions in opposite directions along the diameter at $\phi \approx -15^o$.

Calculation of the Liquid Moments

Conservation of angular momentum for the steady flow in a control volume V with surface S rotating with constant rate Ω about a fixed axis requires

$$\mathbf{M} + \int_S (\mathbf{r} \times \mathbf{F}) dS = \int_V \mathbf{r} \times (2\Omega \times \mathbf{v}) \rho \, dV$$

$$+ \int_V \mathbf{r} \times [\Omega \times (\Omega \times \mathbf{r})] \rho \, dV + \int_S (\mathbf{r} \times \mathbf{v}) \rho (\mathbf{v} \cdot d\mathbf{S}) \qquad (15)$$

where the velocity $\mathbf{v}$ is measured relative to the aeroballistic frame. On the left-

hand side, $\mathbf{M}$ is the resultant torque on the control volume, $\mathbf{r}$ is the position vector, and $\mathbf{F}$ the stress acting on the cylinder. The presence and meaning of certain terms depend on the choice of the control volume. The surface integral on the right-hand side of Eq. (15) vanishes if the surface of the control volume is closed.

For ease of practical application, we express the moment $\mathbf{M} = (M_x, M_y, M_z)$ in terms of cartesian components which provide yaw, pitch, and roll moment, respectively. Analogue to Eq. (1) we decompose the moments into

$$\mathbf{M} = \mathbf{M}^r + \mathbf{M}^d \tag{16}$$

where $\mathbf{M}^r$ corresponds to the pure rigid-body motion while $\mathbf{M}^d$ originates from the deviation velocity and pressure. For the cylindrical control volume, the rigid-body rotation causes only a pitch component

$$M_y^r = 2\pi\epsilon\eta[1 + \frac{\epsilon}{\tan\theta}(\frac{1}{2} - \frac{2}{3}\eta^2)] \tag{17}$$

while $M_x^r = M_z^r = 0$. Note that $\mathbf{M}$ is dimensionless; the reference moment is $\rho a^5\omega^2$.

The evaluation of the components of $\mathbf{M}^d$ bears some ambiguity that can be exploited for advantages. Previous computational work [3, 4, 5, 6] employed a control volume consisting of an "empty" closed cylinder with only the pressure and stresses acting on the inside surface. In this case, the right hand side of Eq. (15) vanishes and the moments are obtained from the stresses $\mathbf{F}$ at the inside wall of the control volume. Here, we use a different choice that bears great advantages especially for computational work.

We consider a control volume consisting of a solid cylindrical surface completely enclosing the liquid. The moment calculation for this "full" control volume rests on the relation

$$\mathbf{M}^d = \int_V \mathbf{r} \times (2\Omega \times \mathbf{v}^d)\rho\, dV \tag{18}$$

Using analytical relations derived by Rosenblat et al.,[6] the components of $\mathbf{M}^d$

can be shown to take the form

$$M_x^d = -I_1 \cos\theta \tag{19a}$$

$$M_y^d = I_2 \sin\theta - I_3 \cos\theta \tag{19b}$$

$$M_z^d = I_4 \sin\theta \tag{19c}$$

where

$$I_1 = -I_4 = \int_V z\,(v_r \cos\phi - v_\phi \sin\phi) r dr d\phi dz \tag{20a}$$

$$I_2 = \frac{1}{2}\int_V v_\phi r^2 dr d\phi dz \tag{20b}$$

$$I_3 = -\int_V v_z \sin\phi\, r^2 dr d\phi dz \tag{20c}$$

Finally, we obtain the moments in the form

$$M_x^d = \frac{2\epsilon}{\tan\theta} \int_{-\eta}^{\eta}\int_0^{2\pi}\int_0^1 v_z r^2 \cos\phi\, dr d\phi dz \tag{21a}$$

$$M_y^d = \epsilon \int_{-\eta}^{\eta}\int_0^{2\pi}\int_0^1 v_\phi r^2 dr d\phi dz + \frac{2\epsilon}{\tan\theta}\int_{-\eta}^{\eta}\int_0^{2\pi}\int_0^1 v_z r^2 \sin\phi\, dr d\phi dz \tag{22b}$$

$$M_z^d = M_x^d \tan\theta \tag{22c}$$

The volume integral approach thus leads to handy expressions which involve only the radial and azimuthal velocity components. Integration over $d\phi$ reduces the requirements in fact to the knowledge of the aperiodic component of v_ϕ and the simply periodic components of v_z. Therefore, the volume approach can also be applied to the analytical results given above and provides yaw and pitch moments without explicit knowledge of the pressure.

Results for the Liquid Moments

While velocity and pressure fields are primarily of basic fluid mechanical interest, the practical need for the moments dictates the measure for efficiency of the code. The moments derived from the volume approach and the surface

approach applied to the same spectral solutions are shown in Tables 1 and 2, respectively. The Reynolds number $Re = 20$ is in the range of maximum despin moment M_z.

It is obvious that the volume approach provides results of superior quality and more rapid convergence. The required (absolute) accuracy of 10^{-3} for engineering applications can be achieved with the low truncation $K = 4$, $L = 3$, $M = 4$. This accuracy has to be seen in the light of considerable uncertainty in the moments governing the exterior aerodynamics of the projectile. As a rule of thumb, an increase in the aspect ratio requires additional expansion functions in axial direction while increasing Reynolds number requires higher resolution in both radial and axial direction.

Figure 8 compares the calculated roll moments for a wide range of Reynolds numbers with the experimental results of Miller [2] and with computational results.[4, 6] The deviation of the results of the Sandia code [4] is caused by using inappropriate formulas for the moments in the nutating coordinate system.[7] The agreement with the other computational data is good. Test runs with high resolution suggest that the small difference from the results of Rosenblat et al.[6] is due to lower resolution of the finite-element code in combination with the application of the surface approach for the moments. The experiments were made in a range of spin rates ω between 2000 and 4000 rpm. While $\omega = 3000$ rpm has been used in Figure 8, assumption of a lower value would improve the comparison with respect to the maximum values.

Figure 9 shows a similar comparison for the yaw and pitch moments. The results of the Sandia code are suppressed since they suffer from a dimensional inconsistency.[7] While the agreement for the yaw moment at high Reynolds numbers is surprisingly good, the deviation in the pitch moment is likely to originate from insufficient resolution of the steep pressure gradients. This effect of discretization errors has been reduced in the spectral code by using the volume approach for calculating the moments.

Figure 10 shows the dependence of the yaw and pitch moments per unit length (the roll moment is proportional to M_z) on the aspect ratio of the cylinder and compares with results of the code written by Strikwerda & Nagel [5, 7] and the analytical results for $\eta \to \infty$. This diagram indicates that a reduction in the overall liquid moments for a given fluid mass can be achieved by splitting the cylindrical volume into slices of low aspect ratio.

Discussion

The codes previously in use may serve for establishing some basic results but are too inefficient for routine applications. The finite-difference code developed at Sandia Laboratories [3, 4] rests on Chorin's method of artificial compressibility and provides the steady solution at $11 \times 24 \times 21$ grid points in r, ϕ, z-direction by integrating over typically 10^4 to $8 \cdot 10^4$ time steps, a task that requires 6 to 48 minutes of CPU time on a Cray-1S. The result consists of over 22,000 values of the velocities v_r, v_ϕ, v_z and the pressure p at the grid points.

Strikwerda & Nagel [5] briefly describe a code using finite differences in radial and axial direction and pseudospectral differencing in the azimuthal direction. Nonuniform grids are introduced for increased resolution near the walls. The difference equations are solved by an iterative method based on successive over-relaxation. The computer time required is comparable to that of the Sandia code. A thorough evaluation of the two codes is currently conducted at BRL.[7]

The experience with the present version of the spectral code shows that high performance can be achieved. The solution is obtained in semi-analytical form with only $N = 4 \cdot K \cdot L \cdot M$ (typically less than 500) numerical coefficients. This low data volume is especially attractive for storage and for communication with remote supercomputers. The code is very well suited for vectorization, since practically all CPU time is spent on constructing and solving an algebraic system. The code demands larger memory than other codes, because 64-bit arithmetic is highly recommended for spectral methods in general, and the algebraic system requires $N(N+1)$ words of storage. A run with $N = 500$ requires about 2 Mbyte of memory and can easily be carried out on engineering workstations

within a few minutes, while moment calculations with $N = 192$ are a matter of seconds. Since the memory requirement is acceptable even if higher resolution is desired, the method applied here is a viable alternative in numerous other fluid mechanical problems. The ability to obtain accurate solutions for the steady problem directly from (large) algebraic systems bears valuable potential to answer the question whether the steady solution is stable, and allows analysis of unsteady motions with implicit time-stepping. The design of a reliable code for the unsteady problem can take profit from the knowledge of the eigenvalue spectrum for small unsteady disturbances of the steady flow.

While the calculation of velocity and pressure fields provides insight into the physics of the flow, the practical interest in the moments for the quasi-steadily changing parameters in flight simulations can be satisfied with modest amounts of computer time. This is due to using a modified Newton method which updates the Jacobian only when demanded by deteriorating convergence.

In general, the volume approach provides much more accurate results than the surface approach. This improvement is due to the additional smoothing of fluctuating data by integrating over three instead of two space directions and to using fewer, less fluctuating, and more accurate input data. The absence of v_r in the volume formulation is welcome. This velocity component is small over most of the cylinder length but oscillatory in the radial direction [10] with considerable gradients near the wall. Near the end walls, v_r is of the same order as v_z with steep gradients toward the end wall. Inspection of the velocity plots of Vaughn et al.[4] indicates that these gradients were difficult to resolve by the finite difference method. The aperiodic component of v_ϕ is a relatively small streaming term of smooth and almost uniform behavior along the cylinder axis. The large azimuthally periodic components of v_ϕ near the end walls do not affect the moment calculation.

Probably the greatest advantage of the volume formulation is the absence of the pressure from the moment equations. This property favors the use of pressure-free sets of basic equations, e. g. in terms of vorticity or vector potential.

The smaller number of dependent variables can be exploited for further increasing the efficiency. Even in natural variable formulations, the pressure is difficult to obtain with high accuracy because of the invalidity of the equations in the joints of the flat end walls to the cylindrical side wall. As shown in Figure 3, the pressure may assume extrema near the corners and, therefore, inaccuracies in this region may strongly influence yaw and pitch moment. In this context, it is instructive to evaluate the convergence history of the artificially time-dependent method implemented in the Sandia code.[3] While the velocity rapidly reaches a quasi-steady state, about 75% of the iterations are spent on improving the pressure field. We estimate that by use of the volume approach equivalent or superior values for the moments could be obtained with less than 20% of the iterations. It is worthwhile to note that the analytical results of Rosenblat et al.,[6] and equations (19), (20) for the moments are valid for closed containers of more general shape and thus can be used for other interior flow problems.

Our analytical and numerical tools allow quick estimates and efficient calculation of accurate liquid moments. These results also suggest guide lines for the suppression of the flight instability caused by the viscous-liquid payload. For a given cavity and fluid, a reduction in the overall liquid moments can be achieved in two ways. The first method is the split of the cylindrical volume into slices of low aspect ratio. The second way is the longitudinal split into k^2 "straws" of high aspect ratio $k\eta$. The change of the radius reduces the Reynolds number which may or may not be desirable. The nondimensional moment per straw increases due to the increasing aspect ratio. An essential reduction of the overall moments, however, originates from the fact that the dimensional moments are proportional to the fifth power of the radius. The dimensional factor is therefore reduced by k^{-5} per straw or k^{-3} for all straws together. As a raw estimate, the effective moments can be reduced by a factor k^{-2}.

ACKNOWLEDGMENT

We greatly appreciate discussions with S. Rosenblat and M. Nusca and the availability of their results prior to publication. The technical monitor of this project, M. C. Miller, deserves our gratitude for his sustained interest and the support of this work by the U. S. Army AMCCOM under Contract DAAA15-85-K-0012.

REFERENCES

1. R. Sedney 1985 "A Survey of the fluid dynamic aspects of liquid-filled projectiles," AIAA Paper No. 85-1822-CP.

2. M. C. Miller 1982 "Flight instabilities of spinning projectiles having nonrigid payloads," *J. Guidance, Control, and Dynamics*, vol. 5, pp. 151-157.

3. H. R. Vaughn, W. L. Oberkampf, and W. P. Wolfe 1983 "Numerical solution for a spinning nutating fluid-filled cylinder," Sandia Report SAND 83-1789.

4. H. R. Vaughn, W. L. Oberkampf, and W. P. Wolfe 1985 "Fluid motion inside a spinning nutating cylinder," *J. Fluid Mech.*, vol. 150, pp. 121-138.

5. J. C. Strikwerda and Y. M. Nagel 1985 "A numerical method for computing the flow in rotating and coning fluid-filled cylinders," in *Proc. 1984 Scientific Conf. on Chemical Defense Research, Aberdeen Proving Ground, Maryland*, ed. M. Rausa, pp. 523-527, CRDC-SP-85006.

6. S. Rosenblat, A. Gooding, and M. S. Engleman 1986 "Finite-element calculations of viscoelastic fluid flow in a spinning and nutating cylinder," Chemical Research, Development & Engineering Center, Report CRDEC-CR-87021.

7. M. J. Nusca and W. P. D'Amico 1986 "Parametric Study of low Reynolds number precessing/spinning incompressible flow," Ballistic Research Laboratory, Interim Memorandum Report BRL-IMR-881.

8. H. R. Vaughn, W. P. Wolfe, and W. L. Oberkampf 1985 "Six degree of freedom simulation of fluid payload projectiles using numerically computed fluid moments," Sandia Report SAND 85-1166.

9. Th. Herbert 1986 "Viscous fluid motion in a spinning and nutating cylinder," *J. Fluid Mech.*, vol. 167, pp. 181-198.

10. Th. Herbert, R. Li, and S. D. Greco 1988 "Perturbation analysis of the viscous flow in a spinning and nutating cylinder of large aspect ratio." *Phys. Fluids.* In preparation.

11. Th. Herbert 1987 "Analytical and computational studies of the fluid motion in liquid-filled shells," in *Proc. 4th Army Conf. on Appl. Math. and Computing, Ithaca, New York, 1986*, pp. 627-636, ARO Report 87-1.

12. Th. Herbert 1987 "A spectral Navier-Stokes solver for the flow in a spinning and nutating cylinder," in *Proc. 1986 Scientific Conf. on Chemical Defense Research, Aberdeen Proving Ground, Maryland*, ed. M. Rausa, pp. 455-460, CRDC-SP-87005.

13. R. Li and Th. Herbert 1988 "Calculation of the liquid moments in a spinning and nutating cylinder," *J. Guidance, Control, and Dynamics.* In preparation.

14. Th. Herbert and D. Pierpont 1986 "Visualization of the flow in a spinning and nutating cylinder," in *Proc. 1985 Scientific Conf. on Chemical Defense Research, Aberdeen Proving Ground, Maryland*, ed. M. Rausa, pp. 989-994, CRDC-SP-86007.

15. M. C. Miller 1981 "Void characteristics of a liquid filled cylinder undergoing spinning and nutating motion." *J. Spacecraft Rockets*, vol. 18, pp. 286-288.

CAPTIONS OF TABLES

Table 1. Volume approach for the moments at $\eta = 4.368$, $\tau = .1667$, $\theta = 20$, Re = 20.

Table 2. Surface approach for the moments at $\eta = 4.368$, $\tau = .1667$, $\theta = 20$, Re = 20.

CAPTIONS OF FIGURES

Figure 1. Definition sketch.

Figure 2. Vector plot of the axial and radial velocities in the planes $\phi = 45^o$ (left, scale 0.075) and $\phi = 135^o$ (right, scale 0.0375) at $Re = 20$ for $z \geq 0$.

Figure 3. Contour plot of the pressure field in the planes $\phi = 45^o$ (left) and and $\phi = 135^o$ (right) at $Re = 20$ for $z \geq 0$. Levels every 0.0025.

Figure 4. Vector plot of the azimuthal velocity v_ϕ in the center plane at $z = 0$, $Re = 20$. Scale 0.003.

Figure 5. Vector plot of the axial and radial mean velocity v_ϕ for $Re = 20$. Scale 0.002.

Figure 6. Vector plot of the axial and radial velocities in the planes $\phi = 0^o$ (left, scale 0.05) and $\phi = 90^o$ (right, scale 0.2) at $Re = 300$ for $z \geq 0$.

Figure 7. Contour plot of the pressure field in the planes $\phi = 0^o$ (left) and $\phi = 90^o$ (right) at $Re = 300$ for $z \geq 0$. Levels every 0.005.

Figure 8. Roll moment M_z vs. Reynolds number Re for $\eta = 4.368$,

$\tau = 0.16667$, and $\theta = 20°$. Comparison with numerical and experimental data.

Figure 9. Yaw moment M_z and pitch moment M_y vs. Reynolds number Re for $\eta = 4.368$, $\tau = 0.16667$, and $\theta = 20°$. Comparison with numerical data.

Figure 10. Yaw moment M_z and pitch moment M_y per unit length vs. aspect ratio η at $Re = 10$, $\tau = 0.16667$, and $\theta = 2°$. Comparison of present numerical results with analytical results for $\eta \to \infty$ and data obtained by Nusca with Strikwerda's code.

Table 1. Volume approach for the moments at $\eta = 4.368$, $\tau = .1667$, $\theta = 20$, $\mathrm{Re} = 20$.

K	L	M	M_x	M_y	M_z
3	3	3	0.08305	0.07475	0.03023
4	3	4	0.08260	0.07334	0.03006
5	3	5	0.08300	0.07332	0.03021
5	3	6	0.08317	0.07353	0.03027
6	3	5	0.08300	0.07332	0.03021
6	3	6	0.08317	0.07353	0.03027
4	5	4	0.08280	0.07353	0.03014
5	5	5	0.08322	0.07355	0.03029
6	5	6	0.08340	0.07374	0.03035
6	5	8	0.08335	0.07385	0.03034

Table 2. Surface approach for the moments at $\eta = 4.368$, $\tau = .1667$, $\theta = 20$, Re $= 20$.

K	L	M	M_x	M_y	M_z
3	3	3	0.07394	0.09396	0.03308
4	3	4	0.07247	0.08133	0.02992
5	3	5	0.07904	0.07291	0.03024
5	3	6	0.08178	0.07039	0.03028
6	3	5	0.07864	0.07354	0.03023
6	3	6	0.08137	0.07115	0.03027
4	5	4	0.07289	0.08354	0.02999
5	5	5	0.07894	0.07700	0.03032
6	5	6	0.08152	0.07491	0.03036
6	5	8	0.08289	0.07415	0.03034

Figure 1. Definition sketch.

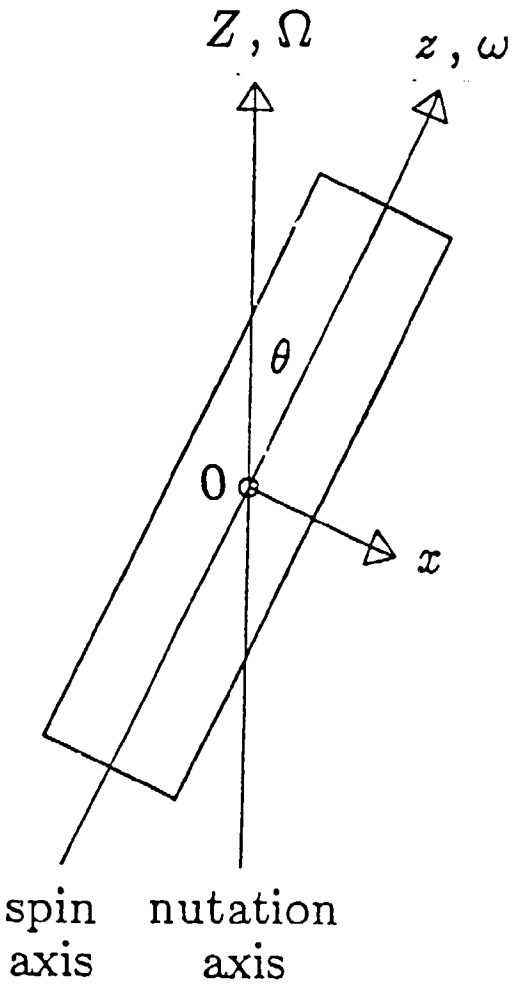

Figure 2. Vector plot of the axial and radial velocities in the planes $\phi = 45^{\circ}$ (left, scale 0.075) and $\phi = 135^{\circ}$ (right, scale 0.0375) at $Re = 20$ for $z \geq 0$.

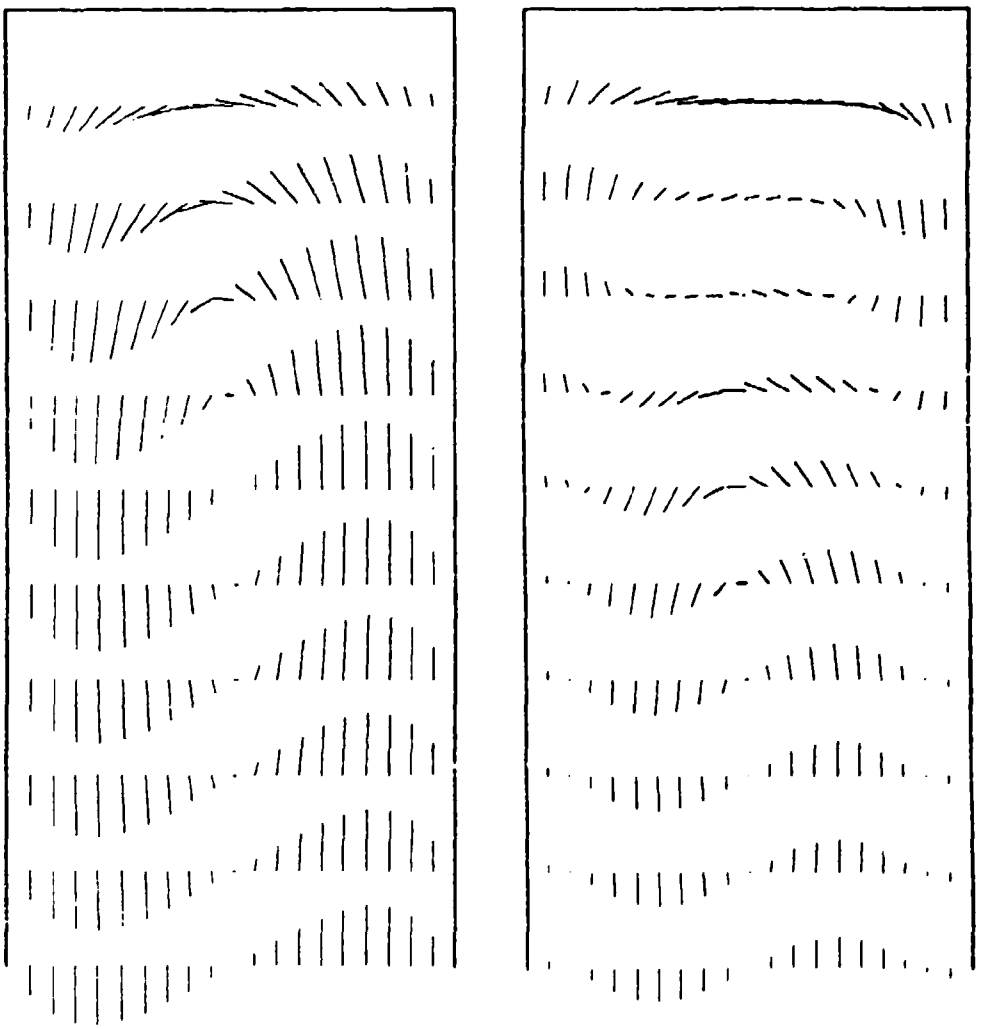

Figure 3. Contour plot of the pressure field in the planes $\phi = 45^o$ (left) and and $\phi = 135^o$ (right) at $Re = 20$ for $z \geq 0$. Levels every 0.0025.

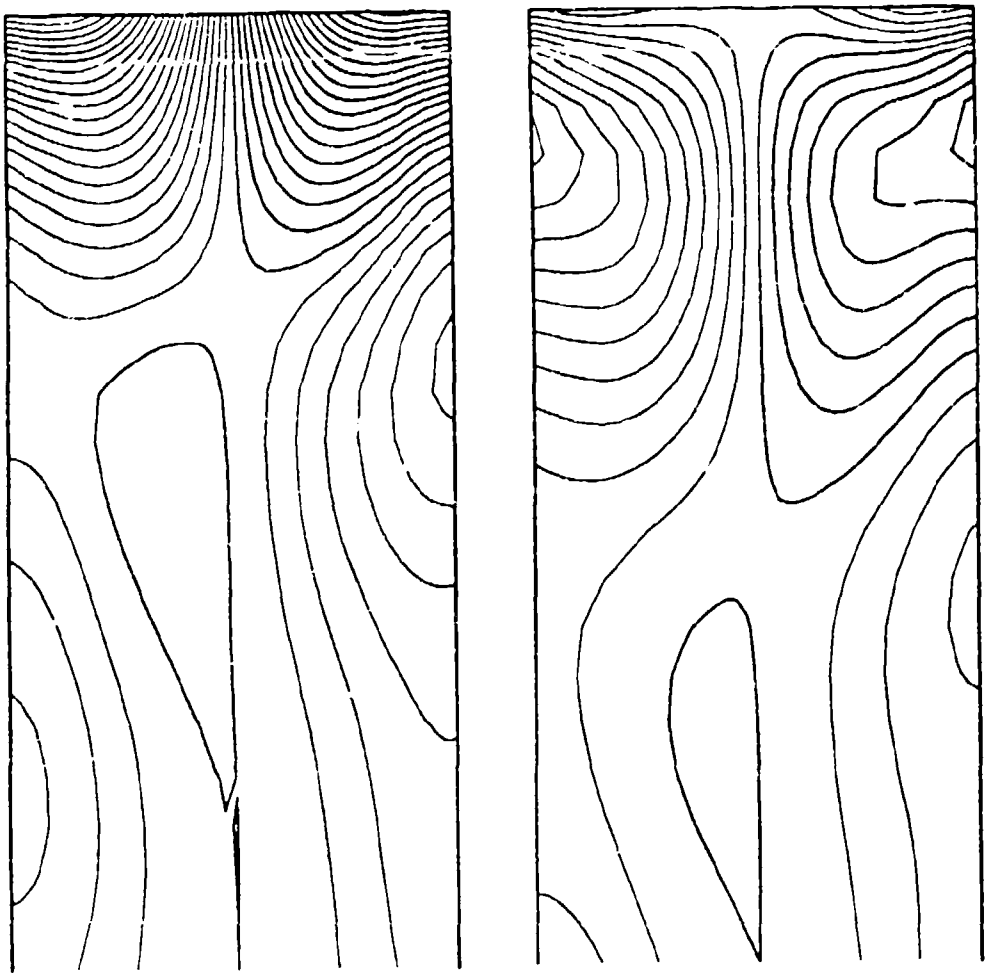

Figure 4. Vector plot of the azimuthal velocity v_ϕ in the center plane at $z = 0$, $Re = 20$. Scale 0.003.

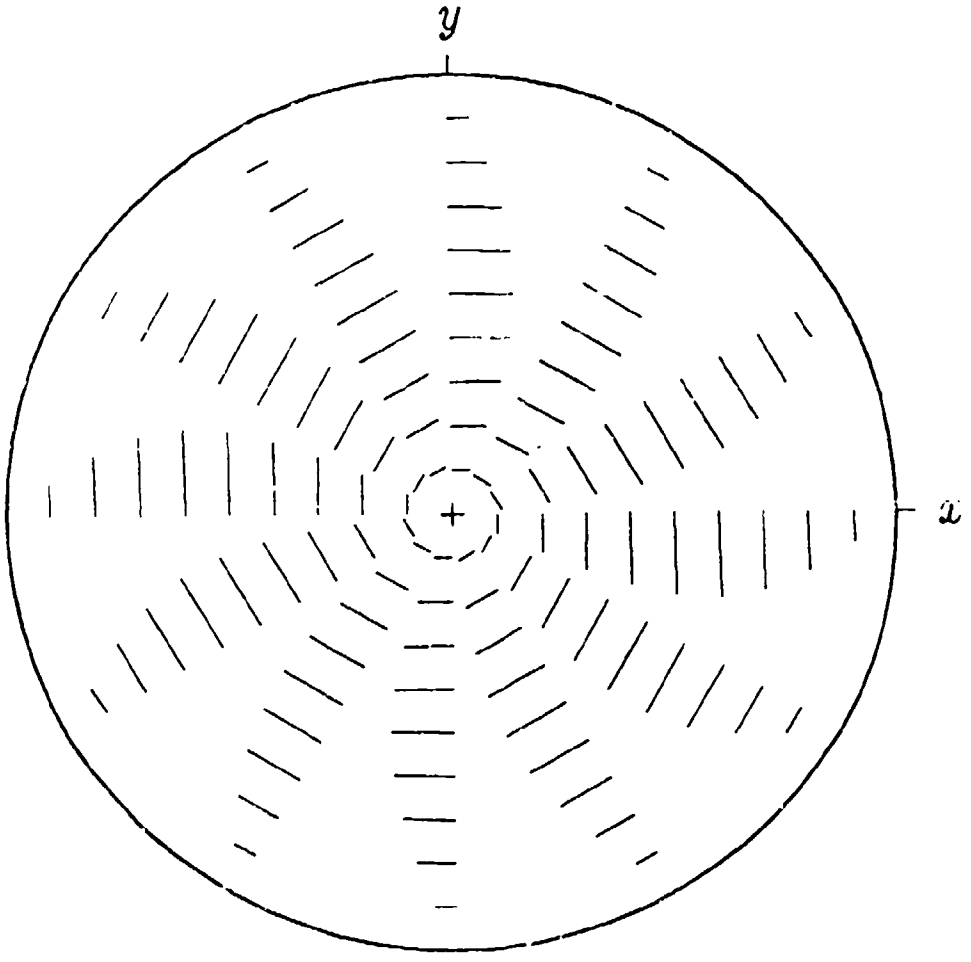

Figure 5. Vector plot of the axial and radial mean velocity v_ϕ for $Re = 20$. Scale 0.002.

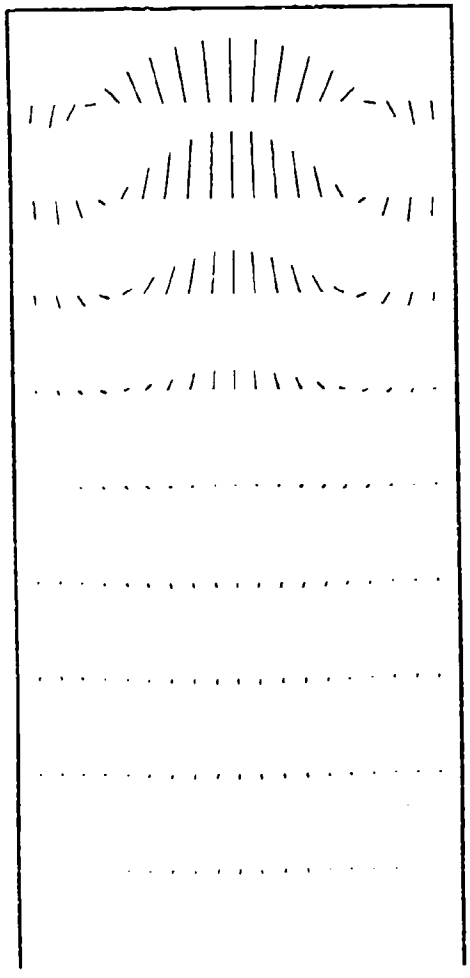

Figure 6. Vector plot of the axial and radial velocities in the planes $\phi = 0^o$ (left, scale 0.05) and $\phi = 90^o$ (right, scale 0.2) at $Re = 300$ for $z \geq 0$.

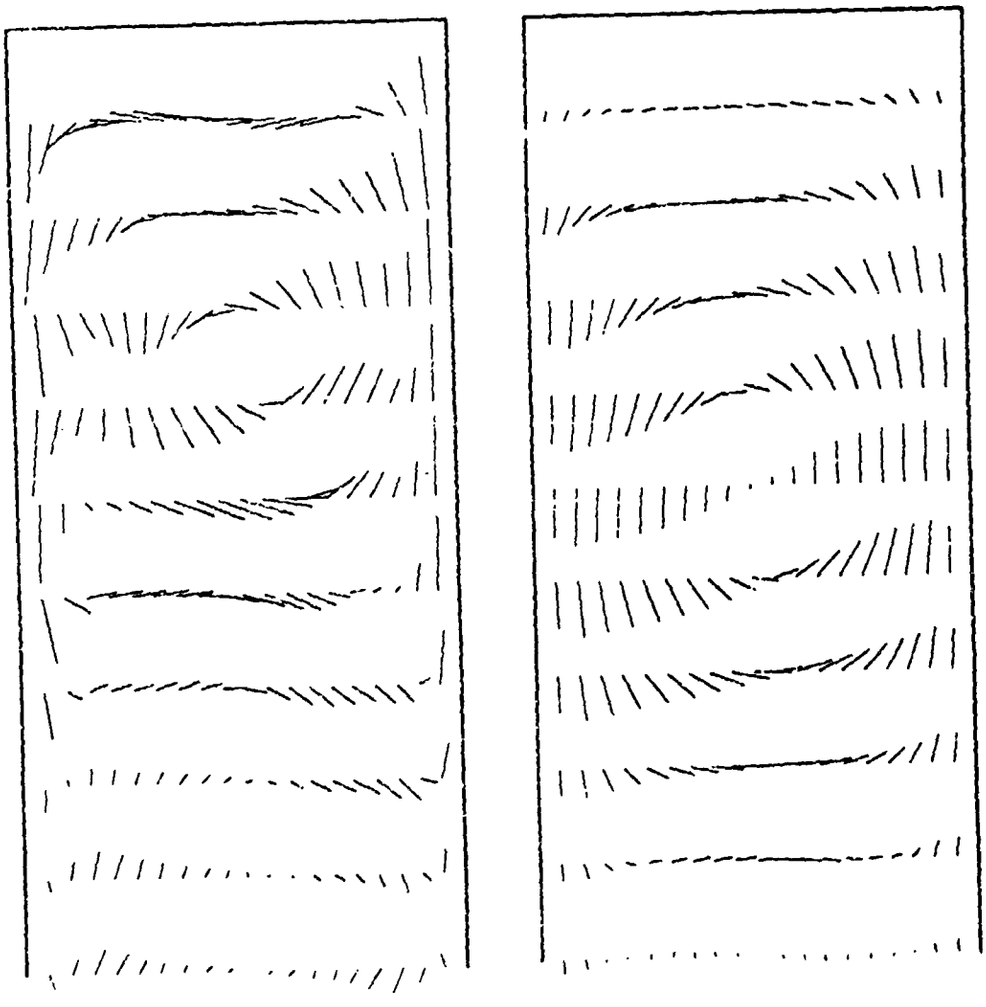

Figure 7. Contour plot of the pressure field in the planes $\phi = 0^o$ (left) and $\phi = 90^o$ (right) at $Re = 300$ for $z \geq 0$. Levels every 0.005.

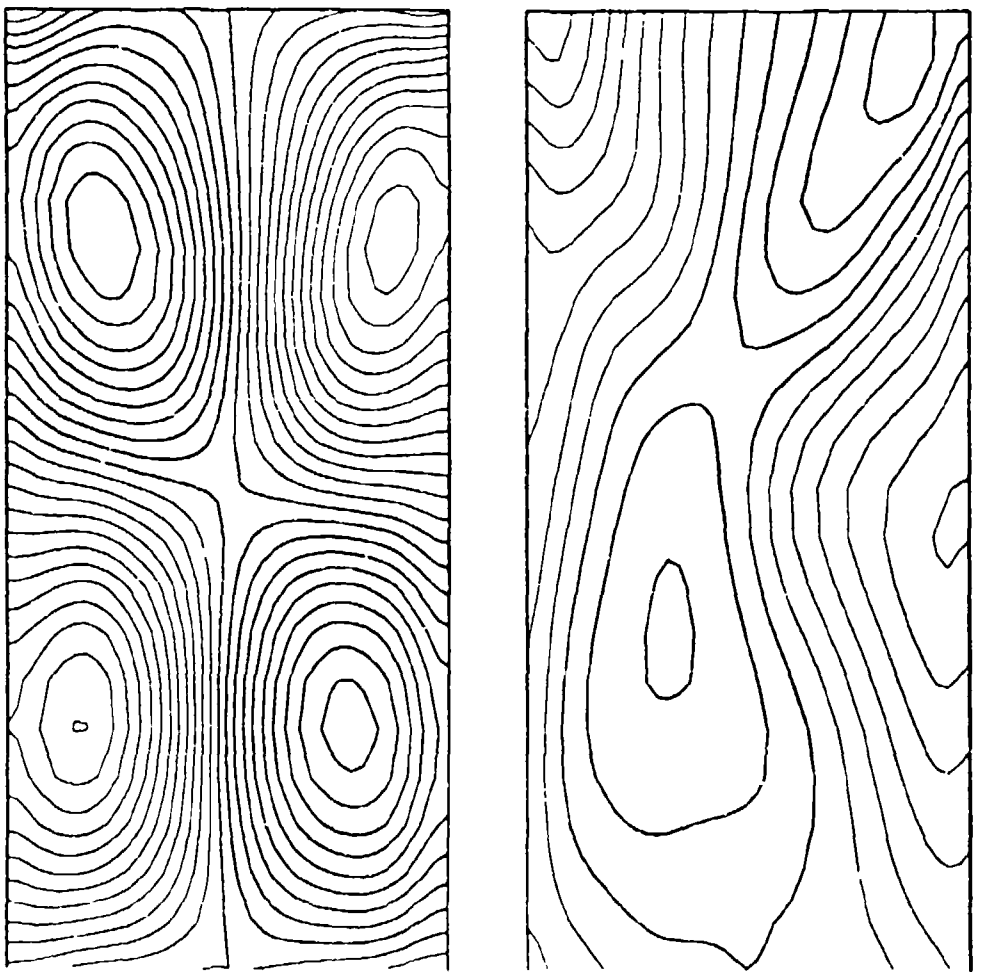

Figure 8. Roll moment M_z vs. Reynolds number Re for $\eta = 4.368$, $\tau = 0.16667$, and $\theta = 20°$. Comparison with numerical and experimental data.

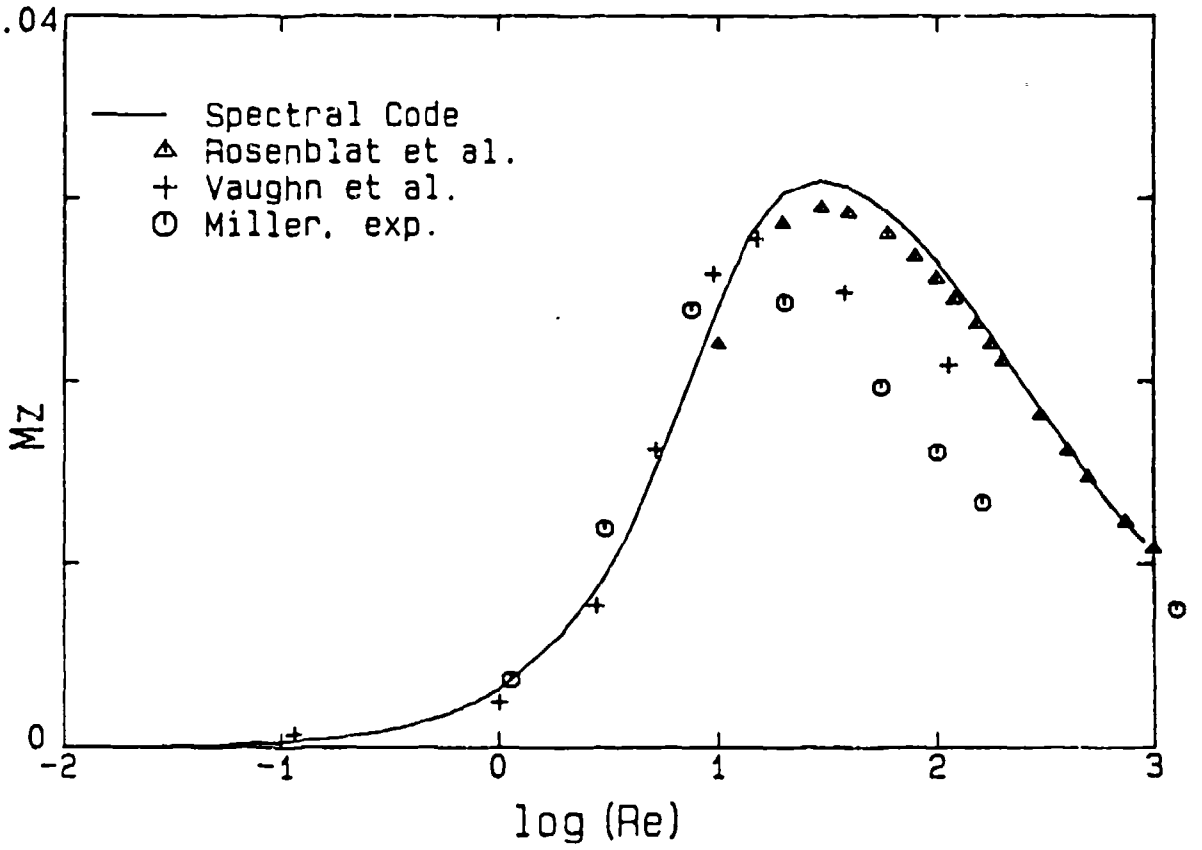

Figure 9. Yaw moment M_z and pitch moment M_y vs. Reynolds number Re for $\eta = 4.368$, $\tau = 0.16667$, and $\theta = 20°$. Comparison with numerical data.

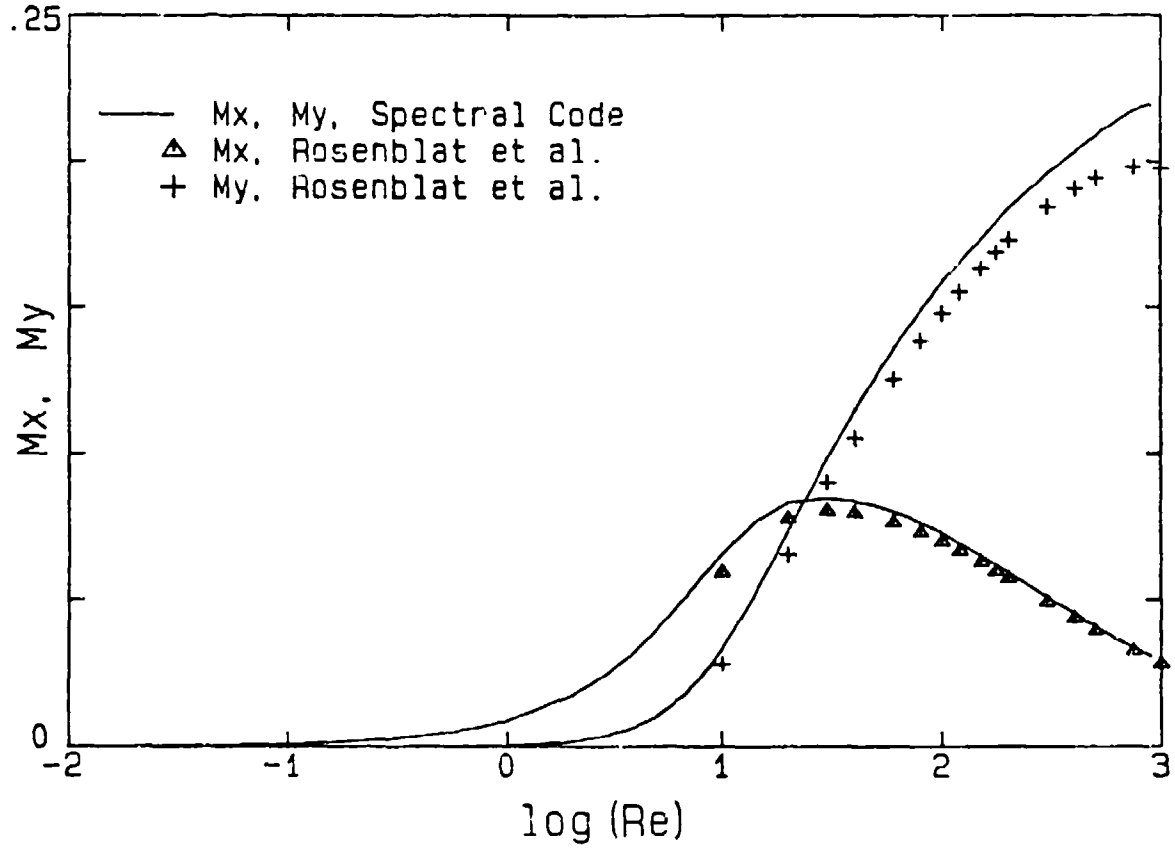

Figure 10. Yaw moment M_x and pitch moment M_y per unit length vs. aspect ratio η at $Re = 10$, $\tau = 0.16667$, and $\theta = 2°$. Comparison of present numerical results with analytical results for $\eta \to \infty$ and data obtained by Nusca with Strikwerda's code.

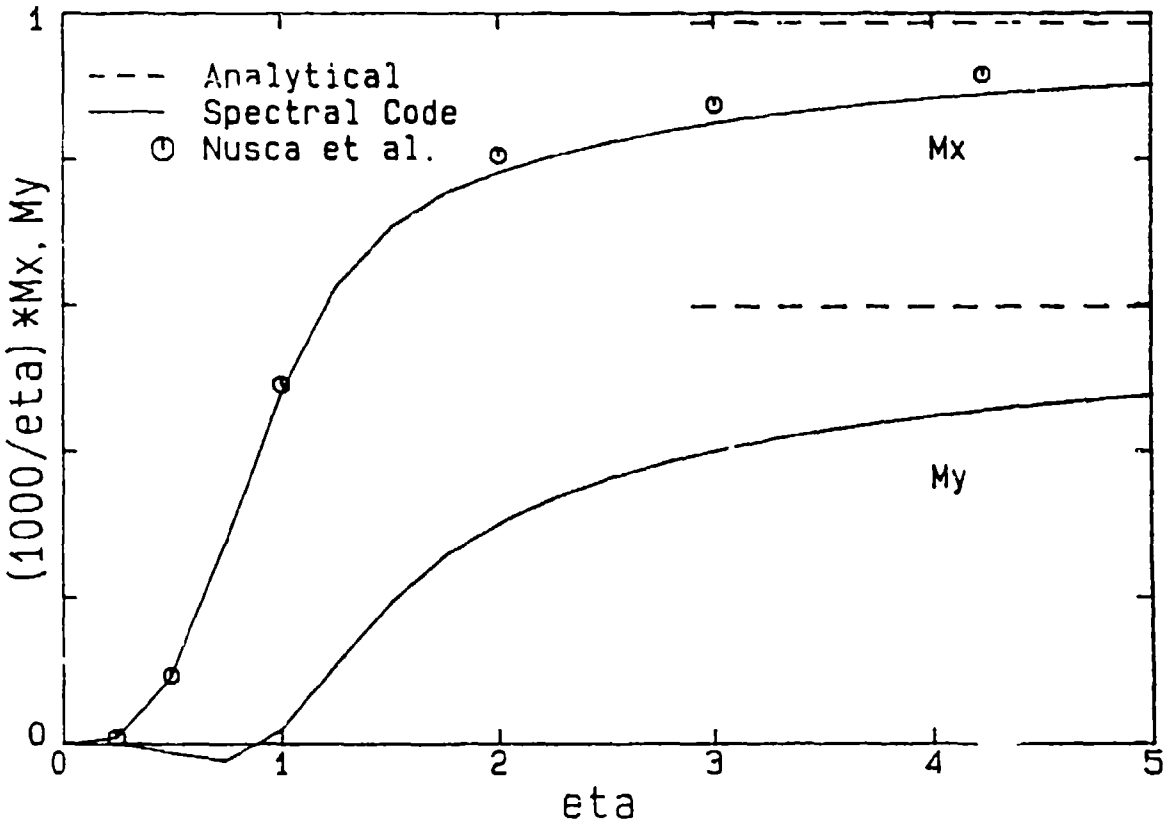

BLANK

APPENDIX G

SYMBOLIC COMPUTATIONS WITH SPECTRAL METHODS

By

Thorwald Herbert

Symbolic Computations with Spectral Methods

Thorwald Herbert

Department of Mechanical Engineering
Department of Aeronautical and Astronautical Engineering
The Ohio State University
Columbus, Ohio 43210

Abstract

The use of distributed workstations instead of mainframes has enabled us to adapt the software to our needs and to implement symbolic manipulation into our research environment. Our applications are primarily the simplification and verification of tedious manual procedures rather than solving complete problems in symbolic form. We report our experience using Macsyma for the derivation, coding, and documentation of complex equations, development of improved algorithms for spectral methods, and generation of Fortran code to provide test data. Example problems are in the area of viscous flow computation and hydrodynamic stability.

1. Introduction

The exploration of fluid dynamic phenomena and their underlying mechanisms often requires solving the complex equations of motion in relatively simple geometry. The arsenal of tools for solution ranges from brute-force computation to sophisticated asymptotic methods each of which has merits and shortcomings. Pure computation with finite-difference or finite-element methods is usually the shortest and most direct route to results but leaves the investigator with vast amounts of data for tedious postprocessing. Computation and postprocessing must be repeated for every new set of parameters. Analytical methods, on the other end, often provide generic results that are easy to understand and clearly reveal the role of parameters. Derivation of analytical results for complex problems, however, can be time-consuming and prone to errors, and the necessary approximations may blur the quantitative aspects. Only in rare cases can closed-form solutions be found. Usually, analytical work reduces the partial differential equations to ordinary differential equations which can be solved numerically with relative ease.

In our strive for quantitative information and insight, we have successfully applied a combination of analytical modeling and spectral methods for the numerical work. Spectral methods have very attractive numerical properties [1] and are closely related to the mathematical formulation of the problem. Inconsistencies in the approach do not remain localized, e.g. to a few grid points in a finite-difference solution, but affect the overall solution. The sensitivity of spectral methods to even small errors - in the formulation or due to round-off - is frustrating for the beginner but a welcome indicator for the experienced user. Often, the inconsistencies arise from inappropriate treatment of singularities, e.g. corners of the domain, from errors in equations or code, or from loss of significant digits that may remain undetected in other calculations. The successful effort of debugging the whole approach is rewarded with very pleasant performance of the method.

The development and implementation of correct equations can be a task of unexpected difficulty. Repetition of derivations and coding is time-consuming but not fail-safe. The a posteriori check of results with existing work or intuition is insufficient for verification of research computations. We have, therefore, incorporated symbolic manipula-

tion with Macsyma into our studies on linear and nonlinear stability of shear flows and on viscous rotating flows.

In our applications, Macsyma has been used less for problem solving than for reproducing and verifying the steps of the analysis. Like most computer tools, Macsyma requires major learning efforts, while tutorial examples for a specific step in a practical application are hard to find. With increasing skills, however, the efficiency in performing symbolic manipulation dramatically increases. The gain in overall efficiency is high enough to consider new classes of problems and new approaches that would hardly be feasible without symbolic manipulation. We have also experienced that this tool trains the user to clearly formulate the steps of the analysis and to "play" with alternatives which at times provide new insight into the structure of the problem and stimulate more elegant formulations.

1. The Computational Environment

We have Macsyma Version 309.6 installed on a Sun 3/180S with 575MB disk. This server is connected to Ethernet and to the campus-wide Sonnet fiber-optic link. Therefore, we can access Macsyma locally and remotely from other workstations or dial in through the university's Micom lines from home. The system is currently used by about ten faculty and graduate students with little or no prior experience in Lisp or any symbolic manipulators. Some members of this group have worked with Unix-based workstations and superminis for the past five years and had a short encounter with Macsyma on a Masscomp workstation with insufficient disk space. The Macsyma software is not under maintenance, therefore, the reference manual [2] and users guide [3] are the only common sources of information for self-study. Although our applications vary over a wide range of topics in fluid mechanics and heat transfer, we have not yet fully explored the capabilities of Macsyma.

Our primary applications of symbolic manipulation are in the following areas:

(1) Derivation of equations

(2) Generation of Fortran code

(3) Comparison and selection of algorithms

(4) Documentation

We outline in the following sections the major steps involved in solving some sample problems and indicate areas of application for symbolic manipulation.

2. The Flow in a Spinning and Nutating Cylinder

Calculation of the flow in a spinning and nutating cylinder is a prototype problem arising in the design of spin-stabilized rockets or shells with liquid payloads. Interest is in the moments exerted by the internal fluid motion and their detrimental effect on flight stability. Since the angle between spin axis and trajectory is small and the rate of nutation is smaller than the spin rate, a small dimensionless parameter ε can be identified that governs the deviation of the fluid motion from rigid-body rotation.[4] This viscous secondary flow in the cylinder and the coupling with inviscid inertial waves are analyzed using a perturbation method for long cylinders, an expansion in spatial eigenfunctions, and a Navier-Stokes solver based on a spectral collocation method. All these methods rest on the continuity equations and momentum equations for the reduced pressure and the secondary velocities (deviation from rigid-body motion). The equations are written in cylindrical coordinates with respect to a rotating coordinate system.[4] In this system, the secondary motion appears steady and forced by an azimuthally periodic force of order $O(\varepsilon)$.

This set of equations, the characteristics of the variables (*scalar, real*), dependencies, and frequently occuring operators can be defined once and saved in a file. The branching into different approaches suggests a hierarchical file structure as in Unix. We found it advantageous - especially in the learning phase - to develop segments of this hierarchy interactively and to save the successful commands in relatively small files which terminate with cleanup commands (*kill*). This mode is very conveniently executed on multi-window systems with easy scroll and screen-to-screen copy. The proper sequence of files to be loaded can be specified in a master file.

2.1 Perturbation Analysis for Long Cylinders

For a sufficiently long cylinder, the solution can be assumed independent of the axial direction and the boundary conditions on the end walls can be neglected. The essential steps of the perturbation expansion are: specify axial gradients to be zero (*gradef*), expand velocities and pressure in a truncated power series in ε (*sum*), expand azimuthally in a complex Fourier series, and substitute the double sum into the basic equations. Extraction of terms in the nth power of ε and like exponentials $e^{im\phi}$ in the azimu-

thal variable ϕ with *ratcoeff(ev(...))* provides ordinary differential equations for the coefficient functions which depend on the radial variable r. This procedure shows an interesting pattern, since numerous equations are identically satisfied: odd n are associated with odd m and contribute only to the axial velocity component, while even n are associated with even m and contribute to radial and azimuthal velocities and the pressure. With homogeneous boundary conditions on the cylinder wall and proper conditions on the axis, the lowest-order axial velocity component can be obtained in closed form and expressed in terms of the modified Bessel function $I_1(\alpha r)$, where $\alpha^2 = iRe$ and Re is the Reynolds number. The mean velocity (m even) is of order $O(\varepsilon^2)$ and consists only of an azimuthal component. This component is associated with a viscous roll moment on the cylinder.

We have manually developed a closed-form solution in terms of Bessel functions for the periodic second-order terms.[5] We have not yet reproduced this result with Macsyma. The effort to obtain closed-form solutions increases dramatically with the order. Therefore, we solve for the terms of order $n \geq 2$ by use of a spectral collocation method. The expansion functions are linear combinations of even and odd Chebyshev polynomials in the interval $0 \leq r \leq 1$ that satisfy the boundary conditions and conditions at $r = 0$. The case $n = 2$ serves for comparison with the closed-form solutions.

Given the (linear) differential equation $Lf = g$, where $f = f(x)$ and $g = g(x)$ and the expansion functions $h_k(x)$, spectral collocation directly leads to a linear algebraic system $\mathbf{Ma} = \mathbf{g}$.[1] The vector $\mathbf{g}$ consists of the values $g(x_j)$ at the collocation points x_j. In our work, the vector $\mathbf{a}$ consists of the expansion coefficients a_k of f with respect to $h_k(x)$, and $\mathbf{M} = (m_{jk})$ is the matrix representation of the differential operator applied to h_k (columns) at x_j (rows). The key to solving the given differential equation is to accurately define the elements m_{jk} of the matrix $\mathbf{M}$ and the right-hand side $\mathbf{g}$. The algebraic system can then be solved with standard procedures.

With Macsyma, it is straightforward to replace the right hand side g by a vector form $g[n]$ and to do the same for the r dependent coefficients of the differential equation. What remains then, is to replace *diff(f,r,n)* by $H[j,k,n]$, $n \geq 0$, where j indicates the collocation point, k the expansion function, and n the order of differentiation. The result can be converted to Fortran and inserted into a generic Fortran framework. The Macsyma output usually requires some editing for inconsistencies (e.g. *sqrt(2)*) with our compiler. After this editing and modifications to account for the specific parameters of the problem, printout, etc., the spectral code is ready to run, provided the array $H(j,k,n)$ contains the required data. These data are generated by one of a number of problem-independent subroutines in our individual library. Different versions account for different symmetries, intervals, variable transformations, and the specific choice of collocation points (see section 4).

2.2 Volume Integration of the Moments

Given the deviation velocities and reduced pressure, the calculation of the moments exerted by the fluid on the cylinder is a formidable task. In previous finite-difference codes, these moments are obtained by integrating normal and tangential stress components over the surface of the cylinder. Unfortunately, the input data - surface pressure and velocity gradients - are not very accurate. In addition, this procedure obtains the moments as the small difference of large numbers (pressure and viscous contribution) and consequently the results suffer from insufficient resolution.

With some analytical effort, the moments can be obtained by integrating over the volume of the cylinder. The final equations given by Herbert & Li[6] show that neither the pressure nor derivatives of the velocity are required; only the mean azimuthal velocity and the first Fourier mode ($\sim e^{i\phi}$) of the axial velocity need to be known. The expressions do not involve small differences of comparable terms.

The original derivations of the moment equations by Rihua Li consumed weeks of intense work. The smaller part of this time, obviously, served to find the proper steps of the analysis. The remainder was used to derive and verify the detailed equations and to insert and correctly integrate the spectral representation of the velocity components. Since Chebyshev polynomials are closely related to powers of the variable x as well as to trigonometric functions of the transformed variable $\theta = \cos^{-1}x$, the spectral moment equations give the result in an easy-to-interpret semi-analytical form. Meanwhile, we have repeated Li's derivation with Macsyma in a few hours.

2.3 Expansion in Spatial Eigenfunctions

For cylinders with smaller aspect ratios, above perturbation solution deteriorates. The problem is then to solve the basic equations for a finite cylinder. While previous finite-difference codes suffer from insufficient resolution and lack of convergence at higher Reynolds numbers, the problem appears to be well suited for a spectral approach. Two alternatives to consider are: (1) spectral expansions in generic functions, with azimuthal Fourier series, radial and axial series in combinations of Chebyshev polynomials (even or odd to satisfy the conditions at $r = 0$ and to exploit the symmetries of the problem), or (2) expansion in azimuthal Fourier series and spatial eigenfunctions that can be obtained from the linearized problem.

Expansions in spatial eigenfunctions to solve the linear problem were pursued by Hall et al.[7] who determined the eigenfunctions in a separate step by numerical integration of homogeneous ordinary differential equations in the axial variable z. The three-dimensional boundary value problem reduces in this way to the one-dimensional problem of satisfying the boundary conditions at the end wall with a collocation or least square method.

Li & Herbert [8] have developed a single partial differential equation for the spatial eigenfunctions that can be solved by separation of variables. The general solution consists of the product of cosines of complex arguments in the axial and modified Bessel functions of complex arguments in the radial direction. Eigensolutions can be found by determining the constant of separation from a characteristic system of equations. The remaining one-dimensional problem here is to satisfy three rather complicated boundary conditions at the cylinder wall. With the numerical expansion coefficients determined by collocation or least square method, the moments of the linear approach are obtained in semi-analytical form.

The notes and derivations for this approach fill a file of well over 200 pages. The results are still unpublished since a small error was detected in the final results for the moments. Rederivation of the complete formulation with Macsyma by a relatively unexperienced student required two days and showed one sign error in the manual derivation that led to cancellation, not summation of two small terms. At the end of the second day, we obtained the correct result from the Fortran code.

The expansion in spatial eigenfunctions is very interesting from a fluid dynamic point of view since it clearly reveals inertial-wave type functions and the formation of boundary layers at higher Reynolds numbers. However, the evaluations of convergence and computational demand lead to the conclusion that spatial eigenfunction expansions may not be the optimum approach. Reliable calculation of the roots of the characteristic equations in the large range of Reynolds numbers ($10^{-1} \le Re \le 10^6$, say) is numerically very demanding and can only be achieved after detailed studies on the asymptotic form of the eigenvalue spectrum. Symbolic manipulation of the equations and the ultimate *solve* command simplified this task enormously. Currently, we obtain reliable and accurate results up to Reynolds numbers of the order 10^3. While we have mastered the calculation of the eigenvalues up to $Re = 5 \cdot 10^6$, more analytical reformulation is required to avoid floating point overflows and loss of significant digits in the numerical solution for the expansion coefficients. Based on existing batch files, this work will be done in an interactive mode with Macsyma alternating with sketching new attempts on the note pad.

2.4 Spectral Navier-Stokes Solution

From previous work we have learned that the solution of the cylinder problem is essentially governed by linearized equations plus nonlinear corrections that increase with ε. Linearization can be performed in different ways. The first is a linearization in ε. A second linear system can be obtained by linearization of the velocity components and pressure about some known solution which may be identically zero. The latter procedure is very efficient if the solution is sought for a densely spaced sequence of parameter combinations as in flight simulations.

The algebraic form of the equations is obtained by use of spectral collocation with generic functions.[6] Instead of a single array $H(j,k,n)$ above, various preset arrays H_{ir}, $H_{i\phi}$, H_{iz} are required, where i indicates the dependent variables. The spectral form of the basic equations is not difficult to code manually but - with the Macsyma input available - can be quickly generated per computer. The generic framework reflects the increased number of dimensions and variables as well as the nonlinear nature of the problem: the dimension of the matrix increases to the product of the numbers of expansion functions in r, ϕ, z times four (variables). The linear algebraic system

takes the form $M^{\nu}a^{\mu} = g^{\mu}$ that is obtained by applying Newton's method ($\mu = \nu+1$) or the modified Newton's method ($\mu > \nu+1$). In the latter case, the Jacobian M^{ν} is only updated when indicated by deteriorating rate of convergence. The solution procedure starts with $\nu = 0$, $\mu = 1$ from zero or from a previously obtained solution at neighboring parameters. Once the iterative solution converges, the moments are calculated from volume integrals.

In the Reynolds number range covered by previous finite-difference codes, accurate moments can be obtained with $4 \times 3 \times 4$ expansion functions in r, ϕ, z, respectively, and a matrix dimension of 192. The measured computer times are smaller than 10^{-3} times those required by finite-difference codes. These three-orders-of-magnitude savings in computing time and cost permit routine application of the spectral code in flight simulations performed for design purpose which was not possible with previous codes. The cost per solution increases with the Reynolds number but is still less than with eigenfunction expansions at $Re \approx 10^3$ and is for the nonlinear result, not the linear approximation. For higher Reynolds numbers, methods based on the boundary-layer approximation are effective although their accuracy at Reynolds numbers of the order 10^3 remains to be verified.

The overall design of the spectral code and the volume approach to the calculation of moments was made possible only by good understanding and intense exploitation of the analytical properties of the problem. Unavailability of any symbolic manipulator in our earlier computer environment had forced us to do most of the work manually. In retrospect, symbolic manipulation had easily saved one year of qualified labor on this problem alone. We have purchased the license for Macsyma for $1,800 (for educational institutions), to be shared by various users - a worthwhile investment.

3. Hydrodynamic Stability

The situation in our studies of hydrodynamic instability and transition in shear flows is quite similar to the above. Decomposition of the velocity and pressure fields into various components, Fourier decomposition in two spatial directions, and extraction of linearized or nonlinear equations for single components are tedious tasks. Even more tedious are the common steps of eliminating the pressure by taking the curl of the momentum equations and eliminating one of the velocity components by use of continuity. These steps require manipulations of derivatives of the basic equations and subsequent substitutions. We have made much progress in performing these steps with Macsyma although elegant commands for some detailed steps have not yet been found. In our procedures, we prevent Macsyma from evaluating differentiations to maintain differential equations in the original variables (not their derivatives). Since Macsyma distinguishes, e.g. between $(u_x)_y$ and $(u_y)_x$, a formal substitution for u_x and subsequent evaluation *ev(%,diff)* does not always provide the result we desire. Our skills, though, are still open to improvement.

A particular example for the fruitful application of symbolic manipulation is our study of nonlinear secondary instability in boundary layers.[9,10] In spite of thorough checks of equations and Fortran code, we ended up with two independent codes that provided different results. In view of some ambiguity in certain substitutions and arrangement of terms, we were unable to find the source of the discrepancy and to decide for either one of the codes to be correct. While we were caught for months in this dilemma and faced a third and fourth pass through the analysis, Macsyma became available for MC68000-based workstations. Although we had to install and run the software on a workstation with insufficient disk space and had to learn the use of Macsyma from the very basics, the correct code was obtained within a few weeks. The printout of the equations and detailed output from this code enabled correction of the manually derived equations and of the faster hand-written code shortly after.

Weaponed with the new capabilities, we currently implement non-parallel effects and the streamwise variations of the disturbances into the analysis. Besides the creation of the matrices and vectors for the algebraic systems, symbolic manipulation is used to analyze asymptotic properties of the solutions, e.g. at large distance from the wall. Outside the boundary layer, the coefficients of the differential equations are constant. The asymptotic solution can, therefore, be obtained in closed form. Recently, we discovered that the existing theories of stability in non-parallel flows use an incorrect form of these asymptotic solutions.

The complexity of the equations and difficulties of the code verification markedly increase when we change from the previous incompressible problems to similar problems in supersonic and hypersonic flows.

The main reasons are the increased number of variables and functional relations, e.g. between viscosity and temperature (or species distribution). In joint work with Dr. G. Erlebacher at NASA Langley, we performed the first critical step: to develop and verify a spectral code for compressible stability studies. The verification used Macsyma to generate the matrix elements of the high-dimensional linear eigenvalue problem. With little effort, the effect of approximations employed in other codes could be studied and a small error in another available code discovered.

Over time, the use of symbolic manipulation produces a variety of relatively small input files that are worthwhile saving and developing into an archive of procedures comparable to a subroutine library. Improved versions can be created as skills develop. New projects can take profit of this archive of reoccuring sets of equations or formal manipulations making the application of Macsyma increasingly efficient.

4. Algorithms for Spectral Methods

While the foregoing applications were primarily concerned with the derivation of error-free equations and codes, there is a wealth of algorithms that are mathematically correct but useless for numerical applications - often because of the finite word length for handling numbers in a computer. The finite word length and round-off errors are of particular concern in context with spectral methods and their sensitivity to small errors. It is inevitable to secure accurate numerical results, especially for those subroutines that produce the problem-independent spectral data such as the matrices $H(j,k,n)$ mentioned above.

An early example of a numerical pitfall with spectral methods is associated with the first spectral solution of the Orr-Sommerfeld equation of the hydrodynamic stability theory by Orszag.[11] This work employed the tau method instead of collocation but rests on matrices similar to $H(j,k,n)$ to express the derivatives of the expansion functions in terms of expansion functions. For the fourth derivative, the matrix elements take the form

$$k\,[k^2(k^2-4)^2 - 3j^2k^4 + 3j^4k^2 - j^2(j^2-4)^2]$$

For $j \approx k$, the result of evaluating this expression with 32-bit floating point arithmetic deteriorates rapidly for $j, k > 25$, as shown by Orszag's results for the eigenvalues of the Orr-Sommerfeld equation. The obvious reason is the small difference between the large numbers k^6 and j^6. The effect of round-off can be easily studied with Macsyma by obtaining first the accurate result and then the result of bigfloat operations with different settings of *fpprec*, the desired precision. It is also easy to see that a numerically more advantageous form of the matrix elements can be obtained by substituting $k = l + j$:

$$(l+j)[l^4(l^2-8) + jl^3(6l^2-32)$$
$$+ (12j^2l^2 + 8j^3l)(l^4-4) + 16l^2 + 32jl]$$

This substitution is a trivial symbolic step but the effect of round-off errors is practically removed.

Every step in the subroutines for initializing the matrices $H(j,k,n)$ has been carefully selected to minimize round-off errors. Calculations of data for the sequence of trigonometric functions or Chebyshev polynomials are often recursive and bear the danger of dramatic error propagation. Error analyses in the literature and comparison of results for different floating-point precision were earlier used as criteria. More recently, these studies have been repeated with Macsyma, although no improvements were achieved. Accuracy of the basic subroutines has been verified for up to 180 expansion functions. For larger numbers of functions (which are irrelevant for our purpose), round-off errors slowly creep in.

5. Documentation

Availability of workstations and virtually unlimited access to a computer (and laser printer) at no nominal charge has modified our mode of operation over the past few years. Besides program development and computation, the computer also serves for documentation and as a "note book." While documentation earlier involved piles of scratch notes, program listings, and results before the first draft of a publication, we usually begin this draft before the first line of coding. The use of Unix has led us to still adhere to *troff* as the common typesetting system (although *TeX* is available). With the *typeset: true* command, intermediate steps and results of our Macsyma scripts can be directly converted to *eqn* | *troff* form for inclusion in the descriptive text. For lengthy expressions, the Macsyma output frequently requires some manual modification. The short notation of the scripts also suggests global redefinition of the quantities for *troff* output. The printout of the Macsyma batch script provides all the details of the derivations. The draft can be extended as the work progresses and provides an unambiguous description of the equations used in the computer codes. Conver-

sion to a publication requires major editing, more text, fewer equations, inclusion of the results, etc. The procedure prevents, however, the discrepancies between what has been done and what has been published. Symbolic manipulation serves here to save tedious typing of equations and to reduce sources of error.

6. Conclusions

Symbolic manipulation does not solve our research problems. We still have to develop the ideas and work out the details of the analysis. However, the description of the various steps can be sketchy, and the accurate formulation for documentation and computer code can be obtained by symbolic manipulation. Macsyma can also be used as a powerful and efficient "calculator" to test and improve numerical algorithms.

We consider symbolic manipulation as a tool similar to programming languages and computers: initially, their use helped to reduce the amount of human labor and human errors. Soon, these tools enabled solutions to problems that were not feasible without their use. Learning and mastering these tools require some effort, but their use educates us to more rigorously formulate ideas and relieves us from time-consuming tasks. Today, symbolic manipulation should be an integral part of the engineer's research environment.

Acknowledgment

I am grateful to Gordon Erlebacher, NASA Langley, for his cooperation in the development of a spectral code for compressible stability analysis. This work is supported by the U. S. Army AMCCOM under Contract DAAA15-85-K-0012 and by the Air Force Office of Scientific Research under Contract F49620-87-K-0005.

References

References

1. C. Canuto, M. Y. Hussaini, A. Quarteroni, and T. A. Zang, *Spectral Methods in Fluid Dynamics*, Springer-Verlag, 1987.
2. Macsyma Group, "Vax Unix Macsyma Reference Manual Version 11," Document No. SM105010300.011, Symbolics, Inc., 1985.
3. Computer Aided Mathematics Group, "Macsyma Users Guide," Document No. SM105000400.0, Symbolics, Inc., 1987.
4. Th. Herbert, "Viscous fluid motion in a spinning and nutating cylinder," *J. Fluid Mech.*, vol. 167, pp. 181-198, 1986.
5. Th. Herbert, R. Li, and S. D. Greco, "Perturbation analysis of the viscous flow in a spinning and nutating cylinder of large aspect ratio," *Phys. Fluids*, 1988. In preparation.
6. Th. Herbert and R. Li, "Numerical study of the flow in a spinning and nutating cylinder," AIAA Paper No. 87-1445, 1987. Submitted to AIAA Journal.
7. P. Hall, R. Sedney, and N. Gerber, "Fluid motion in a spinning, coning cylinder via spatial eigenfunction expansions," Ballistic Research Laboratory, Technical Report BRL-TR-2813, 1987.
8. R. Li and Th. Herbert, "An eigenfunction expansion for the flow in a spinning and nutating cylinder," *J. Fluid Mech.*, 1988. In preparation.
9. Th. Herbert, "Secondary instability of boundary layers," *Ann. Rev. Fluid Mech.*, vol. 20, pp. 487-526, 1988.
10. J. D. Crouch, "The nonlinear evolution of secondary instabilities in boundary layers," Ph.D. thesis, Virginia Polytechnic Institute and State University, 1988.
11. S. A. Orszag, "Accurate solution of the Orr-Sommerfeld stability equation," *J. Fluid Mech.*, vol. 50, pp. 689-703, 1971.

APPENDIX H

HIGH-REYNOLDS-NUMBER FLOWS IN A SPINNING AND NUTATING CYLINDER

By

Thorwald Herbert
Rihua Li

HIGH-REYNOLDS-NUMBER FLOWS IN A SPINNING AND NUTATING CYLINDER

Rihua Li
Department of Aerospace and Mechanical Engineering,
University of Arizona
Tucson, Arizona 85721

Thorwald Herbert
Department of Mechanical Engineering
Department of Aeronautics and Astronautics
The Ohio State University
Columbus, Ohio 43210

ABSTRACT

The moments exerted by the fluid motion in liquid payloads can jeopardize the stable flight of spin-stabilized projectiles. These moments can be computed with various Navier-Stokes codes for sufficiently small Reynolds numbers. For the linearized problem, Hall, Sedney, and Gerber (1987) have proposed an expansion in radial eigenfunctions that could extend the range of Reynolds numbers. The need to determine eigenvalues and eigenfunctions numerically and the slow convergence of the expansion series, however, make this approach less efficient than solving the Navier-Stokes equations with spectral methods. We have derived a new formulation of the linear problem that permits closed-form solutions for radial or axial eigenfunctions and calculation of the eigenvalues from a closed-form characteristic equation. The formulation is also suited for solution by spectral methods at a fraction of the computational expense of other codes.

1. Introduction

Spin-stabilized projectiles with liquid payloads may experience severe flight instabilities. Two types of liquid-induced instability are currently known. Both types are excited by the coning motion of the projectile about the trajectory.[1] The first type is caused by resonance with inertial waves at critical frequencies τ (ratios of coning rate Ω to spin rate ω). This resonance is most pronounced for low-viscosity liquid fills, i.e. at high Reynolds numbers, and depends sensitively on the cylinder's aspect ratio η. Theoretical analysis of this instability usually involves the boundary-layer approximation and therefore provides design criteria for sufficiently large Reynolds numbers, $Re > 1000$, say. Analysis based on the Navier-Stokes equations [2] shows, however, that resonance with inertial waves may severely influence the liquid moments at Reynolds numbers as low as $Re \approx 100$. (We define the Reynolds number by $Re = \rho\omega a^2/\mu$, where ρ is the density, a the radius of the cylindrical cavity, and μ the viscosity.) The second type of instability is of viscous nature and is most pronounced at low and medium Reynolds numbers for a wide range of aspect ratios and frequencies. This instability is characterized by a negative roll moment that opposes the spinning motion of the projectile.

Theoretical analysis of the moments must be based on the Navier-Stokes equations or on a linearized form of these equations if the nutation angles θ are sufficiently small.

Since both types of instability appear simultaneously for a wide range of Reynolds numbers, it would be highly desirable to develop a unified approach that bears potential for computing the moments in a wide range. Moreover, the efficiency of the moment computation is crucial since flight simulations require either large tables for interpolation or frequent evaluation of the moments for varying parameters.[3]

The analysis of liquid moments for engineering design is based throughout on the quasi-steady motion in the aeroballistic system. Direct solution of the three-dimensional nonlinear Navier-Stokes problem typically requires 5 - 200 seconds per solution on today's workstations (Sun 3/140 FPA) when using spectral methods.[2] The time increases with the Reynolds number and the formation of boundary layers. For practical purpose, the application ranges up to $Re \approx 1000$. For larger Reynolds numbers, $Re > 1000$, the analysis rests on linearized equations and use of the boundary-layer approximation.[4] At $Re = O(10^3)$, this approximation causes errors of about 10% [5] which decrease with increasing Re. Estimates of the moments for large aspect ratios η can be obtained at negligible cost from a perturbation expansions in $\varepsilon = \tau \sin\theta$.[6] Although this expansion is valid for all Reynolds numbers, it disregards the finite length of the cylinder and hence excludes the effect of resonances with inertial waves that depend on this length.

An alternative approach to solving the lowest-order equations of such an expansion has been suggested by Hall, Sedney, and Gerber (HSG).[7] This approach expands velocity components and pressure in a series of products of trigonometric functions in axial direction and radial "eigenfunctions" that satisfy homogeneous boundary conditions at the side wall. The coefficients of the series can be found from the boundary conditions at the end wall by collocation or least squares methods. Since only the linearized equations are solved, the HSG method provides yaw and roll moments but the pitch moment requires solving for nonlinear terms. While the nonlinear extension may be a matter of time, the shortcoming of the method is in the numerical determination of eigenvalues and eigenfunctions. Practical application is restricted to the range up to $Re = 1000$ with CPU times of 10 - 1800 seconds per solution (VAX 8600).

For given parameters, the eigenvalues for the HSG expansion are obtained by iterative solution of a sixth-order complex system of ordinary differential equations and are difficult to find. Good initial guesses are required for the iteration to converge. This problem is currently overcome by precalculating voluminous tables for interpolation of the initial estimates. The generation of these tables requires approximately 40 hours CPU time on a Cray (Murphy 1988, personal communication).

In the following, we discuss an alternative to the HSG method. We first outline what quantities are needed for the calculation of the moments. We derive a single sixth-order partial differential equation for the axial velocity component. This equation can be solved by using axial or radial eigenfunctions. The eigenfunctions are given in closed form and the eigenvalues are determined by numerically solving a closed-form characteristic equation. The partial differential equation in two variables also provides a new basis for efficient solution by spectral methods.

2. Calculation of the Moments

For the moments, we use cartesian coordinates x, y, z, where z is the spin (or cylinder) axis while x is normal to z and coplanar with spin axis and nutation axis. Velocity and pressure fields,

however, are more conveniently expressed in cylindrical coordinates r, ϕ, z. The nondimensional moments can be obtained from the following relations:[8]

$$M_x = 2\frac{\Omega}{\omega}\cos\theta \int_{-\eta}^{\eta}\int_{0}^{2\pi}\int_{0}^{1} v_z\, r^2 \cos\phi\, dr\, d\phi\, dz\ , \tag{1}$$

$$M_z = M_x \tan\theta\ , \tag{2}$$

$$M_y = 2\frac{\Omega}{\omega}\cos\theta \int_{-\eta}^{\eta}\int_{0}^{2\pi}\int_{0}^{1} v_z\, r^2 \sin\phi\, dr\, d\phi\, dz + \frac{\Omega}{\omega}\sin\theta \int_{-\eta}^{\eta}\int_{0}^{2\pi}\int_{0}^{1} v_\phi\, r^2\, dr\, d\phi\, dz\ . \tag{3}$$

The reference moment is $\rho\omega^2 a^5$ and $\mathbf{v} = (v_r, v_\phi, v_z)$ is the velocity vector of the deviation from rigid-body motion. We represent the velocity field by the Fourier series

$$\mathbf{v}(r, \phi, z) = \sum_{n=-\infty}^{\infty} \mathbf{v}_n(r, z)\, e^{in\phi}\ ,\quad \mathbf{v}_n = (u_n, v_n, w_n)\ . \tag{4}$$

After performing the integrations over ϕ in eqs. (1) and (3), it is obvious that the calculation of the moments requires only the two Fourier components $w_1(r, z)$ and $v_0(r, z)$. From perturbation expansion in $\varepsilon = \tau\sin\theta$ [6] it becomes immediately clear that w_1 is of order $O(\varepsilon)$ and hence the dominating component directly related to the periodic forcing with $\tau_r = -\varepsilon\cos\phi$. In contrast, v_0 is an aperiodic (streaming) component and hence of order $O(\varepsilon^2)$. Since ε is small in cases of practical interest, we concentrate in the following on determining w_1 from the linearized equations, leaving the nonlinear corrections for future investigation.

3. Linearized Equations for the Axial Velocity

We write the Navier-Stokes equations for the deviation $\mathbf{v}$, p from rigid-body motion in the nutating (aeroballistic) coordinate system.[9] Linearization in $\varepsilon = (\Omega/\omega)\sin\theta$ provides

$$\nabla \cdot \mathbf{v} = 0\ , \tag{5}$$

$$\frac{\partial}{\partial\phi}\mathbf{v} + 2\boldsymbol{\tau}\times\mathbf{v} + \nabla p - \frac{1}{Re}\nabla^2\mathbf{v} = -2r\tau_r\mathbf{e}_k\ , \tag{6}$$

where

$$\nabla^2 = \frac{\partial}{\partial r^2} + \frac{1}{r}\frac{\partial}{\partial r} + \frac{1}{r^2}\frac{\partial^2}{\partial\phi^2} + \frac{\partial^2}{\partial z^2} \tag{7}$$

and

$$\boldsymbol{\tau} = (\tau_r, \tau_\phi, 1 + \tau_z)\ ,\ \tau_r = -\frac{\Omega}{\omega}\sin\theta\cos\phi\ ,\ \tau_\phi = \frac{\Omega}{\omega}\sin\theta\sin\phi\ ,\ \tau_z = \frac{\Omega}{\omega}\cos\theta\ . \tag{8}$$

We take the curl of the momentum equations (6) to obtain the vorticity equations that are free of the pressure. We further take the curl of the vorticity equations and apply $\partial/\partial\phi - (1/Re)\nabla^2$ to the resulting equations. Since τ_r and τ_ϕ are functions of ϕ only, we obtain the following homogeneous system of partial differential equations for $\mathbf{v}$:

$$\frac{1}{Re^2}\nabla^6\mathbf{v} - \frac{2}{Re}\frac{\partial}{\partial\phi}\nabla^4\mathbf{v} + \frac{\partial^2}{\partial\phi^2}\nabla^2\mathbf{v} + 4(1+\tau_z)^2\frac{\partial^2\mathbf{v}}{\partial z^2} = 0\ . \tag{9}$$

We introduce the Fourier series (4) for $\mathbf{v}$ and the scaled variables

$$w_1 = \varepsilon w \ , \quad \bar{r} = qr \ , \quad \bar{z} = qz \ , \quad q = (1+i)\sqrt{Re/2} \ , \tag{10}$$

and obtain for w

$$\nabla^6 w - 2\nabla^4 w + \nabla^2 w - 4(1+\tau_z)^2 \frac{\partial^2 w}{\partial \bar{z}^2} = 0 \ , \tag{11}$$

where

$$\nabla^2 = \frac{\partial^2}{\partial \bar{r}^2} + \frac{1}{\bar{r}}\frac{\partial}{\partial \bar{r}} - \frac{1}{\bar{r}^2} + \frac{\partial^2}{\partial \bar{z}^2} \ . \tag{12}$$

Equation (11) is a single sixth-order partial differential equation for $w(\bar{r}, \bar{z})$. The derivation of the boundary conditions at the end walls and side wall is tedious and will be given elsewhere. The boundary conditions at the end walls $\bar{z} = \pm q\eta$ are

$$w = 0 \ , \quad \frac{\partial w}{\partial \bar{z}} = 0 \ , \quad \frac{\partial^5 w}{\partial \bar{z}^5} + (2\nabla_1^2 - 1)\frac{\partial^3 w}{\partial \bar{z}^3} = 0 \ , \tag{13}$$

with

$$\nabla_1^2 = \frac{\partial^2}{\partial \bar{r}^2} + \frac{1}{\bar{r}}\frac{\partial}{\partial \bar{r}} - \frac{1}{\bar{r}^2} \ . \tag{14}$$

The boundary conditions at the side wall $\bar{r} = q$ take the form

$$w = 0 \ , \tag{15a}$$

$$\frac{\partial}{\partial \bar{r}}(\nabla_1^4 w) + 2\frac{\partial}{\partial \bar{r}}\nabla_1^2 \frac{\partial^2 w}{\partial \bar{z}^2} + \frac{\partial^5 w}{\partial \bar{r}\,\partial \bar{z}^4}$$

$$- \frac{\partial}{\partial \bar{r}}\nabla_1^2 w - \frac{\partial^3 w}{\partial \bar{r}\,\partial \bar{z}^2} - 2(1+\tau_z)\frac{1}{\bar{r}}\nabla_1^2 w = \frac{2(1+\tau_z)}{iq} \ , \tag{15b}$$

$$2(1+\tau_z)\left[\frac{\partial w}{\partial \bar{r}} - \frac{\partial}{\partial \bar{r}}\nabla_1^2 w - 2\frac{\partial^3 w}{\partial \bar{r}\,\partial \bar{z}^2} + \frac{1}{\bar{r}^2}\frac{\partial w}{\partial \bar{r}}\right]$$

$$- \frac{1}{\bar{r}}\nabla_1^2 w + \frac{1}{\bar{r}}\nabla_1^4 w + \frac{2}{\bar{r}}\nabla_1^2 \frac{\partial^2 w}{\partial \bar{z}^2} = \frac{2(1+\tau_z)}{iq} \ . \tag{15c}$$

Three of the boundary conditions (13), (15) contain only derivatives with respect to $\bar{z}$ while the other three involve derivatives in both variables. In this form, the end-wall conditions are homogeneous while the axial velocity is forced by the side-wall conditions (15b, c). The problem can also be reformulated with inhomogeneous end-wall conditions and homogeneous conditions at the side wall by subtracting from w a multiple of the closed-form solution

$$w_\infty(\bar{r}) = \frac{\bar{r}}{q} - \frac{I_1(\bar{r})}{I_1(q)} \tag{16}$$

for the axial flow in an infinite cylinder.[9] I_1 denotes the modified Bessel function. The solution of the problem can be found by appropriate numerical methods or by expansions in spatial eigenfunctions. We note that the latter method belongs to the class of spectral methods and is distinguished from more generic methods by the special definition of the expansion functions.

4. A Note on Spectral Solution with Chebyshev Series

Previous work [2] has shown that spectral methods with Chebyshev-Fourier-Chebyshev series in r, ϕ, z, respectively, are efficient in solving the Navier-Stokes equations in the four natural variables v_r, v_ϕ, v_z, and p. If K, L, M denote the degrees of freedom in the three space directions, then the spectral solution requires determination of $N_{NS} = 4 \times K \times L \times M$ coefficients for all natural variables. The no-slip boundary conditions are independent of the variables and can be implicitly satisfied by using linear combinations of Chebyshev polynomials for the velocities.

Solving the governing equations for the single function w with Chebyshev-Chebyshev series in $\bar{r}$ and $\bar{z}$, respectively, requires the determination of only $N_w = (K + 2) \times (M + 1)$ expansion coefficients. The small increases in the degrees of freedom in $\bar{r}$ and $\bar{z}$ account for the three boundary conditions that involve derivatives with respect to both variables; the other three conditions can be implicitly satisfied. The projected CPU time for a single solution is reduced by the considerable factor $(N_w/N_{NS})^3 \approx 0.016/L^3$. These savings should permit spectral solutions for Reynolds numbers well in excess of $Re = 10^4$.

The spectral code was suggested by M. Selmi and is currently in development. The high order of differentiation demands extreme care for preventing round-off errors in the implementation.

5. Spatial Eigenfunctions

For brevity, we consider here only the case of axial eigenfunctions that satisfy the homogeneous boundary conditions (13). We solve the governing equation (12) by separation of variables:

$$w(\bar{r}, \bar{z}) = F(\bar{r})\,G(\bar{z})\,, \tag{17}$$

where

$$\nabla_1^2 F = BF\ ,\quad F(\bar{r}) = I_1(\sqrt{B}\,\bar{r})\,, \tag{18}$$

and B is a constant of separation. Equation (17) with

$$G(\bar{z}) = \sum_{i=1}^{3} c_i \cos a_i \bar{z} \tag{19}$$

is a solution of equation (12) if the three a_i are roots of

$$a^6 - (3B - 2)a^4 + [3B^2 - 4B + 1 - 4(1 + \tau_z)^2]a^2 - (B^3 - 2B^2 + B) = 0\,. \tag{20}$$

The other three roots are redundant by reasons of symmetry in $\bar{z}$. The boundary conditions at the end walls are satisfied if

$$\begin{aligned}
&(a_1^2 - a_2^2)(2B - 1 - a_1^2 - a_2^2)\,a_1 \tan(a_1 q\eta)\,a_2 \tan(a_2 q\eta) \\
&+ (a_2^2 - a_3^2)(2B - 1 - a_2^2 - a_3^2)\,a_2 \tan(a_2 q\eta)\,a_3 \tan(a_3 q\eta) \\
&+ (a_3^2 - a_1^2)(2B - 1 - a_3^2 - a_1^2)\,a_3 \tan(a_3 q\eta)\,a_1 \tan(a_1 q\eta) = 0\,.
\end{aligned} \tag{21}$$

and two of the coefficients c_i are properly chosen. Equations (20) and (21) represent a transcendental nonlinear system that provides an infinite set of solutions for the four unknown quantities B and a_i and associated eigenfunctions (17).

Finding the eigenvalue quadrupels (B, a_1, a_2, a_3) is a nontrivial task, and details will be described elsewhere. The relatively simple form of eqs. (20) and (21), however, permits application

of analytical tools unavailable in the numerical approach.[7] Equation (20) has four isolated roots with real B. Only the double root $B = 1$ (with $a_1 = 0$) satisfies eq. (21) and provides an isolated eigenfunction. For sufficiently large Reynolds numbers (and q), it can be shown that one of the a_i's, a_1 say, must be located near the diagonal $arg(a_1) \approx -\pi/4$. We observe that eq. (20) can be interpreted as determining either the a_i for given B or three solutions B_j, $j = 1,2,3$ for any given a. Varying a along the diagonal $-\pi/4$ provides three branches as the locus of the B_j, two of them, B_1 and B_2, originating at $B = 1$, the third, B_3, at $B = 0$, as shown in figure 1. A small correction to these branches and the position of the eigenvalues along the branches is provided by eq. (21). The larger the Reynolds number, the denser is the spacing of the eigenvalues.

Given a triplet B_j, we obtain for each B_j the associated values of a_{ji}, $i = 1,2,3$, where the a_{j1} are located in a small neighborhood near the diagonal $-\pi/4$. Figure 2 shows the curves generated by the first 50 eigenvalues for $Re = 20$, $\eta = 4.368$, $\tau = 0.16667$, and $\theta = 20$. Full, dashed, and dotted lines indicate the three families associated with the B_j in figure 1. At higher Reynolds numbers, the lines with $arg(a_{j1}) \approx -\pi/4$ are hardly distinguishable. Since each quadrupel $(B_j; a_{j1}, a_{j2}, a_{j3})$ defines one eigenfunction, these functions are ordered into triplets with approximately the same a_{j1}. The triplets can be ordered by increasing $|a_{11}|$. We finally obtain the ordered eigenvalue quadrupels $(B_n; a_{n1}, a_{n2}, a_{n3})$, $n = 1, 2, \cdots \infty$, with $|a_{n1}| < |a_{(n+1)1}|$.

The complex eigenfunctions are oscillatory, and the number of zeroes of real and imaginary part increases with n. Analysis of this oscillatory behavior suggests accounting for the isolated eigenfunction with $B = 1$. At larger Reynolds numbers, the eigenfunctions exhibit a pronounced boundary-layer character near $z = \eta$.

6. Numerical Solution for the Axial Velocity

With given eigenvalues and eigenfunctions, the axial velocity can be represented in the form

$$w(\bar{r}, \bar{z}) = \sum_{n=1}^{N} \sum_{j=1}^{3} A_{nj} F_{nj}(\bar{r}) G_{nj}(\bar{z}) , \tag{22}$$

where the yet unknown constants are determined by the boundary conditions (15) at the side wall, $\bar{r} = q$. As Hall, Sedney, and Gerber,[7] we find these constants numerically by using a collocation method or the method of least squares and calculate the associated yaw moment M_x. The convergence of the expansion series in terms of M_x is shown in figure 3. A relatively large number of eigenfunctions is necessary to obtain the accurate result within an error of a few percent. The accuracy improves rapidly and systematically as more eigenfunctions are taken into account.

The method is currently operational up to $Re = 2000$. We have calculated the eigenvalues for Reynolds numbers as high as $Re = 10^6$. The calculation of the eigenfunctions and expansion coefficients, however, still suffers from problems with large numbers caused by the exponential behavior of trigonometric and Bessel functions of large complex arguments. Work is conducted to circumvent these problems by proper scaling.

7. Summary

We have developed a new analytical formulation to obtain the liquid moments in the linear approximation by solving a single partial differential equation for the axial velocity. This equation can be solved by standard spectral methods or by use of expansions in spatial eigenfunctions. In

contrast to earlier work,[7] we obtain the eigenfunctions in closed form, and the eigenvalues are governed by a closed-form characteristic equation. Our formulation reveals the structure of the eigenvalue spectrum and permits direct calculation of the eigenvalues without costly lookup tables. The computer time for obtaining the spatial eigenfunctions is of the order of seconds and hence negligible. The calculation of the expansion coefficients requires essentially the time for solving an algebraic system with $3N$ complex unknowns, where N depends on the desired accuracy and increases with the Reynolds number. The computational efficiency of the spatial eigenfunction expansion is comparable to the spectral Navier-Stokes solver of Herbert and Li.[2] We expect higher efficiency from solving for the axial velocity by standard spectral methods.

ACKNOWLEDGMENT

The assistance of Mohamed Selmi in the analytical and numerical work and discussions with Miles C. Miller, CRDEC, are greatly appreciated. This work is supported by the U. S. Army AMCCOM under Contract DAAA15-85-K-0012.

REFERENCES

1. R. Sedney (1985) "A Survey of the fluid dynamic aspects of liquid-filled projectiles," AIAA Paper No. 85-1822-CP.
2. Th. Herbert and R. Li (1987) "Numerical study of the flow in a spinning and nutating cylinder," AIAA Paper No. 87-1445. Submitted to AIAA Journal.
3. Th. Herbert (1988) "Flight Simulation for Liquid-Filled Projectiles," in *Proc. 1987 U.S. Army CRDEC Scientific Conference on Chemical Defense Research, Report CRDEC-CR-88013*, ed. M. Rausa, pp. 377-385.
4. C. M. Murphy (1983) "Angular motion of a spinning projectile with a viscous liquid payload," *J. Guidance, Control, and Dynamics*, Vol. 6, pp. 280-286.
5. C. H. Murphy (1988) "An extension of the HSG theory for moments produced by very viscous rotating and coning liquid payloads," in *Proc. 1988 U.S. Army CRDEC Scientific Conf. on Chemical Defense Research, Nov. 1988, Aberdeen Proving Ground, MD*, ed. M. Rausa.
6. Th. Herbert and R. Li (1988) "Perturbation analysis of the viscous flow in a spinning and nutating cylinder," *Phys. Fluids*. In preparation.
7. P. Hall, R. Sedney, and N. Gerber (1987) "Fluid motion in a spinning, coning cylinder via spatial eigenfunction expansion," Ballistic Research Laboratory, Technical Report BRL-TR-2813, Aberdeen Proving Ground, MD.
8. R. Li and Th. Herbert (1988) "Calculation of the liquid moments in a spinning and nutating cylinder," *J. Guidance, Control, and Dynamics*. In preparation.
9. Th. Herbert (1986) "Viscous fluid motion in a spinning and nutating cylinder," *J. Fluid Mech.*, Vol. 167, pp. 181-198.

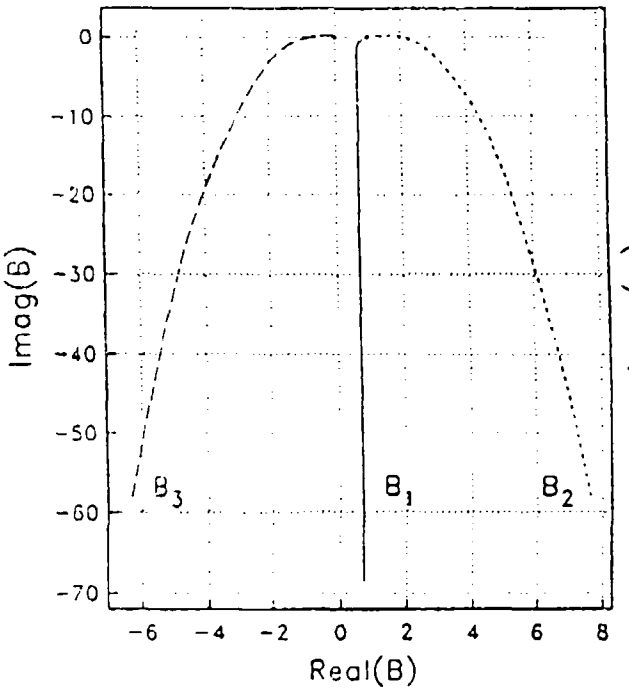

Figure 1. The three branches of $B(a)$ according to eq. (20) for $arg(a) = -\pi/4$ generated by the first 150 eigenvalues for $Re = 20$, $\eta = 4.368$, $\tau = 0.16667$, and $\theta = 20^{\circ}$.

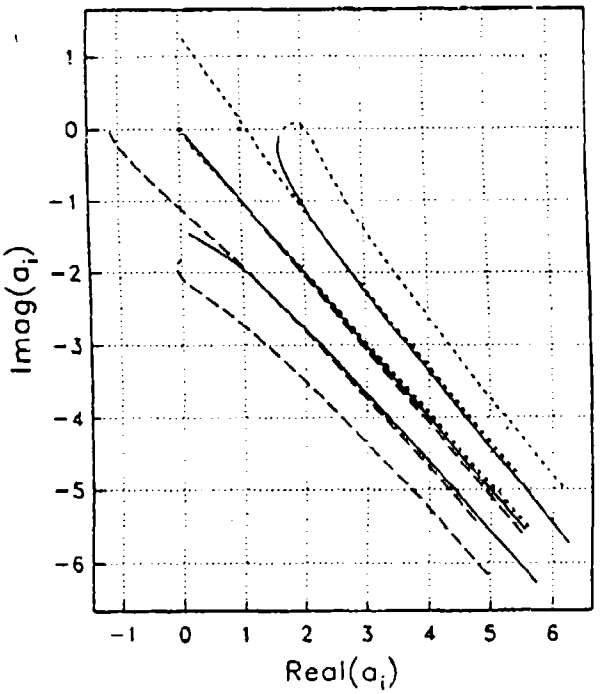

Figure 2. The three families of three eigenvalues a_{ji}, $i = 1,2,3$, associated with the B_j of figure 1. Full, dashed, and dotted line [illegible] for $j = 1,2,3$, respectively.

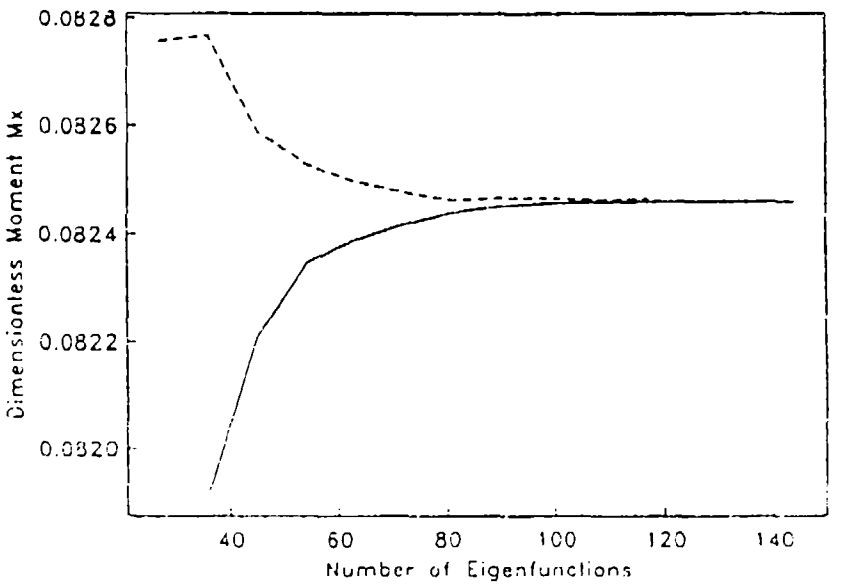

Figure 3. Convergence of the values of M_x obtained by collocation method (full line) and method of least squares (dotted line) with the number $3N$ of eigenfunctions. $Re = 20$, $\eta = 4.368$, $\tau = 0.16667$, and $\theta = 20^{\circ}$.